NASALR-170407

NASA Contractor Report 170407

NASA-CR-170407
19840012497

Space Shuttle Flying Qualities Criteria Assessment – Phase III

T. T. Myers, D. E. Johnston, and D. T. McRuer

LIBRARY COPY

MAR 23 1984

LANGLEY RESEARCH CENTER
LIBRARY, NASA
HAMPTON, VIRGINIA

Contract NAS4-3005
February 1984

National Aeronautics and
Space Administration

NASA Contractor Report 170407

Space Shuttle Flying Qualities Criteria Assessment – Phase III

T. T. Myers, D. E. Johnston, and D. T. McRuer
Systems Technology, Inc., 13766 Hawthorne Boulevard, Hawthorne, California 90250

Prepared for
Ames Research Center
Dryden Flight Research Facility
Edwards, California
under Contract NAS4-3005

1984

National Aeronautics and
Space Aeronautics
Ames Research Center
Dryden Flight Research Facility
Edwards, California 93523

N84-20565#

This Page Intentionally Left Blank

TABLE OF CONTENTS

		Page
I.	INTRODUCTION	1
II.	PILOT/VEHICLE IDENTIFICATION FROM FLIGHT DATA	5
	A. Overview of Flight Data Analysis	5
	B. Identification of the Effective Augmented Vehicle from Fight Data	9
	C. Pilot Technique Identification	28
	D. Summary of Flight Data Problems and Recommendations for OFQ	46
III.	CREW QUALITATIVE ASSESSMENTS	65
	A. STS-5 and -6 Crew Commentary	66
	B. Revised Crew Interview/Debriefing Questionnaire	69
IV.	HAND CONTROLLER EXPERIMENT	71
	A. Key Concepts for Assessing Sensitivity to Task Variables	72
	B. Experimental Plan	77
	C. Results	79
	D. Conclusions	81
V.	RESULTS, CONCLUSIONS, AND RECOMMENDATIONS	83
	A. Major Results	83
	B. Conclusions	84
	C. Recommendations for OFQ	85
REFERENCES		R-1
APPENDIX A.	DERIVATION OF NIPIP ESTIMATION EQUATION FOR THE SHALLOW GLIDE AND FLARE MODEL	A-1
APPENDIX B.	SPACE SHUTTLE FLYING QUALITIES QUESTIONNAIRE	B-1

LIST OF FIGURES

		Page
1.	Shuttle Approach and Landing (Nominal Characteristics).....	6
2.	Attitude Control Time Histories STS-4.....	8
3.	Superaugmentation Concept.....	11
4.	Shuttle Airframe Longitudinal Stability, Flexible-Approach and Landing (Adapted from Ref. 6).....	14
5.	Schedule for Pitch Rate Loop Gain, K_q (GDQ_COMP).....	16
6.	Effective Pitch Gain Scheduling of Shuttle.....	17
7.	FREDA Output for q/δ_{RHC} STS-4 Preflare Through Touchdown.....	20
8.	FREDA Output for q/δ_{RHC}, STS-4 Shallow Glide and Final Flare.....	22
9.	Definition of Cost Function in MFP Program.....	23
10.	Comparison of Flight-Derived Effective q/δ_{RHC} with $1/T_q$ Fixed and Free.....	24
11.	Asymptotic Comparison of $\lvert q/\delta_{RHC} \rvert$ with Three Different Numerator Constraints.....	27
12.	Comparison of NIPIP and FREDA Results for Shuttle Effective Vehicle Identification.....	29
13.	Elements of Preflare Oscillation Analysis.....	31
14.	Idealized Trajectory for the Shallow Glide and Flare Trajectory Model.....	33
15.	Effect of Pilot's Flare Time Constant on Final Flare.....	35
16.	Shallow Glide and Final Flare Pilot Model.....	36
17.	Idealized Altitude/Sinkrate Phase Plane Trajectory for the Shallow Glide and Flare Pilot Model.....	38
18.	Altitude-Sinkrate Phase Plane Analysis of STS-4 Shallow Glide and Final Flare Complementary Filtered $\dot{h}$.....	39
19.	Variations of Touchdown Variables in the Pilot's T_f-γ_o Control Plane, STS-4.....	42

LIST OF FIGURES (Concluded)

		Page
20.	Y_{p_θ} From NIPIP Interpreted in w′ Domain	47
21.	Comparison of Altitude Time Histories from Radar and IMU Channels in DFRF STS-4 MMLE Files	49
22.	Interpolated Radar Altitude, Shallow Glide and Final Flare	50
23.	Comparison of Sinkrate Signals	52
24.	Sinkrate from Complementary Filter	53
25.	Altitude-Sinkrate Trajectory, STS-4 Shallow Glide and Final Flare, $\dot{h}$ from Reference 18	55
26.	Frequency Response Comparison of θ/δ_{RHC} from Attitude Processor and ACIP	56
27.	NASA JSC Master Product Data Base for Shuttle	60
28.	Typical Page from the STS-6 Computer Compatible Tape (CCT) Report for the NASA JSC MPDB	61
29.	Generation and Use of the OFQ Archive Files	63
30.	Shuttle Orbiter RHC Feel/Command Gradient Characteristics in Landing	72
31.	The "Critical-Instability" Task (First Order)	74
32.	Structural-Isomorphic Model of Pilot-Aircraft System	75
33.	Critical Instability vs. Type of Control Stick	76
34.	RHC Configuration	78
35.	Manipulator Experiment Set-Up	78
36.	Pitch Axis CCT Raw Scores	80
37.	Roll Axis CCT Raw Scores	80
38.	Effective Pilot Latency; Shuttle vs. DFRF Simulation Controller	82
39.	Comparison of Experimental Results with Free and Stiff Manipulator Data of Reference 13	82

LIST OF TABLES

		Page
1.	Comparison of Parameter Extracted from STS-4 Flight Data with the Superaugmentation Model	25
2.	Contribution of FCS Elements to Effective Time Delay	26
3.	Shallow Glide and Flare Parameters	41
4.	Summary of Shuttle Flight Data Desired and Sources for OFQ	58

NOMENCLATURE

A_x, A_y, A_z	Acceleration components along the body x, y, z axes
c	Reference chord length
C_D	Drag coefficient; $\frac{2D}{\rho U^2 S}$
C_{D_o}	Zero lift drag coefficient
C_{D_u}	$\frac{U}{2}\frac{\partial C_D}{\partial U}$
C_{D_α}	$\frac{\partial C_D}{\partial \alpha}$
C_L	Lift coefficient; $\frac{2L}{\rho U^2 S}$
C_{L_o}	Lift coefficient, $\alpha = \delta_e = 0$
C_{L_u}	$\frac{U}{2}\frac{\partial C_L}{\partial U}$
C_{L_α}	$\frac{\partial C_L}{\partial \alpha}$
$C_{L_{\dot\alpha}}$	$\frac{\partial C_L}{\partial (\dot\alpha c/2U)}$
C_{L_q}	$\frac{\partial C_L}{\partial (qc/2U)}$
C_{L_δ}	$\frac{\partial C_L}{\partial \delta}$
C_M	Pitching moment coefficient; $\frac{2M}{\rho U^2 Sc}$

C_{M_u}	$\frac{U}{2}\frac{\partial C_M}{\partial U}$
C_{M_α}	$\frac{\partial C_M}{\partial \alpha}$
$C_{M_{\dot{\alpha}}}$	$\frac{\partial C_M}{\partial(\dot{\alpha}c/2U)}$
C_{M_q}	$\frac{\partial C_M}{\partial(qc/2U)}$
C_{M_δ}	$\frac{\partial C_M}{\partial \delta}$
d	Beam deviation
D	Aerodynamic drag
E_k	Specific kinetic energy
f_N	Nyquist frequency, Hz
FD	Flight director signal
g	Acceleration due to gravity (32.2 ft/sec^2)
G_{wo}	Washout equalization
h	Path deviation; altitude
h_c	Desired path
h_e	Path error
h_f	Flare initiation altitude
h_o	Altitude at start of shallow glide
h_B	Depth of flare asymptote
h_{IMU}	Altitude from IMU
h_R	Radar altitude
$\dot{h}_{TD}$	Touchdown sinkrate
I_y	Moment of inertia in pitch
K	Gain

K_q Controller gain

$K_V^{\bullet}$ Averaged value of -dV/dt

L Aerodynamic lift

ℓ_p Distance between pilot and c.g., positive for pilot forward

m Aircraft mass

M Aerodynamic pitching moment; Mach number

M_q (Single degree of freedom) pitch damping; Pitching acceleration per unit pitching velocity;

$$M_q = \frac{\rho S U c^2}{4 I_y} C_{M_q}$$

M_u Pitching acceleration per unit forward velocity;

$$M_u = \frac{\rho S U c}{I_y} (C_M + C_{M_u})$$

M_w, (M_α) Weathercock stability; Pitching acceleration per unit vertical velocity (angle of attack);

$$M_\alpha = U_o M_w \quad ; \quad M_w = \frac{\rho S U c}{2 I_y} C_{M_\alpha}$$

$M_{\dot{\alpha}}$ Pitching acceleration per unit angle of attack rate

$$M_{\dot{\alpha}} = \frac{\rho S U c^2}{4 I_y} C_{M_{\dot{\alpha}}}$$

M_δ Pitching acceleration per unit control surface deflection

$$M_\delta = \frac{\rho S U^2 c}{2 I_y} C_{M_\delta}$$

n Load factor

n_z Load factor in z direction

$N_{\delta_e}^{h}$	Altitude-to-elevator numerator
$N_{\delta_e}^{\theta}$	Pitch attitude-to-elevator numerator
P, Q, R	Angular velocity components about the x, y, z axes
q	Pitching velocity (pertubation)
q_e	Pitching velocity error
q_{ss}	Steady-state pitching velocity
$\bar{q}$	Dynamic pressure
R	Radius, (Fig. 1)
R_o	Equilibrium yaw rate
s	Laplace Operator
S	Reference planform area
t'_{TD}	Touchdown time measured from flare initiation
T	Time constant; sampling period
T_f	Flare time constant
T_{h_1}, T_{h_2}, T_{h_3}	Time constants, altitude numerator
T_q	Lead time constant in augmentaion system
T_r	Rise time
T_{RUN}	Length of a time response for parameter identification
T_{SP_1}, T_{SP_2}	Time constants, real short period roots
T_{θ_1}, T_{θ_2}	Time constants, pitch attitude numerator
T_{θ_2}	Lead time constant in short-period θ/δ transfer function for conventional airplane dynamics. Lag time constant between flight path angle, γ, and pitch attitude, θ.

$$1/T_{\theta_2} = -Z_w + Z_\delta M_w/M_\delta \doteq -Z_w$$

U	Speed (x stability axis)
U_o	Speed in reference condition
V	Speed
V_f	Speed at flare initiation
V_o	Velocity at start of shallow glide
V_E	Equilibrium speed
V_{TD}	Touchdown speed
w	Vertical velocity
w_g	Vertical gust velocity
W	Gross weight; Aircraft weight
X_f	Flare distance
X_u	Forward acceleration per unit speed change $X_u = \frac{\rho SU}{m}(-C_D - C_{D_u})$
X_w, X_α	Forward acceleration per unit vertical velocity $X_\alpha = U_o X_w \quad ; \quad X_w = \frac{\rho SU}{2m}(C_L - C_{D_\alpha})$
Y_c	Controlled element (augmented Shuttle) describing function
Y_{P_h}	Pilot describing function for pilot control action on path deviation
$Y_{P\theta}$	Pilot describing function for pilot control action on attitude
Z_u	Vertical acceleration per unit forward velocity $Z_u = \frac{\rho SU}{m}(-C_L - C_{L_u})$
Z_w, $(Z\alpha)$	Heave damping; vertical acceleration per unit vertical velocity (angle of attack); $Z_\alpha = U_o Z_w \quad ; \quad Z_w = \frac{\rho SU}{2m}(-C_{L_\alpha} - C_D)$

Z_δ	Vertical acceleration per unit control surface deflection $Z_\delta = \frac{\rho S U^2}{2m} \left(-C_{L_\delta}\right)$
α	Angle of attack
α_A	Aerodynamic angle of attack, $(w - w_g)/U_o$
α_I	Inertial angle of attack, w/U_o
β	Sideslip angle, v/U_o
γ	Flight path angle
γ_o	Selected flight path angle, Fig. 22
δ	Generic control (elevator, horizontal tail, etc.) surface deflection
δ_a	Aileron deflection
δ_{BF}	Body flap deflection
δ_{BFC}	Body flap controller
δ_e	Elevator deflection
δ_{e_p}	Pilot command input
δ_{PED}	Rudder pedal deflection
δ_{RHC}	Rotational hand controller deflection
δ_r	Rudder deflection
δ_{SB}	Speed brake
δ_{SBC}	Speed brake controller
δ_T	Throttle deflection
ΔX_f	Distance traveled in flare
$\Delta \ell_p$	Distance between pilot and ICR, positive for pilot forward
ε_v	Visual angle error

ζ	Damping ratio
ζ_{sp}	Short period damping ratio
θ	Pitch attitude (perturbation)
$\dot{\theta}$	Pitch attitude rate
θ_c	Attitude Command
θ_e	Attitude Error
ρ	Atmospheric Density; coherence function (Eq. 7)
σ	Real component of complex variable, s
τ	Time delay
τ_M	Delay margin, ϕ_M/ω_c
τ_p	Pilot's time delay
Φ, ϕ	Bank Angle
$\Phi_{mm}(\omega)$	Power spectral density functions
$\Phi_{mn}(j\omega)$	Cross-spectral density functions
ϕ_M	Phase Margin
Ψ, Θ, Φ	Euler angles to aircraft body axes (heading, pitch, roll sequence)
ω	Imaginary component of complex variable, s
ω_c	Crossover Frequency
ω_{c_a}	Crossover frequency of amplitude ratio asymptote
ω_{min}	Theoretical lower bound on an identified frequency response, $2\Pi/T_{RUN}$
ω_n	Natural frequency
ω_{SP}	Short period frequency

ACRONYMS AND ABBREVIATIONS

ACIP	Aerodynamic Coefficient Identification Package
ADI	Attitude director instrument
ADS	Air data system
AFFTC	Air Force Flight Test Center
AGL	Above ground level
ALT	Approach and Landing Test
AMI	Shuttle display (α, A_x, M, V)
APU	Auxiliary power unit
AR	Aspect ratio
ARC	Ames Research Center
AVVI	Shuttle display ($\ddot{h}$, $\dot{h}$, h)
BET	Best estimated trajectory
BFCS	Backup flight control system
CCIT	Cross coupled instability task
CHPR	Cooper Harper Pilot Rating
CSS	Control stick steering
CTT	Critical task tester
DAP	Digital autopilot
DFA	Describing function analysis
DFI	Developmental flight instrumentation
DFRF	Dryden Flight Research Facility
EPR	Eye-point-of-regard
FAR	Federal Air Regulations
FBW	Fly-by-wire

FCS	Flight control system
FD	Flight director
FREDA	Frequency domain analysis (computer program)
FSAA	Flight simulator for advanced aircraft
FSL	Flight Simulation Laboratory
FWD	Forward
GPC	General purpose computer
HAC	Heading alignment cylinder
HSI	Heading situation indicator
HUD	Head-up display
Hz	Hertz
ICR	Instantaneous center of rotation for elevator inputs
IMU	Inertial measurement unit
JSC	Johnson Space Center
KEAS	Knots equivalent airspeed
LAHOS	Landing and Approach Higher Order System
LOES	Lower order equivalent system
LRC	Langley Research Center
MMLE	Modified maximum likelihood estimator
MPDB	Master products data base
NIPIP	Non-intrusive parameter identification program
NLR	National Aerospace Laboratory (the Netherlands)
OEX	Orbiter experiment
OFT	Orbiter Flight Test
OFQ	Flying qualities and flight control system design criteria experiment
OI	Operational instrumentation

PCM	Pulse code modulation
PIO	Pilot induced oscillation
PTI	Programmed test input
RGA	Rate gyro assembly
RHC	Rotational hand controller
RSS	Relaxed static stability
SMS	Shuttle Mission Simulator
STA	Shuttle training aircraft
STI	Systems Technology, Inc.
STS	Space Transporation System
TAEM	Terminal area energy management
TIFS	Total Inflight Simulator
TRFN	STI transfer function computer program
USAM	STI unified servo analysis method computer program
VMS	Vertical Motion Simulator

SECTION I

INTRODUCTION

This study is a continuation of work initiated under Contracts NAS4-2834 and NAS4-2940, Space Shuttle Flying Qualities and Flight Control System Criteria Assessment, Phases I and II. It provides continuation and refinement of a program for the Orbiter Experimental Program (OEX) titled Flying Qualities and Flight Control Systems Design Criteria Experiment (OFQ).

Flying qualities criteria for advanced aircraft have been based on many years of experience with civil and military aircraft. For evolutionary designs this experience has provided an orderly and continuous base of data that could be applied to each new design with a modest extrapolation. However, the Space Shuttle combines the characteristics of a spacecraft and aircraft. It is radically different in configuration, operational envelope, and complexity than any vehicle flown before. It is a highly augmented, fly-by-wire vehicle whose control system design preceded by several years those of current military aircraft. Consequently, large extrapolations had to be made to establish handling qualities and flight control system design criteria for the atmospheric flight phases of the Shuttle mission. These criteria are based primarily on Shuttle-specific simulations and on experience with high performance aircraft; however, because the Space Shuttle is a large departure from past experience, much uncertainty has existed as to the validity and application of existing criteria.

The purpose of this continuing effort is to define an effective program of flying qualities and flight control system design criteria experiments (OFQ). The first phase effort, documented in Ref. 1, was devoted to review of existing flying quality and flight control system specification and criteria; review of Shuttle experimental and flight data; identification of specification shortcomings; and preparation of a preliminary OEX approach to produce the optimum use of flight data to develop modified flying qualities criteria for Space Shuttle craft in general.

The Phase I investigation identified several likely problem areas to be addressed in the OEX plan. First, mismatch of Shuttle specification pitch rate response boundaries (and Shuttle response) with available flying qualities data raised the question of whether the specification response boundaries are misplaced or whether the available data base is inadequate for highly augmented relaxed static stability aircraft. The specification boundaries also appeared to allow excessive pitch and roll rate response dead time. Second, comparison of Shuttle characteristics with other criteria, guides, etc., tended to indicate it exhibited excessive longitudinal and lateral effective time delays. This would lower the effective vehicle bandwidth and then reduce pilot-vehicle and autopilot-vehicle attainable closed-loop bandwidth in rolling and path control functions. It would also be expected to produce a tendency for PIO under high stress, precise control situations. Other likely problem areas concerned pilot location effects and hand controller characteristics. While well ahead of the c.g., the pilot is aft of the center of instantaneous rotation for longitudinal control inputs. This location has consequences on longitudinal path control (possibly quite unfavorable for precise control situation) and lateral acceleration at the pilot station. The rotational hand controller (RHC) displacement/force/electrical command, combined characteristics possibly result in larger pilot control latencies (due to near isotonic properties). This can also effect the control bandwidth and contribute to control difficulties in urgent tasks. Finally, the Phase I effort indicated possible problems concerning off nominal cases of critical aerodynamics variation sets, trim extremes, and reduced surface rates.

The Phase II investigation (Ref. 2) continued the review and analysis of applicable experimental and Shuttle flight data and provided further definition of the Orbiter Flying Qualities Experiment (OFQ) Plan. In particular, the influence of "superaugmentation" on vehicle handling characteristics was continued. It was found that the Shuttle qualifies as a superaugmented vehicle and the Shuttle specification pitch rate response boundaries may be appropriate for this class of vehicle. Further, superaugmented aircraft have unconventional attitude/path

response characteristics and lack speed stability. Review of STS-1-4 crew qualitative assessments indicated flying qualities to be adequate at high altitude and speed but support the unconventional, and possibly marginal, flying qualities in terminal control (preflare, shallow glide, and final flare).

The OFQ plan was further refined to address the above superaugmentation considerations and special conditions of Shuttle flights which require a somewhat unconventional, indirect, experimentation approach. The indirect approach consists of inflight experiments combined with a correlated research simulation program. The unconventional features of the approach is the use of non-intrusive flight measurements for effective vehicle and pilot strategy (model) identification. These flight measurements are then used to validate simulations for ground experiment programs involving critical flight situations not likely to be permitted (or encountered) on Shuttle flights.

The purposes of this Phase III study encompass continued analysis of Shuttle flight data, conduct of supportive analytic and simulation efforts, and further refinement of the OFQ plan. A major portion of the effort has been devoted to exploring the crucial, but unperfected, flight data measurement and reduction techniques required for the non-intrusive experiment approach. This is documented in Section II which encompasses an overview of currently available flight data, identification of the effective augmented vehicle from the flight data, pilot technique identification and modeling, and, finally, a summary of flight data problems and recommendations for the OFQ experiment.

Section III continues the Ref. 2 summary of crew qualitative assessments and presents comments on the STS-5 and 6 entry flying characteristics gleaned from systems debriefings and associated press releases. A second subsection outlines considerations which led to a revised questionnaire for crew in-depth debriefing. The revised questionnaire is presented in Appendix B.

A joint STI/DFRF preliminary experiment performed to quantify the influence of Shuttle RHC characteristics on pilot latency is described

in Section IV. Results of this simple experiment lead to the conclusion that the Shuttle RHC configuration and force/displacement characteristics do increase the pilot's neuromuscular time delay.

Overall conclusions and OFQ recommendations are summarized in Section V.

SECTION II

PILOT/VEHICLE IDENTIFICATION FROM FLIGHT DATA

A. OVERVIEW OF FLIGHT DATA ANALYSIS

1. Flight Data Analysis Goals

Three primary goals guided the analysis of flight data in Phase III:

- Identification of the Effective Augmented Vehicle

  While there has been extensive effort to identify the aerodynamic coefficients of the Shuttle airframe from flight data, there appears to have been no effort to similarly identify the effective vehicle, as seen by the pilot, which is dominated by the flight control system. This activity is important to verify analytical models developed in Phase II (e.g., the super-augmented pitch response). Furthermore, a well defined controlled element model is necessary for the second goal -- pilot technique identification.

- Identification of Piloting Technique

  Identification of piloting technique is more difficult because of technique variations among pilots, pilot remnant and uncertainty about cues.

- Refinement of OFQ Procedures

  In addition to obtaining quantitative definition of the vehicle and pilot, refinement and verification of the identification procedures proposed in Phase II was a primary concern because of the emphasis on non-intrusive techniques.

The OFQ plan as developed in Phase II placed first priority on the approach and landing, from the termination of the HAC turn through touchdown (see Fig. 1). The Phase III flight data analysis has involved all flight segments except the steep glide.

2. Shuttle Flight Data Sources

The primary source of data for the Phase III flight data analysis were the computer files available at DFRF for use with the Modified

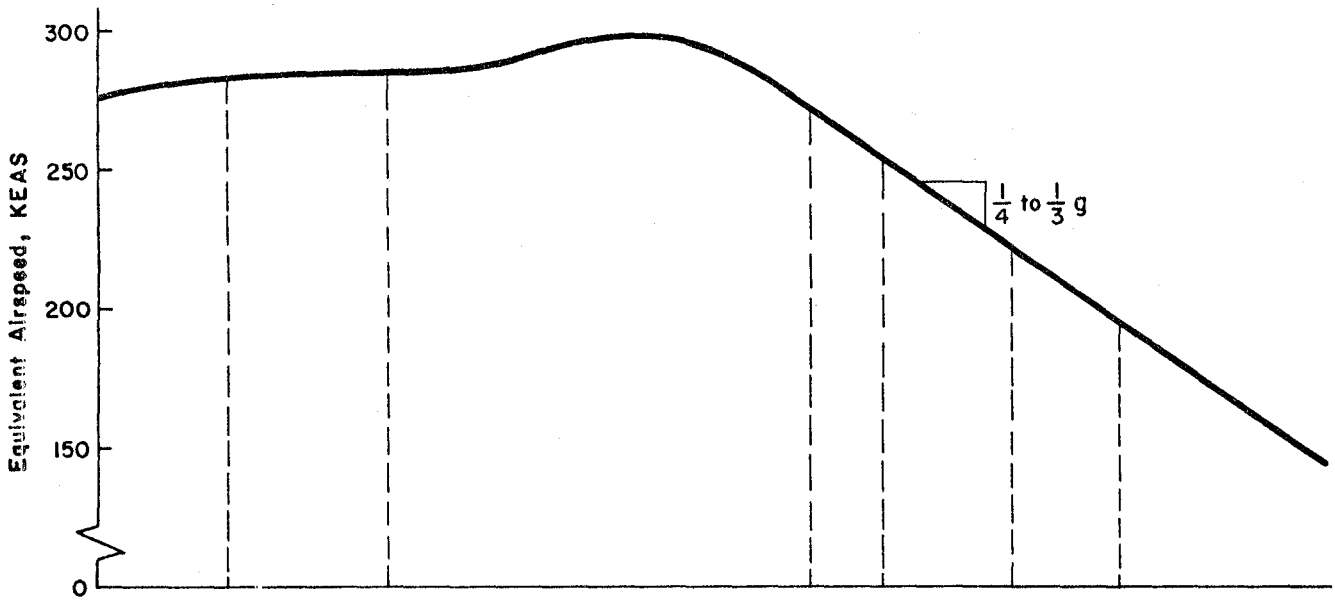

b) Equivalent Airspeed Variation

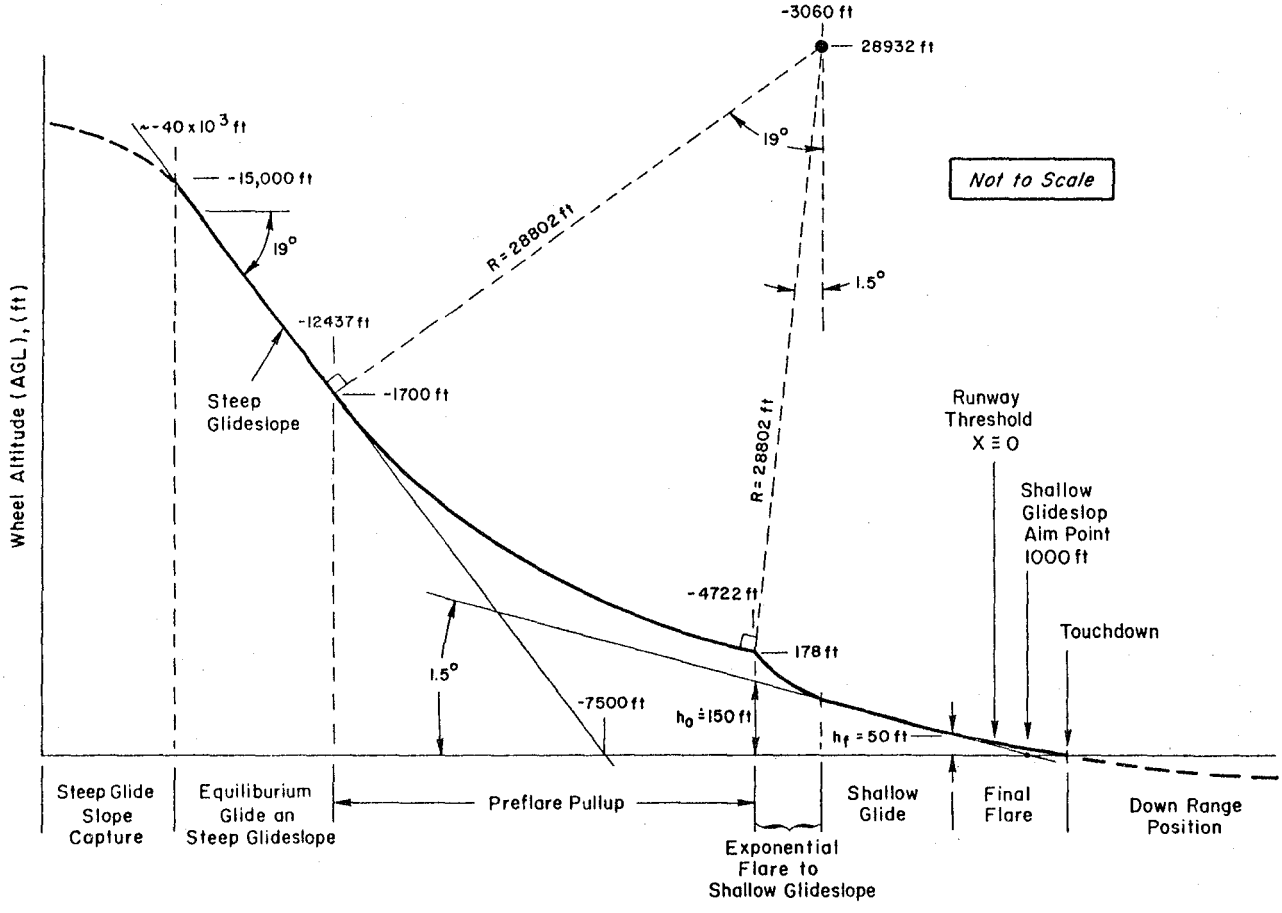

a) Trajectory

Figure 1. Shuttle Approach and Landing
(Nominal Characteristics)

Maximum Likelihood Estimator (MMLE) program. These files exist for all Shuttle flights to date, and have been used extensively for extraction of airframe aerodynamic coefficients. These files may be made available as local files on the DFRF Cyber computer and have been transmitted over telephone lines to the STI PDP-11 computer. Significant effort was required to develop this data transfer procedure; but it is thought to be considerably cheaper, faster, and simpler than physically transferring magnetic tapes. While the MMLE files were set up for airframe aerodynamic identification, they are usable for preliminary Flight Control System (FCS) and flying qualities studies. However, it will be necessary to augment the data available and resolve certain problems before further progress can be made. Specific problems and data needs will be detailed in Subsection D.

Two other sources of flight data were also investigated: the Master Products Data Base (MPDB) at NASA JSC and the Best Estimated Trajectories (BET) computed at NASA LRC. To date, it has not been possible to use these sources. The problems and suggested solutions will also be discussed in Subsection D.

Efforts to obtain the STS-4 data from the DFRF MMLE file were begun in Phase II. However, transfer of the data over phone lines to the STI computer proved more difficult than expected and was not completed until the Phase III effort had begun. It was decided to continue with the STS-4 data since use of data from any later flight would require additional effort and no unusual events occurred in the STS-5 flight -- the only additional flight at the start of the analysis. Also, the most relevant pilot commentary is available for STS-4.

3. Attitude Control Time Histories

Five time histories: Rotational Hand Controller (RHC) deflections, pitch rate, angle-of-attack, pitch attitude, and normal acceleration are shown in Fig. 2 for the preflare through touchdown region of the STS-4 landing. These traces include the variables pertinent to inner loop (attitude) control. To consider outer loop (path) control, sinkrate and altitude are required; however, because of data complications this is

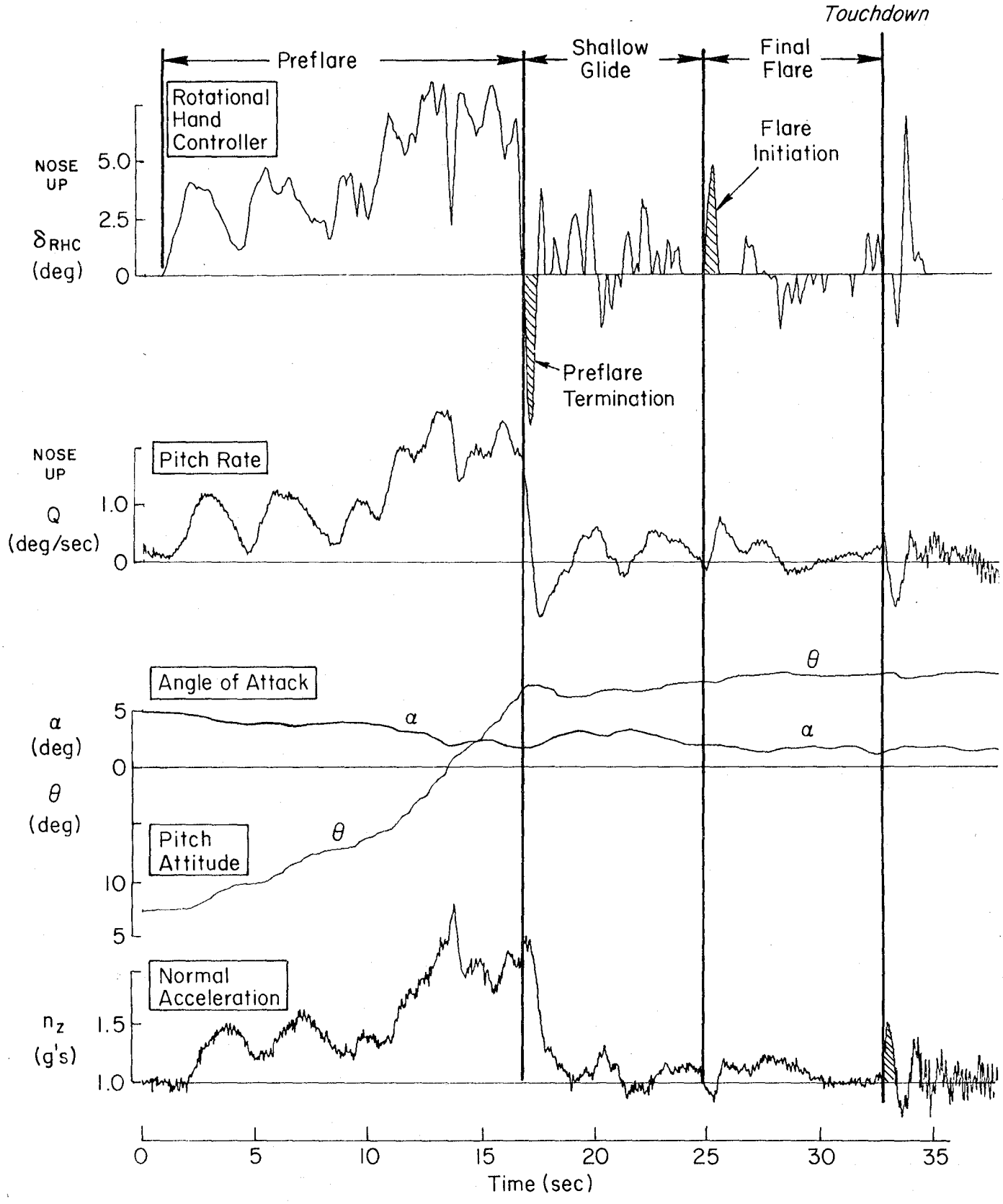

Figure 2. Attitude Control Time Histories
STS-4

deferred until Subsection C. The partitioning of the time histories into preflare, shallow glide, and final flare segments is based, in part, on direct examination of the time histories shown; but also on additional analyses such as the altitude/sinkrate phase plane analysis to be discussed in Subsection D. The transitions between preflare and shallow glide, and between the shallow glide and final flare, may each be associated with a discrete RHC pulse (crosshatched in Fig. 2).

Indications of piloting technique variations among the flight segments may be seen from the traces; in particular the RHC trace. During the preflare maneuver, the RHC trace indicates an initial applied acceleration command followed by a higher command level. The transition from the steep glide to the preflare resulted in a near-neutral stability oscillation in the pilot/vehicle system with a natural frequency of approximately 2 rad/sec. This oscillation will be considered further in Subsection C.

RHC input and pitch response in the preflare task indicates fairly continuous pilot control action. However, in the shallow glide and final flare, the RHC input has a different character and consists of a series of pulses which are either positive or negative and (unlike Q) do not pass through zero. This activity ceased for slightly less than a second before and after the discrete nose-up pulse which initiated the flare, then a pulsive tracking activity continued from preflare to touchdown. Pulsive pilot output is often associated with difficult controlled elements requiring low frequency lead (Refs. 3 and 4) and is currently being investigated for superaugmented configurations in a related study (Ref. 5).

B. IDENTIFICATION OF THE EFFECTIVE AUGMENTED VEHICLE FROM FLIGHT DATA

Because of the dominant effect of the FCS on the Shuttle's pitch response, identification of airframe characteritics alone is not adequate to characterize the effective vehicle seen by the pilot. The superaugmentation model was developed in Phases I and II to deal with this situation. In Phase III an effort has been made to verify this

model from Shuttle flight data. This section will begin with a review of superaugmentation theory to examine the Low Order Equivalent System (LOES) form implied for the pitch rate transfer function q/q_c and also to consider artifacts of the approximation which may contribute to anomalies in identification. With this theoretical background, identification of the Shuttle q/δ_{RHC} transfer function using spectral methods and the Nonintrusive Parameter Identification Program (NIPIP), will be discussed.

1. The Superaugmentation Model

The simplified block diagram (Fig. 3a) shows a representative pitch rate based system appropriate to superaugmented aircraft such as the Shuttle. The basic fedback loop consists of pitch rate measured with a rate gyro fedback to equalization consisting of a lead with time constant T_q and a lag which is a pure integrator. In the Space Shuttle this equalization is created by a δ_e feedback through a first order lag around the elevator servo (Ref. 1). The forward loop contains the actuator, bending mode filters, and other elements which contribute to effective high frequency lag in the system. Provision is also made for turn compensation so that the pilot is not required to maintain RHC pitch deflection in a steady turn.

Perhaps the best way to view the superaugmentation approximation is through the use of the Bode root locus plot. The Bode magnitude plot is sketched in Fig. 3b for the open loop q/q_e transfer function of a near-neutral airframe. This plot is particularly useful for visualizing the important relationship between the dynamics of a relaxed static stability (RSS) airframe (e.g., the Shuttle) and a superaugmented flight control system. The effects of RSS are evidenced by the real short period poles $1/T_{sp_1}$ (stable) and $1/T_{sp_2}$ (unstable). The phugoid appears somewhat more conventionally as a low frequency complex pair and the airframe attitude zeroes $1/T_{\theta_1}$ and $1/T_{\theta_2}$ are relatively uneffected by relaxation of static stability.

The effects of the flight control system design are contained in the equalization zero $1/T_q$ and the asymptotic crossover frequency ω_{c_a} which

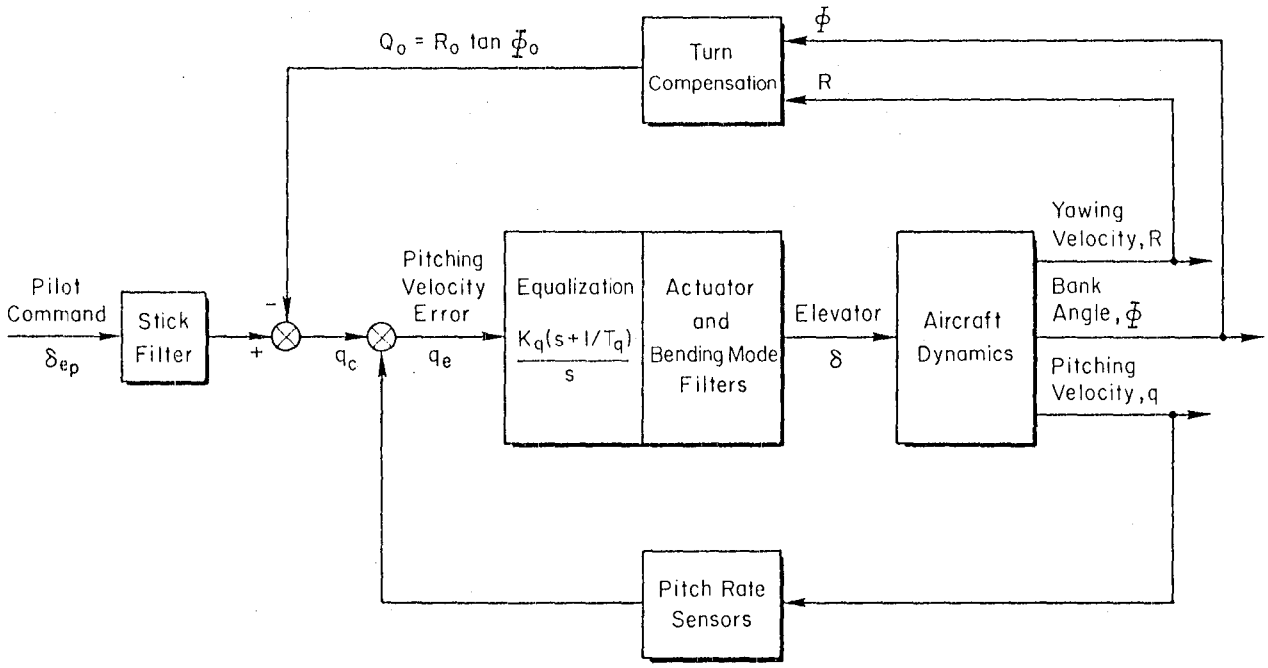

a) Typical Pitch SAS For Superaugmented Aircraft

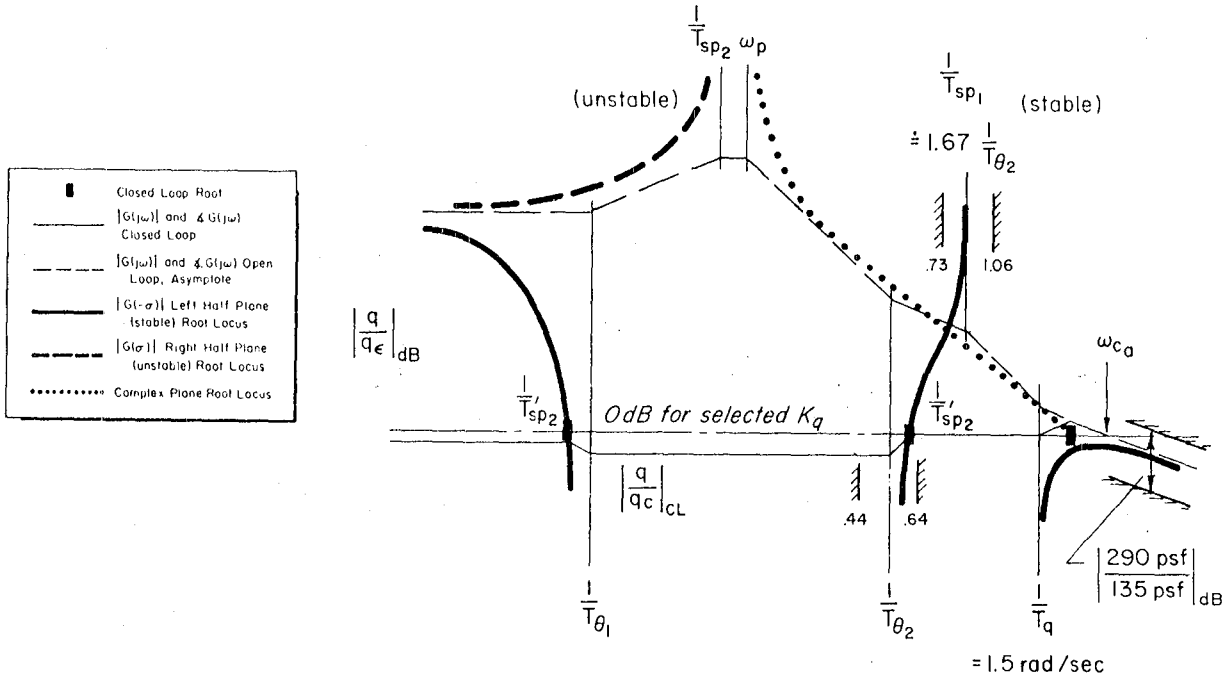

b) Bode Root Locus Sketch, Superaugmented FCS Shuttle Preflare To Touchdown

Figure 3. Superaugmentation Concept

is set by the selection of the loop gain K_q. It may be seen that the crossover region is defined primarily by the FCS parameters. Thus, to a first approximation, the dominant closed loop root is determined by $1/T_q$ and ω_{c_a}. Asymptotic approximations in the crossover region lead to the superaugmentation pitch attitude relation (Ref. 2):

$$\frac{q}{q_c} \doteq \frac{K(1/T_q)e^{-\tau s}}{[\zeta,\ \omega_n]} \tag{1a}$$

$$\zeta \doteq \frac{1}{2}\sqrt{T_q \omega_{c_a}} \tag{1b}$$

$$\omega_n \doteq \sqrt{\omega_{c_a}/T_q} \tag{1c}$$

$$K \doteq \omega_n^2/T_q \tag{1d}$$

The adequacy of these approximations is determined by the behavior of the airframe roots as the pitch rate loop is closed which may be seen in the root loci (heavy lines) in Fig. 3b. The unstable short period root $1/T_{sp_2}$ migrates from the right half plane through the origin and into the left half plane to approach $1/T_{\theta_1}$ and form an approximately canceling dipole. The stable short period root $1/T_{sp_1}$ is driven into $1/T_{\theta_2}$; a situation which will occur whenever $1/T_q > 1/T_{sp_1}$. The adequacy of the superaugmentation approximation shown in Eqs. 1a-d) is dependent on the extent to which $1/T'_{sp_1}$ and $1/T_{\theta_2}$ cancel. The behavior of this dipole, which is fundamental to the superaugmentation concept, is determined by basic RSS airframe characteristics.

The dimensional aerodynamic coefficients which determine the values of $1/T_{sp_1}$ and $1/T_{\theta_2}$ are functions of dynamic pressure $\bar{q}$ which decreases from 290 to 135 psf from preflare through touchdown. However, they are essentially independent of Mach number, which varies from 0.48 to 0.31 in this region of essentially incompressible flow. The high frequency attitude numerator $1/T_{\theta_2}$ may be approximated as

$$\frac{1}{T_{\theta_2}} \doteq -Z_w + M_w \frac{Z_{\delta_e}}{M_{\delta_e}}$$

$$\doteq -Z_w$$

$$\doteq \frac{\rho SU}{2m} C_{L_\alpha} \qquad (4)$$

This approximation is generally adequate for conventional aircraft and even better for RSS aircraft with low values of M_w. Based on this approximation, $1/T_{\theta_2}$ decreases from approximately 0.64 to 0.44 rad/sec at touchdown as indicated in Fig. 3b.

Estimation of the stable short period root requires knowledge of the Shuttle static margin which may be obtained from a 'C_L - C_M' plot such as shown for typical conditions in Fig. 4. Flexibility effects are negligible in this region and the static margin is

$$\frac{dC_M}{dC_L} \doteq 3.7\%\bar{c} \text{ unstable}$$

The maneuver margin is:

$$\frac{dC_M}{dC_L} - \frac{\rho S\bar{c}}{4m} C_{M_q} \doteq 0.9\%\bar{c} \text{ unstable}$$

For an airframe with near neutral maneuver margin, the dipole ratio $(1/T_{sp_1})/(1/T_{\theta_2})$ may be developed in terms of C_{M_q} and C_{L_α} as

$$\frac{1/T_{sp_1}}{1/T_{\theta_2}} \doteq 1 + \frac{M_q}{Z_w}$$

$$\doteq 1 - \frac{1}{2}\left(\frac{\bar{c}}{K_y}\right)^2 \frac{C_{M_q}}{C_{L_\alpha}}$$

$$\doteq 1.67 \qquad \text{(Shuttle)} \qquad (2)$$

Thus the pole and zero maintain a constant and fairly close relationship throughout the region of interest. Several conclusions may be drawn regarding the dipole's effect. The upper end of the airframe

MACH NO.	DEL BF	DEL SB	XCG (IN)	ZCG (IN)	QBAR1-PSF	QBAR2-PSF
0.400	-11.700	25.000	1098.630	375.000	0.0	300.000

QBAR1 = SOLID QBAR2 = DASH

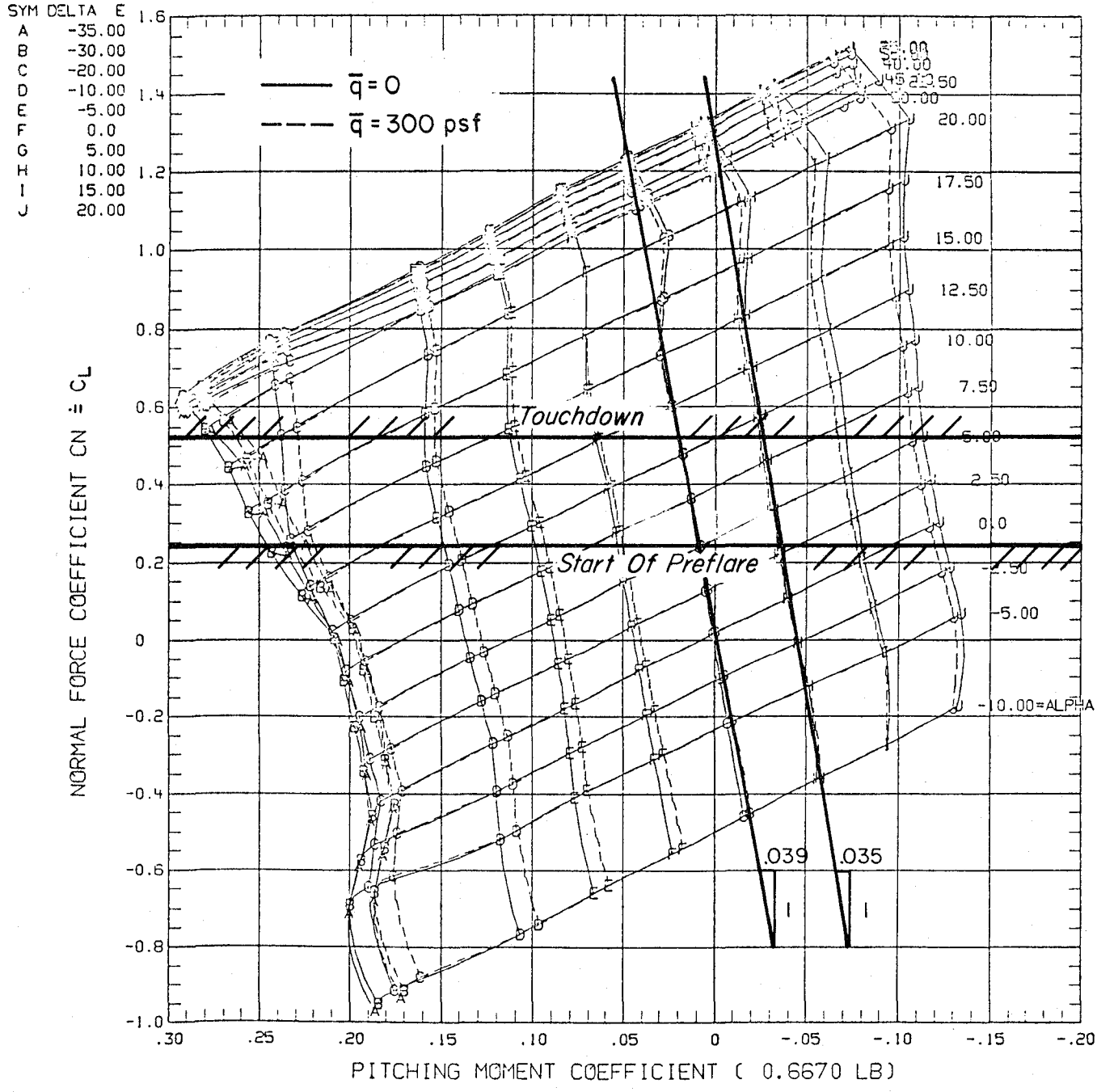

Figure 4. Shuttle Airframe Longitudinal Stability, Flexible-Approach and Landing (Adapted from Ref. 6)

dynamics region is set by the high value of $1/T_{sp_1}$, which is about 1 rad/sec and thus less than $1/T_q$ = 1.5 rad/sec for the Shuttle. The pole and zero have a constant ratio of 1.67, thus even without closure of the $q \rightarrow \delta_e$ loop there is a tendency for dipole cancellation which is increased when the loop is closed. It should be noted for later reference that on the Shuttle there is a first order filter (the 'ELERROR' filter) in the region of the high frequency dipole. The filter zero is near $1/T_{\theta_2}$ and the filter pole is close to $1/T_{sp_1}$, thus producing a lead-lag which increases the phase margin in the crossover region.

The airframe effects are thus limited to higher order artifacts in the superagumented pitch response which is effectively determined by the characteristics of the FCS as implied by Eqs. 1a-d. For the Shuttle, $1/T_q$ is set by the scheduling (GTRE_COMP) in the 'ELFBK' filter as

$$1/T_q = 1.5 \text{ rad/sec} \qquad M \leq 3$$

The variation of the crossover frequency is more involved and is the one area where an airframe characteristic, elevator effectiveness, has a direct effect. The asymptotic crossover frequency is:

$$\omega_{c_a} \doteq -M_{\delta_e} K_q = \left(\frac{S\bar{c}C_{M_{\delta_e}}}{I_y}\right) \bar{q} \, K_q \tag{3}$$

for the Shuttle situation in which $\omega_{c_a} > 1/T_q$. The scheduling of K_q is more complex than for T_q and provides an opportunity to examine the gain scheduling problem for one of the few operational superaugmented aircraft. The basic scheduling (GDQ_COMP) is shown in the block diagram of Fig. 5 and indicates that

$$K_q \propto \frac{f(M)}{\sqrt{\bar{q}}}. \tag{4}$$

It should be noted that none of the relevant nondimensional aerodynamic coefficients are functions of Mach number in this region, thus the

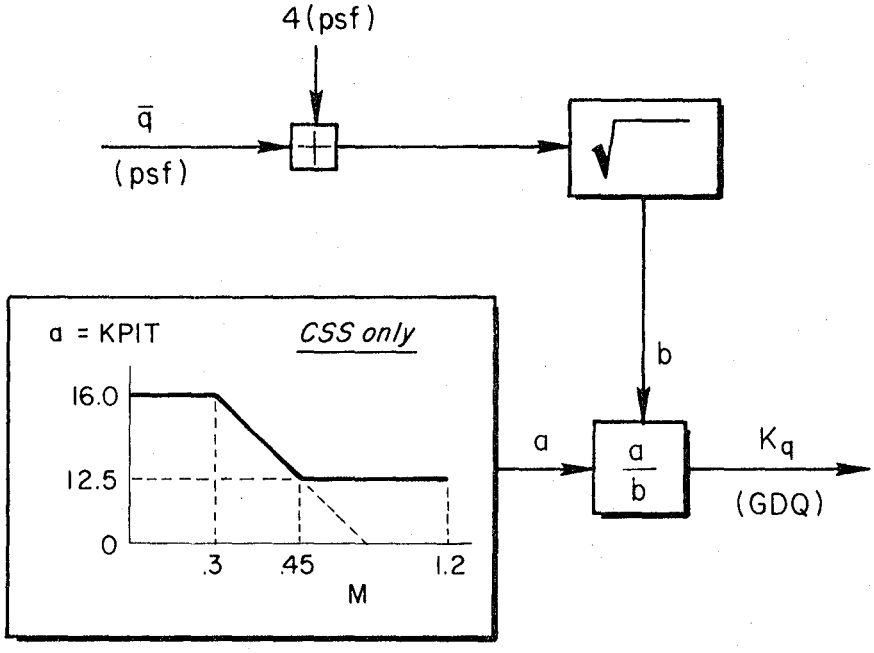

Figure 5. Schedule for Pitch Rate Loop Gain, K_q (GDQ_COMP)

rationale for the Mach number schedule is of interest. At these low altitudes (below 2,000 ft) where density and acoustic velocity are roughly constant, the Mach number schedule effectively performs the function of an additional dynamic pressure schedule. When approximate calculations of this effect are made the resulting crossover frequency schedule is

$$\omega_{c_a} \doteq 0.177(\sqrt{\bar{q}} - 0.026\ \bar{q})\ \text{rad/sec} \qquad (5)$$

Figure 6 shows this ω_{c_a} variation from the start of preflare through touchdown, compared to a fixed crossover schedule (i.e., $K_q \propto \bar{q}^{-1}$) and a crossover frequency schedule proportional to the square root of $\bar{q}$. In the flights of the Approach and Landing Test (ALT vehicle) K_q was scheduled inversely proportional to dynamic pressure Ref. 7, p. 245 thus giving an effectively constant crossover frequency. This has been modified to the present OFT schedule primarily because of problems with elevon saturation at low speeds with the original schedule.

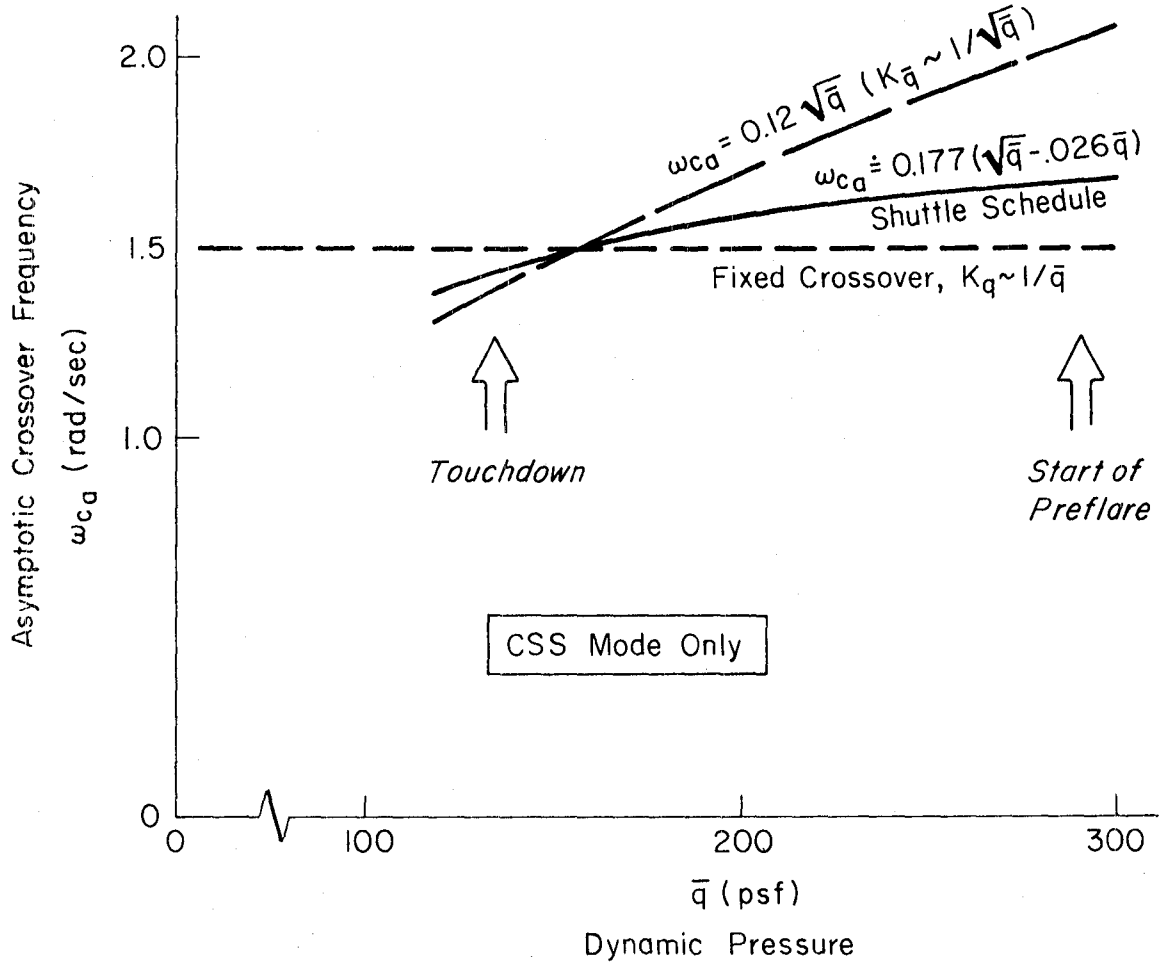

Figure 6. Effective Pitch Gain Scheduling of Shuttle

2. Possible Methods and Inputs for Effective Vehicle Identification

Several identification methods for the effective vehicle are available. First, spectral analysis methods may be used, in particular the use of the fast Fourier transform implemented in programs such as the STI Frequency Domain Analysis program (FREDA), Ref. 8. Secondly, time domain least squares estimation routines are available, such as the STI Non-Intrusive Parameter Identification Procedure (NIPIP), Ref. 9. There are, in addition, the airframe parameter identification programs (e.g., MMLE) extended to augmented vehicles by various means. One approach has

been to assume a conventional linear aircraft model and identify effective stability derivatives; however, this approach has the disadvantage of not identifying unusual effective derivatives (e.g., M_θ) unless these effective derivatives are accounted for in the original model form. This problem may be avoided by structuring the model in terms of the effective poles and zeros of the vehicle response. Some rational basis (e.g., superaugmentation theory) for selecting the number of and constraints on poles and zeros would still be required.

All of the above identification methods require some form of input to the system and there are a number of possibilities. Manual pilot activity accompanying normal flight operations is the simplest, and in the case of the Shuttle OFQ may be the only pilot input available. A sum of sine waves, on the other hand, has theoretical properties which are particularly advantageous for obtaining good signal-to-noise ratios. The frequency sweep, which begins with a low frequency quasi-sinusoidal input and increases to higher and higher frequencies, is particularly useful because it is easily generated by pilots and has a reasonably flat power spectrum. Finally, pulse train inputs can be tailored to have desirable power spectral characteristics. For the OFQ it may ultimately be possible to tailor existing Program Test Inputs (PTI), presently used for airframe identification, to form an approximation of a sum of sine waves disturbance for pilot tracking experiments.

For the Phase III work, both the FREDA and NIPIP procedures have been used on data with normal pilot inputs and will be discussed in the following sections.

3. Identification of Superaugmented q/δ_{RHC} Using Spectral Methods

The spectral identification of the q/δ_{RHC} describing function requires the δ_{RHC} and q time series (Fig. 2). The FREDA program obtains the spectral density distributions $\Phi_{\delta\delta}$ and Φ_{qq} and cross spectral $\Phi_{q\delta}$ by direct Fourier transform of the time series using the Wiener-Khinchin relationship, Ref. 10. The q/δ_{RHC} describing function is then given by

$$\frac{q}{\delta_{RHC}}(j\omega) = \frac{\Phi_{q\delta}(j\omega)}{\Phi_{\delta\delta}(\omega)} \qquad (6)$$

The FREDA program produces discrete magnitude and phase angle pairs for q/δ_{RHC}, $\Phi_{\delta\delta}$ and Φ_{qq}. A coherence function

$$\rho^2(\omega) = \frac{|\Phi_{q\delta}(j\omega)|^2}{\Phi_{qq}(\omega)\Phi_{\delta\delta}(\omega)} \tag{7}$$

is also computed and gives a measure of the degree to which the output is linearly correlated with the input. A ρ^2 of zero implies no correlation and a ρ^2 of 1 indicates perfect correlation between output and input. For vehicle dynamic identification, ρ^2 values between 0.8 and 0.9 are generally indicative of meaningful identification.

Implicit in the use of the spectral procedure is the assumption that the describing function will be time invariant. Because of the properties of superaugmentation this will be true to a first approximation for q/δ_{RHC} in the region of interest given the fixed value of T_q and the small variation of ω_{c_a} with $\bar{q}$ (Fig. 6). This situation would not occur for an airfame transfer function such as q/δ_e and special accommodation would be required. There are in addition system nonlinearities which could, in principal, compromise the use of FREDA; in particular the PIOS filter and the stick shaping (ESHAPE). During the STS-4 landing, the PIOS filter was active only when the commander executed the preflare termination. To examine possible PIOS effects, FREDA runs were made over the entire period from the start of preflare to touchdown and for subsegments excluding the PIOS activity. The above considerations of time varying system parameters and occasional nonlinear events (e.g., PIOS activity) imply a desire for a short identification run length T_{RUN}. On the other hand, maximizing run length is desirable to obtain good low frequency data since the theoretical lower bound on the frequency response ω_{min} is

$$\omega_{min} = 2\pi/T_{RUN} \tag{8}$$

The FREDA output plots for maximum feasible run length (start of preflare to touchdown, T_{RUN} = 30 sec, ω_{min} = 0.2 rad/sec) are shown in Fig. 7. The coherence ρ^2 values are above 0.8 out to approximately

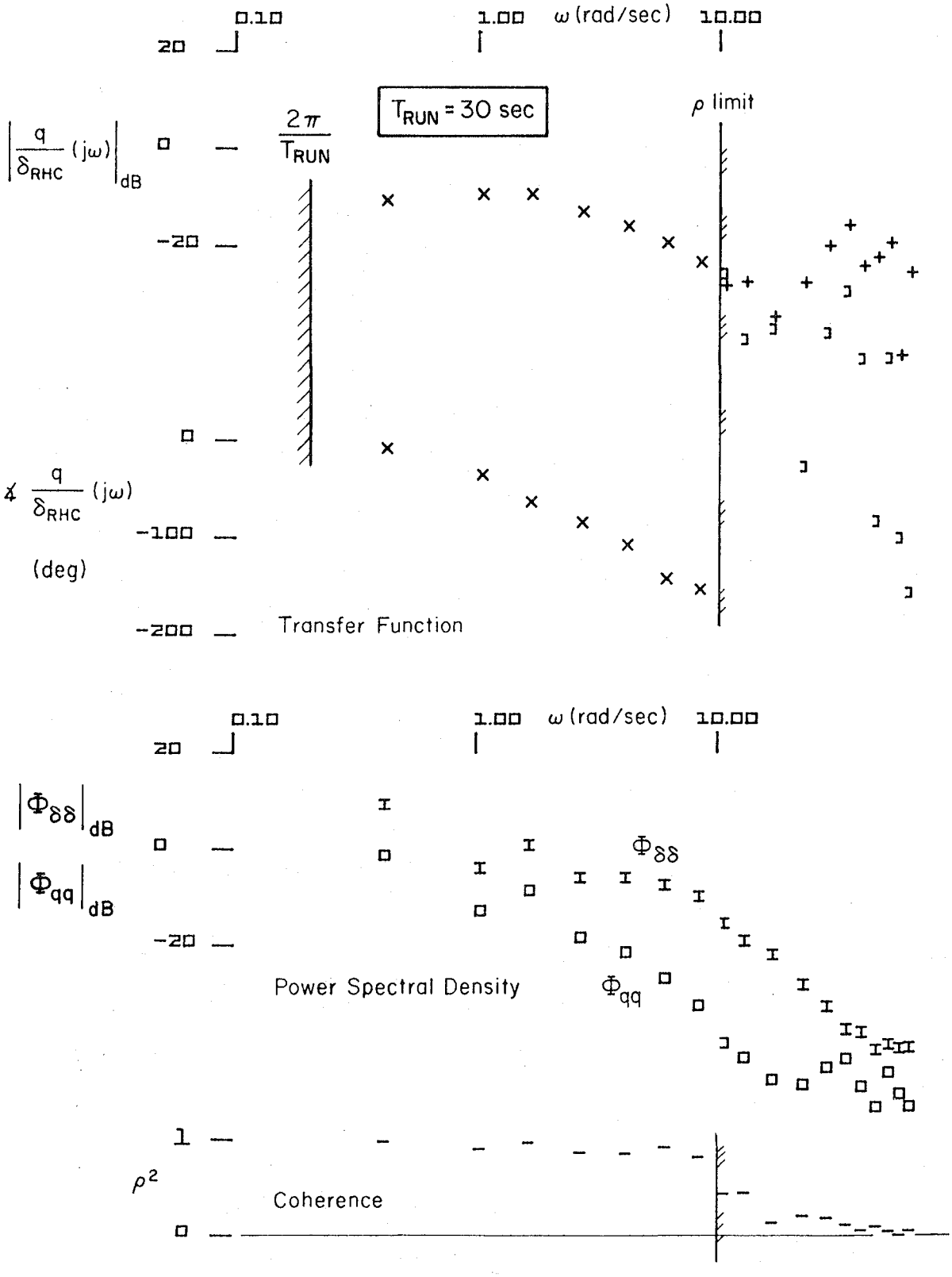

Figure 7. FREDA Output for q/δ_{RHC}
STS-4 Preflare Through Touchdown

10 rad/sec. Above this frequency the coherence decreases and thus 10 rad/sec is taken as limit of validity for the frequency response (the describing function plot symbols are changes when ρ^2 drops below 0.8). This is a very desirable situation which has important implications for the use of non-intrusive procedures in the OFQ, since it indicates that normal pilot RHC activity may be adequate for identification. An indication of the identification potential of the RHC input may be seen in the relatively flat input power spectra $\Phi_{\delta\delta}$ for $1. < \omega < 10.$ rad/sec. Some feeling for this spectra may be obtained by examining the δ_{RHC} trace in Fig. 2 and noting the low frequency trends, especially in the preflare region, combined pulse-like inputs with high frequency content in the shallow glide and final flare which effectively provide a rough approximation to a frequency sweep.

Figure 8 presents the corresponding FREDA output for the shallow glide and final flare starting just after the PIOS activity and terminating just before touchdown. The results are quite consistent with the Fig. 7 data except for the reduction in low frequency data due to the shorter run length (T_{RUN} = 12.0 sec). These results are valuable because they imply usable results may be obtained for T_{RUN} on the order of a flight segment length and they confirm the approximate time invariance of q/δ_{RHC}.

The FREDA program defines the q/δ_{RHC} describing function as a set of discrete magnitude and phase angle points. Definition of the specific parameter values in the superaugmented response form (i.e., the poles and zeroes) requires 'fitting' this form to the FREDA output. This has been done with the Multi-Frequency Parameter identification program (MFP) which provides a weighted least squares fit to the specified response form. For fitting a superaugmented q/δ_{RHC} form, the MFP program was set up to minimize C (see Fig. 9) where

$$C = \sum_{k=1}^{8} w_k^2(j\omega_k)\left|G_{FR}(j\omega_k) - G_{SA}(j\omega_k)\right|^2 \qquad (9)$$

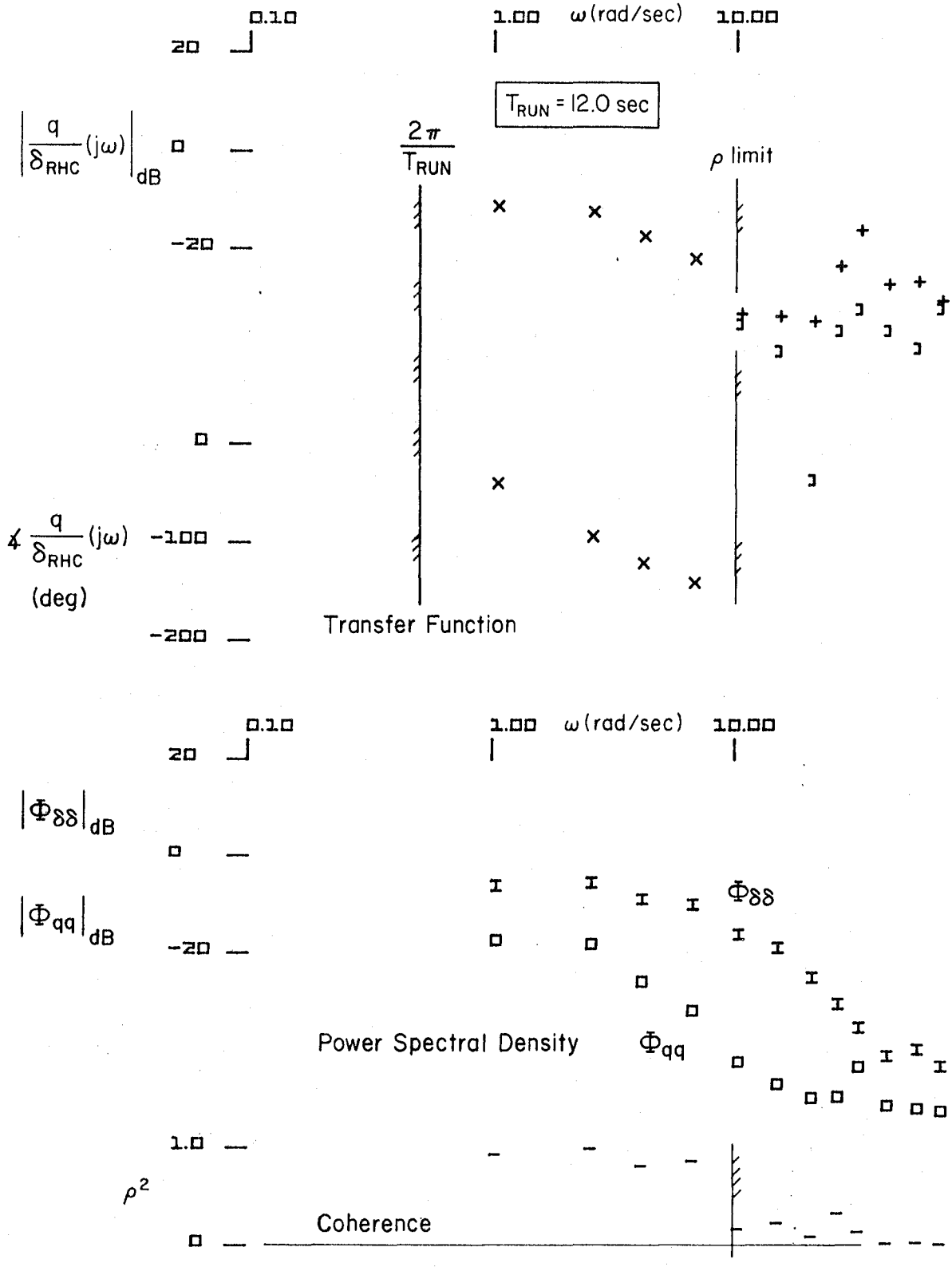

Figure 8. FREDA Output for q/δ_{RHC}, STS-4
Shallow Glide and Final Flare

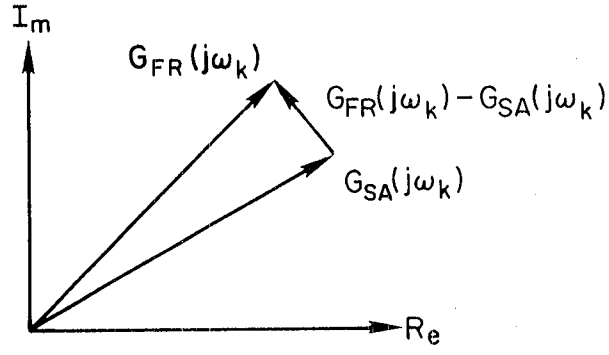

Figure 9. Definition of Cost Function in MFP Program

where

ω_k is the kth matching frequency

w_k is the kth weighting factor

$$G_{SA}(s) = \frac{K(1/T_q)e^{-\tau s}}{[\zeta, \omega_n]} \qquad \text{(superaugmented form)}$$

$$G_{FR}(j\omega_k) = \left|\frac{q}{\delta_{RHC}}(j\omega_k)\right| e^{-\angle q/\delta_{RHC}} \qquad \text{(from FREDA)}$$

The weighting factors were set to

$$w_{k_{dB}} = 20 \log G_{FR}^{-1}(j\omega_k)$$

$$= - G_{FR}(j\omega_k) \text{ dB} \qquad (10)$$

which essentially imposes the same penalty in dB on magnitude mismatches at all frequencies. The fitting operation has been performed both with the lead $1/T_q$ fixed at the Shuttle FCS value ($1/T_q$ = 1.5 rad/sec) and also with the $1/T_q$ free. The two results are shown in Fig. 10a. It may be seen that the two cases are very similar and that both provide a very satisfactory fit. A time domain comparison (Fig. 10b) leads to a similar conclusion.

Table 1 shows a comparison between superaugmentation theory and the values extracted from the STS-4 flight data (both for fixed and free

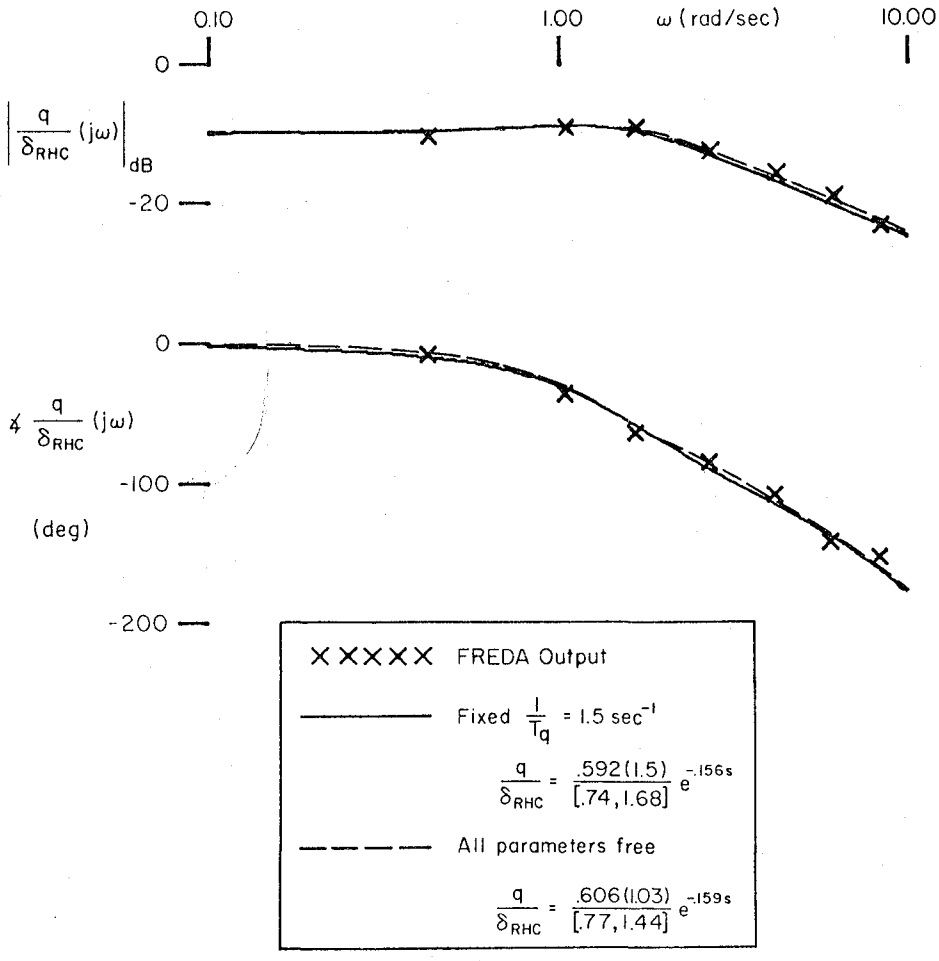

a) Frequency Response Of Fitted Superaugmentation Forms Compared To FREDA Output

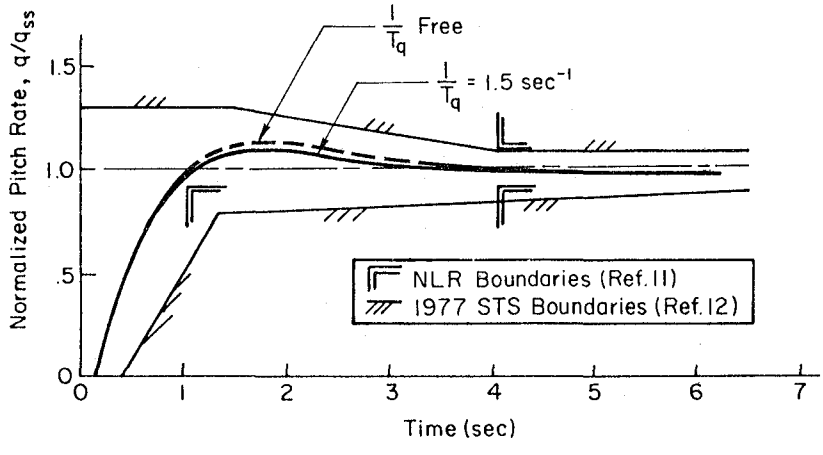

b) Normalized Pitch Rate Response To A δ_{RHC} Step

Figure 10. Comparison of Flight-Derived Effective q/δ_{RHC} with $1/T_q$ Fixed and Free

TABLE 1. COMPARISON OF PARAMETER EXTRACTED FROM STS-4 FLIGHT DATA WITH THE SUPERAUGMENTATION MODEL

PARAMETER	SUPERAUGMENTED MODEL	EXTRACTED FROM STS-4 FLIGHT	
		$1/T_q$ = 1.5 r/s	t/T_q FREE
$q/\delta_{RHC}(0)$ (rad/rad/sec)	0.17	0.31	0.30
$1/T_q$ (rad/sec)	1.5	1.5	1.03
ζ	0.5	0.74	0.77
ω_n (rad/sec)	1.5	1.68	1.44
τ (sec)	0.174	0.156	0.159

numerator time constant) for five q/δ_{RHC} parameters. The first line compares steady state gain values and shows the largest difference of any of the comparisons. The extracted values are approximately 80 percent higher than the estimated values. While the differences have not been resolved, it is presently thought that they may be due to calibration uncertainties in the δ_{RHC} signal. This signal was obtained for the DFRF MMLE file from the Backup Flight Control System (BFCS), which does not contain all of the forward loop elements of the primary system actually used in the STS-4 entry.

The fixed value of flight derived numerator inverse time constant exactly matches the superaugmented model by definition. The extracted value with $1/T_{q_{free}}$ is somewhat lower at 1.03. However, it is still well above the range of values for $1/T_{\theta_2}$ in the identification region (0.44 to 0.64 rad/sec). The values of the damping ratio obtained from flight are approximately 50 percent higher than the superaugmentation theoretical prediction. It is presently felt that the primary cause of the higher in-flight damping ratio, and perhaps also the lower in-flight

value of $1/T_q$, is the 'ELERROR' filter. To a first approximation, the ELERROR filter increases the open loop phase margin in the crossover region which would correspond to the effect of a low value of $1/T_q$. Furthermore, the increased phase margin corresponds to a higher closed loop damping ratio as is seen in the flight extracted results.

The flight extracted values of natural frequency are somewhat higher for the fixed T_q case and somewhat lower for the free T_q case with respect to the theoretical value of 1.5 rad/sec; however, these should be considered in the light of the uncertainty implied by the variation of crossover frequency as shown in Fig. 6. Finally, the flight extracted values of time delay are actually somewhat lower than the value obtained by adding the low frequency phase lag approximates of the forward loop elements (Table 2).

From the standpoint of flight validation of the superaugmentation model, probably the most important issue is whether the attitude zero is really closer to $1/T_q$ than to $1/T_{\theta_2}$. This issue may be addressed by considering an alternative fit with the attitude zero constrained to $1/T_{\theta_2} \doteq 0.50$ rad/sec. Figure 11 shows such a comparison, in terms of asymtotes, between the fits of Fig. 10 and a '$1/T_{\theta_2}$ fit' with ω_n = 1.5 rad/sec. For this alternative fit there is a significant region of

TABLE 2. CONTRIBUTION OF FCS ELEMENTS TO EFFECTIVE TIME DELAY

FCS ELEMENT	EFFECTIVE TIME DELAY (SEC)
Bending Filter	0.039
Smoothing Filter	0.039
Computational Delay	0.046
Actuator	0.050
Total	0.174

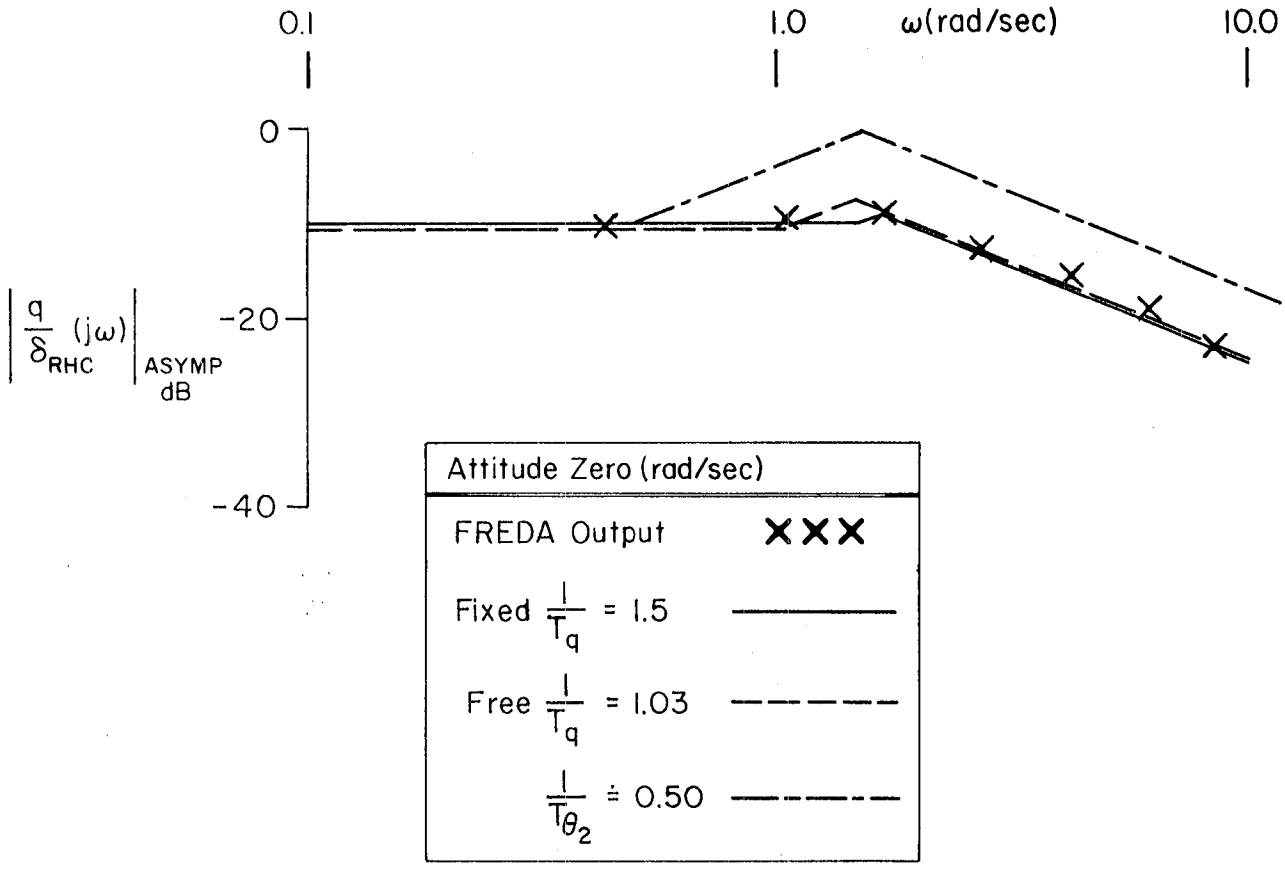

Figure 11. Asymptotic Comparison of $|q/\delta_{RHC}|$ with Three Different Numerator Constraints

+20 dB/decade slope which is inconsistent with the low frequency FREDA points. In this connection it should be noted that these FREDA points are averages of 3 'raw' FFT points and are reliable within the context of this comparison. No adjustments of ω_n would provide a satisfactory '$1/T_{\theta_2}$' fit.

4. Identification of Superaugmented q/δ_{RHC} Using the NIPIP Program

Shuttle vehicle identification has also been performed with the NIPIP program (Ref. 9). This program is a running least squares time domain estimator which was proposed in Phase II as a primary tool for pilot model parameter extraction from Shuttle flight data. However, it may also be used for augmented vehicle identification if a proper

vehicle model structure is employed. Use of NIPIP for this purpose had two primary purposes. First, previous applications of NIPIP to vehicle identification from flight data had been limited and not too successful (Ref. 13). This lack of success is thought to have been due to lack of adequate resolution in the instrumentation system. A second reason for attempting vehicle identification with NIPIP was to test the application of this program to actual Shuttle flight data to obtain confidence in its use for the more difficult pilot identification process.

Figure 12 shows the FREDA data (X's) and the fixed $1/T_q$ fit from Fig. 10 compared to results from NIPIP (O's). The FREDA run was based on the entire region from preflare to touchdown (about 30 sec) and thus the low frequency limit ($2\pi/T_{RUN}$) is lower than for the 7.3 sec NIPIP run. However, in the valid frequency range, the NIPIP result compares quite favorably to the FREDA result.

C. PILOT TECHNIQUE IDENTIFICATION

A major portion of the Phase III work has been devoted to pilot technique identification efforts, both to gain a further understanding of pilot technique and to refine identification procedures for use in the actual OFQ. From this effort a number of data problems and needs have been identified of which altitude and sinkrate problems are the most critical (these will be discussed in detail in Subsection D). The emphasis in the Phase III activity, consistent with the Phase II OEX plan, has been on non-intrusive identification procedures. This is based on the belief that severe constraints on off-nominal Shuttle flight maneuvers must be expected thus placing high priority on methods which can produce useful results from whatever flight data becomes available. Three specific analytical procedures will be discussed in the following section. The first is a simple analysis of the near-neutral closed loop pilot vehicle oscillation which occurred at the initiation of the STS-4 preflare pullup. A value of effective pilot time delay has been extracted from this analysis. The second procedure, the altitude/sinkrate phase plane analysis, produced interesting results and has promise for the OFQ. This procedure has been applied to the shallow

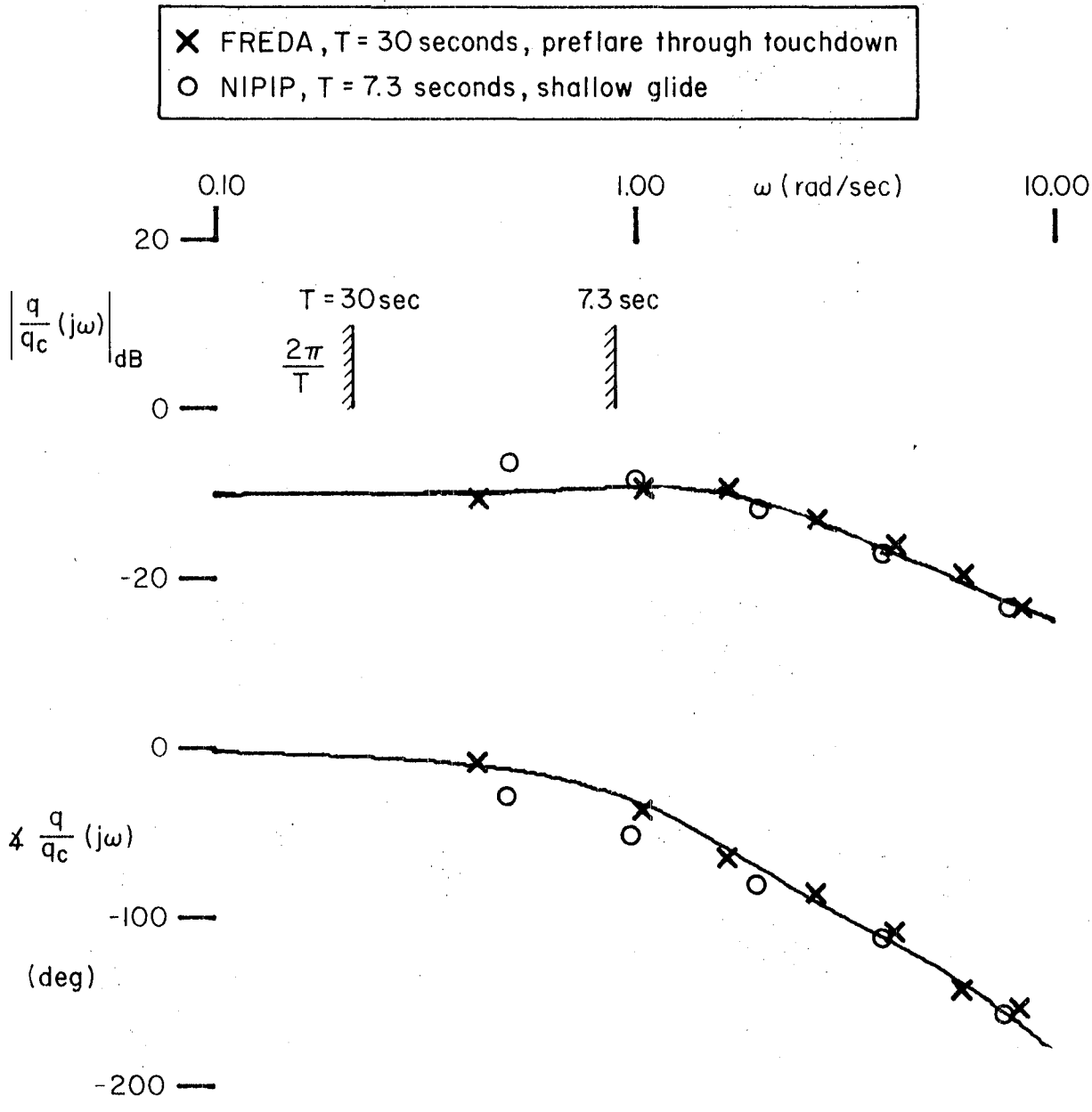

Figure 12. Comparison of NIPIP and FREDA Results for Shuttle Effective Vehicle Identification

glide and final flare maneuver and used to extract parameters of the pilot technique model hypothesized in Phase II. This effort contributed directly to the final effort, the application of the NIPIP program to the shallow glide region. Use of the NIPIP program for pilot model definition was not as successful as for vehicle identification. However, some procedural difficulties have been uncovered, some new procedures have been developed, and some data inadequacies have been found.

1. Effective Pilot Time Delay in Preflare Oscillation

The apparent near-neutral closed loop pilot/vehicle oscillation observed at the initiation of the preflare maneuver is shown in Fig. 13. As indicated, a period of approximately 3.3 sec is observed corresponding to a natural frequency of 1.9 rad/sec with near zero damping. Under the assumption of a closed loop pilot/vehicle system, the product of the open loop pilot and vehicle describing functions Y_pY_c is theoretically -1. Since the Shuttle characteristic Y_c has previously been identified, the value of Y_p (as a complex number) may be computed as

$$Y_p(1.9j) = Y_c^{-1}(1.9j)$$

If the pilot is assumed to operate on attitude information

$$Y_p(1.9j) = \left|\frac{\delta_{RHC}}{\theta}(1.9j)\right| e^{-1.9\tau_p j}$$

$$= \left.\frac{(0)[0.77,\ 1.44]}{0.606(1.03)e^{-0.159s}}\right|_{s\ =\ 1.9j}$$

$$= 6.50e^{-0.436j}$$

If the pilot Y_p is assumed to be a pure gain with a time delay τ_p

$$\tau_p = \frac{-0.436}{-1.9} = 0.23 \text{ sec}$$

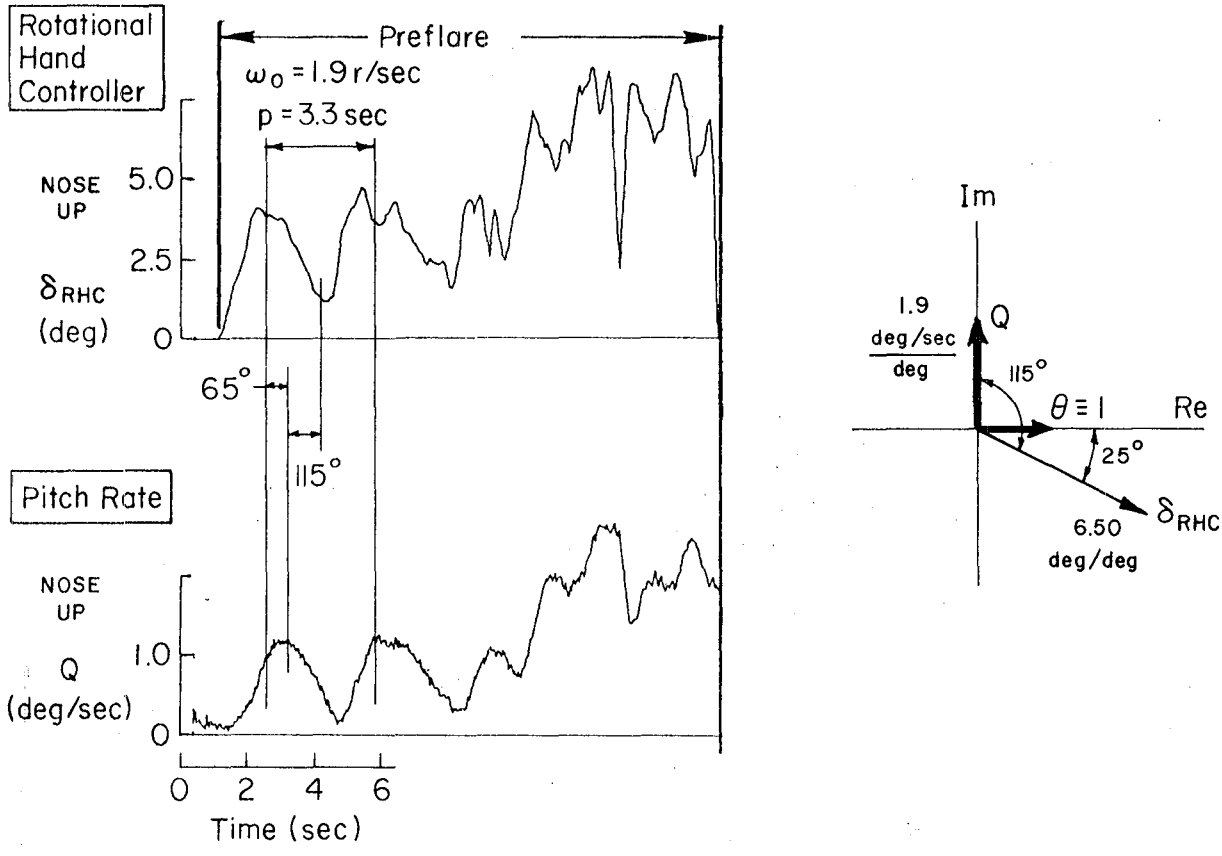

a) Pilot / Vehicle System Response

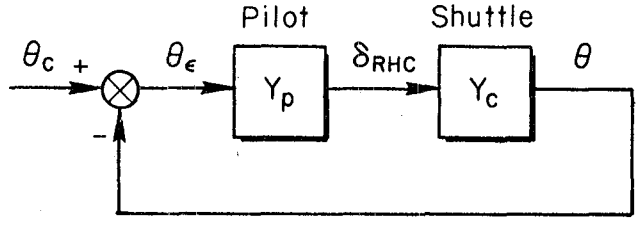

b) Assumed Pilot / Vehicle Model

Figure 13. Elements of Preflare Oscillation Analysis

However, we may expect some (first order) pilot lead in the region of 1-1.5 rad/sec based on the Y_c characteristics (Fig. 10). If this is accounted for

$$\tau_p \doteq 0.7 \text{ to } 0.8 \text{ sec}$$

This is relatively high compared to values usually observed in compensatory tracking, Ref. 3, and may reflect pilot uncertainty in this transition region.

2. Shallow Glide and Final Flare Pilot Model

It was concluded in Phase II that landing, and in particular the shallow glide and final flare, was the most critical flying qualities concern and thus the initial pilot model identification efforts have been concentrated on this task. The Phase II activity also produced a proposed pilot model for this flight segment which will be briefly reviewed and extended here for perspective in the discussion of flight data analysis.

The shallow glide and flare model assumes that the pilot attempts to fly a trajectory of the form shown in Fig. 14. The initial conditions are set by the altitude and speed (h_o and V_o) at the termination of the preflare. The pilot selects a constant value of flight path angle γ_o for the shallow glide which is maintained to some preselected flare altitude h_f at which point a flare is initiated in which the pilot schedules sinkrate proportional to altitude with time constant T_f. This flare law produces an exponential trajectory asymptotically approaching a level h_B below and parallel to the runway.

Analytical treatment is complicated by the fact that the Shuttle decelerates in this region, but it was shown in Ref. 2 that the deceleration is roughly constant ($\dot{V} \doteq 1/4$ to $1/3$ g) which allowed reasonable approximate analysis. The decreasing dynamic pressure does affect the vehicle dynamic characteristics (except for q/δ_{RHC}), but the primary effect for the pilot is the creation of a relatively short 'touchdown

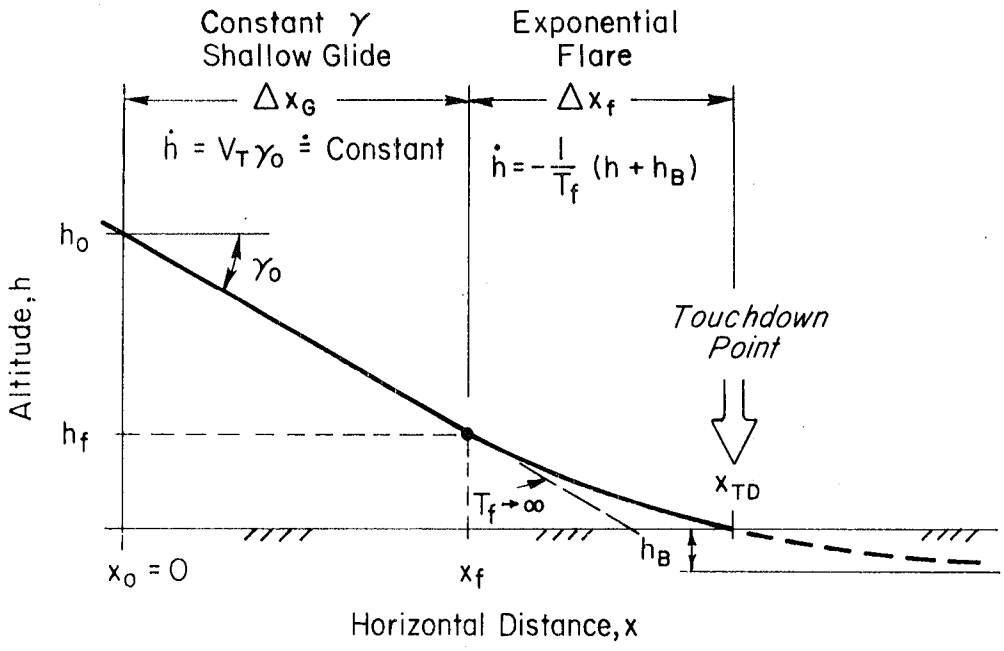

Figure 14. Idealized Trajectory for the Shallow Glide and Flare Trajectory Model

time window' to meet constraints on touchdown energy, speed, and sink-rate. The model assumes that the pilot selects h_f a priori; thus, as γ_o is steepened, the glide distance and time are reduced and the speed at flare initiation is increased. The basic equations derived in Ref. 2 are summarized below:

Speed at flare initiation

$$V_f = [2K_V^*(h_o - h_f)/\gamma_o + V_o^2]^{1/2} \tag{11a}$$

Depth of flare asymptote

$$h_B = -T_f V_f \gamma_o - h_f \tag{11b}$$

Touchdown time measured from flare initiation

$$t'_{TD} = -T_f \ln(h_B/(h_f + h_B)) \tag{11c}$$

Touchdown speed

$$V_{TD} = V_f - K_{\dot{V}} t'_{TD} \tag{11d}$$

Touchdown sinkrate

$$\dot{h}_{TD} = \gamma_o V_f + h_f/T_f \tag{11e}$$

Distance traveled in flare

$$\Delta X_f = V_f t'_{TD} - \frac{K_{\dot{V}}}{2} t'^2_{TD} \tag{11f}$$

The effect of the flare time constant is somewhat more complex, but it may be examined in the curves of Fig. 15 computed for the nominal conditions of Fig. 1 (which are somewhat different than the STS-4 conditions). If the flare is very slow (very large T_f) there is essentially no flare and the trajectory is an extension of the glide. Thus the minimum flare distance is

$$(\Delta X_f)_{min} \doteq -h_f/\gamma_o \quad \text{as } T_f \to \infty \tag{12}$$

As T_f is reduced for a faster flare, the trajectory approches a level parallel to and h_B feet below the runway. When T_f is reduced to

$$T_f^* = -h_f/V_f\gamma_o \tag{13}$$

h_B goes to zero and the runway is approached asymptotically ($\Delta X_f \to \infty$). For still lower T_f values the runway is never reached and a 'ballooning' situation results. Touchdown speed remains fairly constant until $T_f \doteq T_f^*$, at which point the increasing flare time causes considerable speed bleedoff. Touchdown sinkrate is strongly affected by the trajectory slope, and thus decreases steadily as $T_f \to T_f^*$. The Shuttle

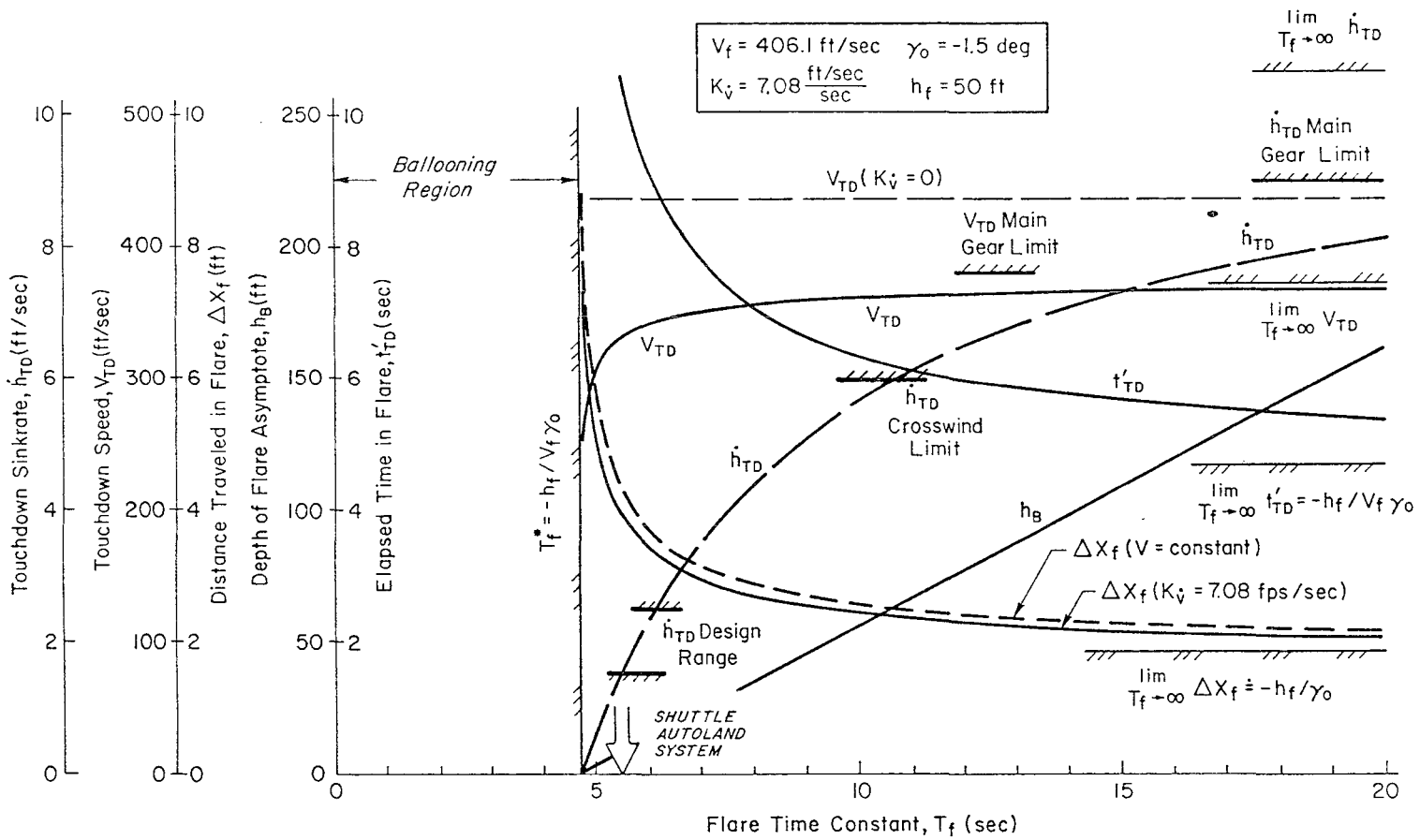

Figure 15. Effect of Pilot's Flare Time Constant on Final Flare

Autoland flare time constant (Ref. 14) is 5-6 seconds. This places $\dot{h}_{TD}$ in the design range, but unfortunately also puts the flare into the sensitive region near the ballooning boundary ($T_f \doteq T_f^*$).

To this point only path and speed control have been considered but these objectives require pitch attitude control. Complete pilot models for the shallow glide and final flare were developed in Phase II (Figs. 27 and 28, Ref. 2). These have been combined and simplified in Phase III to the form shown in Fig. 16. The speed control loop in the Phase II model was not included, in part, because there were no clear indications of path modulation for V_{TD} control in STS-4. The Phase II model also provided for a feed forward loop to the RHC to accommodate precognitive inputs. The STS-4 RHC trace, Fig. 2, indicates that precognitive inputs are probably limited to pulses at the flight segment transitions separated by regions of closed loop tracking. The feed forward was thus replaced by a discrete input δ'_{RHC} in Fig. 16. The transition from glide to flare is accommodated in the present model by a switch on the sinkrate command.

Thus the present model has a series structure as expected for a CTOL technique, especially when pilot lead is anticipated in the inner loop (Ref. 15, pp. 125-142). Some relevant comments are available from the STS-4 commander (T. K. Mattingly) regarding the manner in which the landing is accomplished: "you cannot fly h or $\dot{h}$ in the Shuttle; you have to fly pitch attitude. [I] guess $\dot{h}$ from Hartsfield's altitude calls, then move the nose." The interpretation of this statement, in

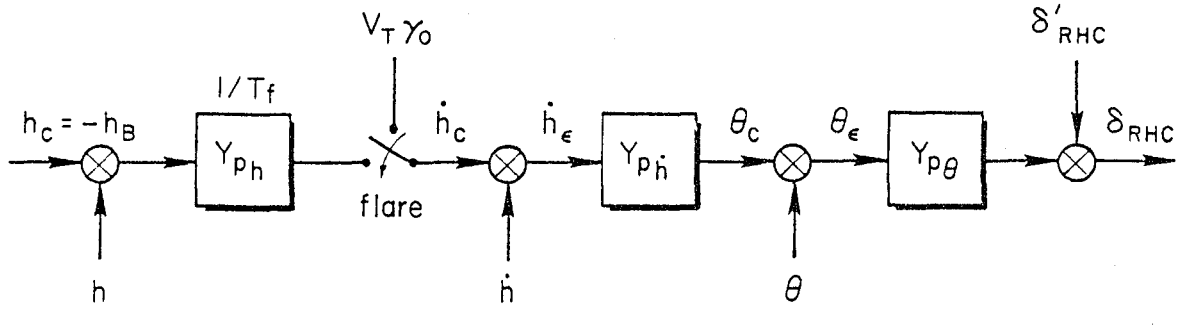

Figure 16. Shallow Glide and Final Flare Pilot Model

light of the Phase II model, is that it is impossible to control altitude or sinkrate directly with elevator, and in fact, an inner pitch attitude loop must be maintained. This is entirely consistent with the series loop structure shown in Fig. 16.

3. Altitude/Sinkrate Phase Plane Analysis

The shallow glide and final flare pilot model of Fig. 16 may be usefully viewed as a trajectory in the altitude/sinkrate phase plane shown ideally in Fig 17. If the shallow glide region has constant flight path angle γ_o as the model implies, the phase plane trajectory will be a straight, sloping line. If the sinkrate were more nearly constant, the glide trajectory would be horizontal. In the final flare region, where sinkrate is assumed to be scheduled proportional to altitude, the phase plane will be a straight line with slope $-1/T_f$. Ideally, touchdown should occur with the sinkrate in the nominal $-\dot{h}_{TD}$ range (1.5 to 2.5 ft/sec).

Application of phase plane analysis to the STS-4 flight was complicated by a number of problems with the available altitude and sinkrate data. These problems and their interim (Phase III) solutions will be discussed in detail in Subsection D. Briefly, the primary requirement to generate a usable phase plane trajectory was generation of a sinkrate signal by complementary filtering of h and a_Z signals. Figure 18 shows the final form of the STS-4 h-$\dot{h}$ trajectory.

The trajectory has been partitioned into final flare, shallow glide, and preflare region based on its shape and the time histories, shown in Fig. 2. The preflare region may be seen to be a region of rapidly decreasing sinkrate consistent with the pull-up maneuver. This is followed by capture and tracking of the shallow glide slope where the trajectory indicates a lightly damped pilot/vehicle system with a settling time comparable to the glide period. Sinkrate in this region varies from 5.5 to 4.3 ft/sec (based on the fitted line shown dashed), however, when the speed variation is accounted for, the variation in flight path angle is smaller, (-0.66 to -0.6 deg).

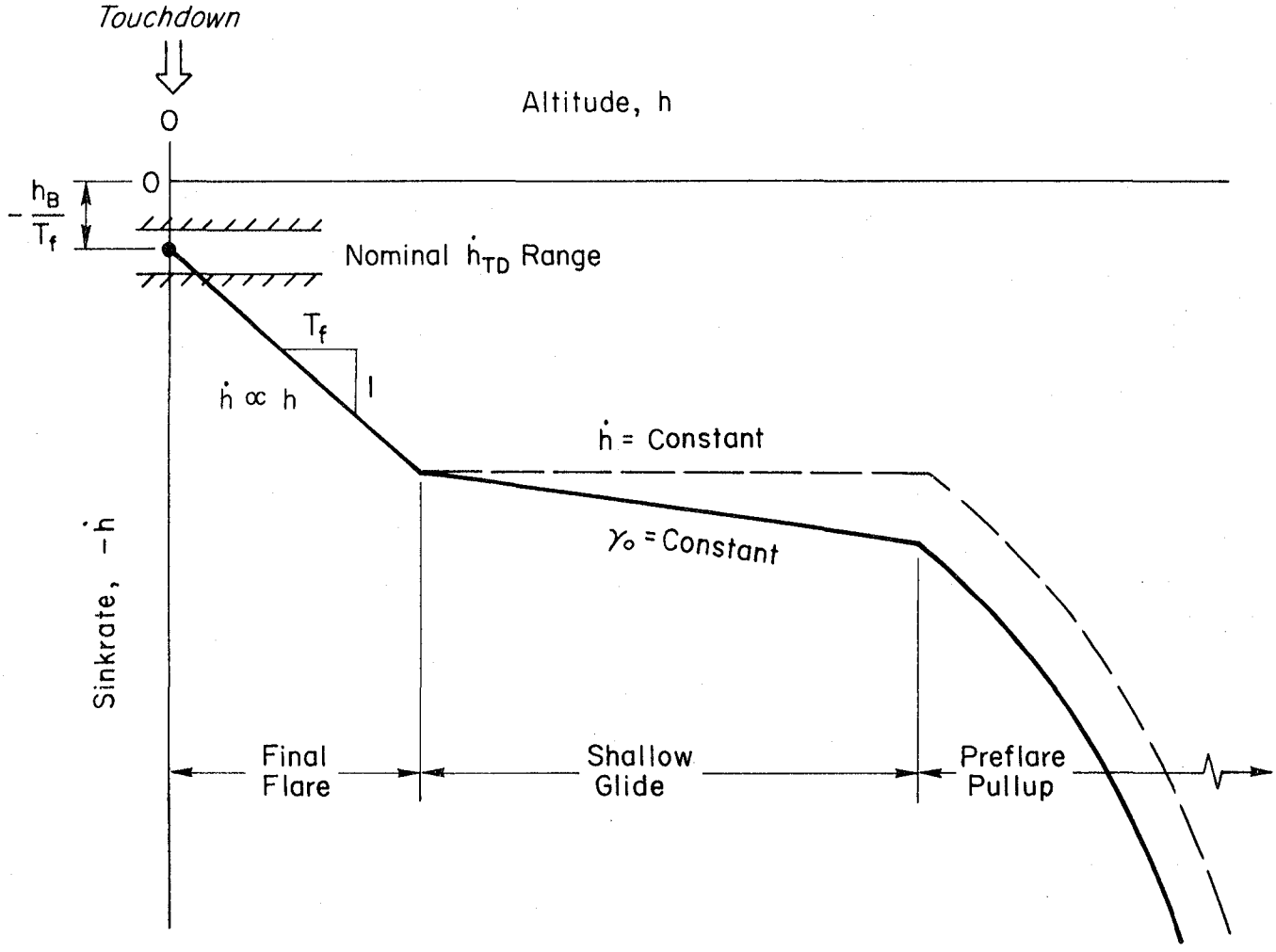

Figure 17. Idealized Altitude/Sinkrate Phase Plane Trajectory for the Shallow Glide and Flare Pilot Model

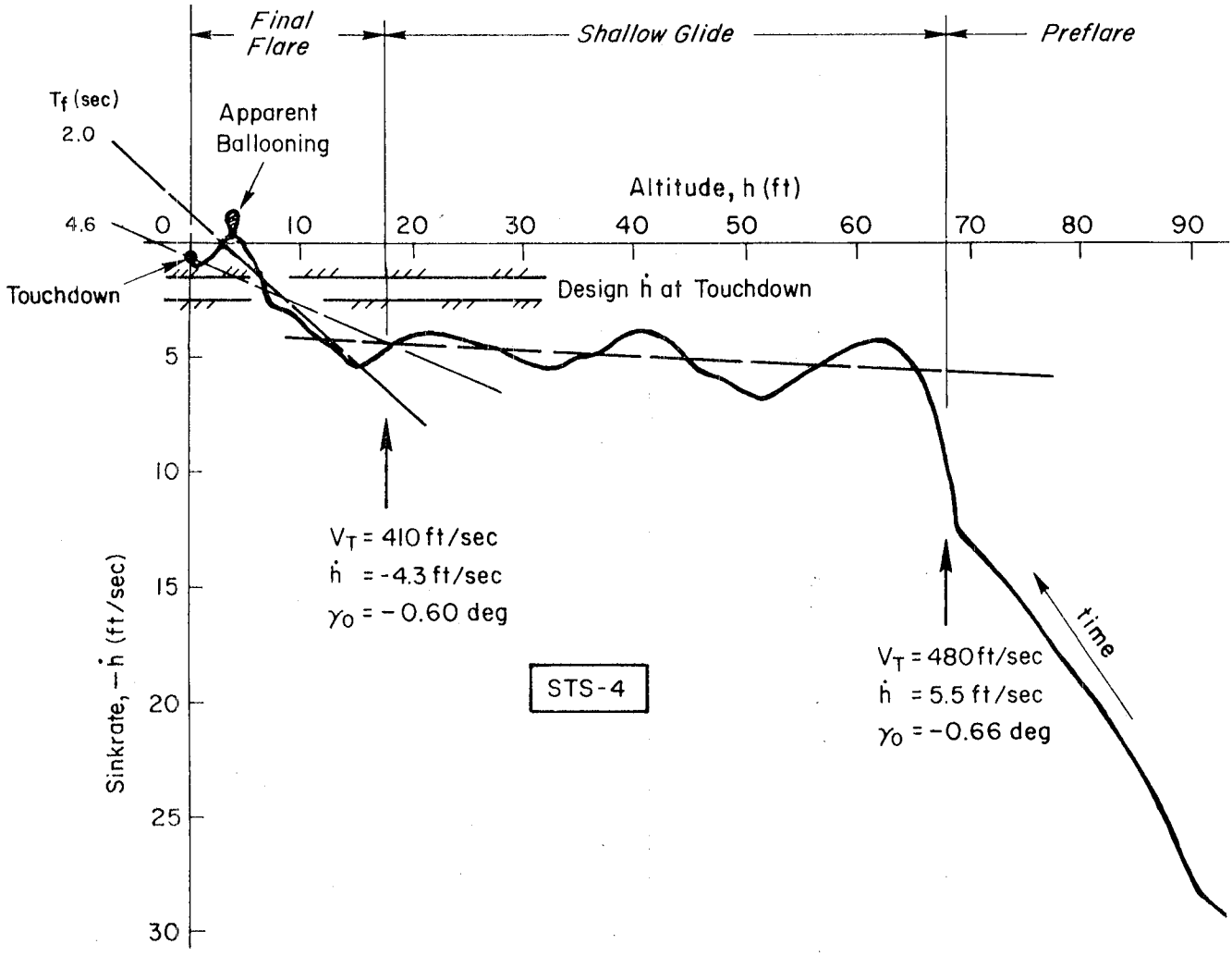

Figure 18. Altitude-Sinkrate Phase Plane Analysis of STS-4 Shallow Glide and Final Flare Complementary Filtered $\dot{h}$

The transition from shallow glide to final flare shown in Fig. 18 corresponds to the RHC flare initiation pulse shown in Fig. 2. The local peak of sinkrate seen immediately after flare initiation may be traced yo the negative download on the elevons associated with the nose-up RHC command. In the flare, sinkrate decreases roughly proportional to altitude with a superimposed oscillation which leads to a region of apparent ballooning about 5 ft above the runway. It should be noted that the altitude scale has been adjusted to give zero altitude at the (known) touchdown time to remove bias present in the altitude signal. A value for the flare time constant T_f can be extracted by fitting a straight line to the final flare region. Because of the oscillatory nature of the actual trajectory, various straight lines could be fitted as shown in Fig. 18 giving $2 \leq T_f \leq 4.6$ sec. If the design $\dot{h}_{TD}$ region is interpreted as an indication of the desired accuracy of control for sinkrate, the implication is that, while the shallow glide and final flare performance is acceptable, the manual control precision is less than might be desired. Beyond this interesting result for STS-4, is the important indication that the Phase II pilot model is reasonable, and that the parameters γ_o and T_f may be simply extracted from the phase plane plot, thus confirming the value of the method for the OFQ experiment.

To analyze the pilot's terminal control problem, based on the shallow glide and flare model, contours of X_{TD}, V_{TD}, and $\dot{h}_{TD}$ were plotted in the pilot's $T_f - \gamma_o$ control plane in the Phase II work. These plots (Fig. 2, Ref. 2) were constructed based on the simplified flight mechanics resulting of Eq. 11 approximation and the nominal V_o, h_o, h_f, and $K_{\dot{V}}$ values shown in Fig. 1 and used in Fig. 15. However, these parameter values were considerably different for STS-4 as shown in Table 3.

Revised V_{TD} and $\dot{h}_{TD}$ plots are shown in Fig. 19 based on the observed STS-4 V_o, h_o, h_f, and $K_{\dot{V}}$ values with the STS-4 (Fig. 18) values of T_f and γ_o shown for comparison, are also indicated in Fig. 19. From the phase plane trajectory, Fig. 18, the STS-4 $\dot{h}_{TD}$ is seen to be near zero with some ballooning indicated. This is consistent with the $\dot{h}_{TD}$

TABLE 3. SHALLOW GLIDE AND FLARE PARAMETERS

PARAMETER	REFERENCE 2 VALUE	STS-4 OBSERVED VALUE
V_o (fps)	468	480
h_o (ft)	150	68
h_f (ft)	50	18
$\dot{K}_V$ (fps/sec)	7.08	8.0

contours in Fig. 19a. The observed V_{TD} was 213 kts which, from Fig. 19b would imply somewhat higher (more positive) values of γ_o and/or T_f than extracted from the phase plane. However, the sensitivity of V_{TD} is very high in this region and γ_o uncertainties of 0.1 deg or less could explain the error. These comparisons are not considered as 'proof' of the Fig. 16 pilot model, but simply as indications of consistencies between the model and observations. Resolution of basic data problems and analysis of data from many more flights are needed; however, these comparisons provide a check on the flight data analysis which will be of value for the OFQ. In addition the Fig. 19 plots allow 'what if' questions to be considered about why the STS-4 crew may have chosen their strategy and the consequences of alternative choices. There are no pilot comments or other explicit indications as to why the STS-4 crew flew a low trajectory (i.e., h_o and h_f lower than the Fig. 1 nominal values); however, given this situation, the Fig. 19 plots provide some possible explanation of the γ_o, T_f choice. Figure 19b indicates that acceptable V_{TD} control would be virtually impossible for $\gamma_o > -0.8$ deg. This is in marked contrast to the 'nominal' situation as shown in Fig. 21b, Ref. 2 and helps explain the apparently low value of γ_o for STS-4. The STS-4 situation occurs because the low h_o limits the time available for speed bleedoff unless a shallow glide is used. The $\dot{h}_{TD}$ situation is not quite so critical, but the STS-4 T_f margins are reduced relative to the Ref. 2 nominal case at a given γ_o. The STS-4 $\gamma_o \doteq$ -0.6 deg produces a relatively large T_f 'sweet spot' but at the expense of ballooning potential.

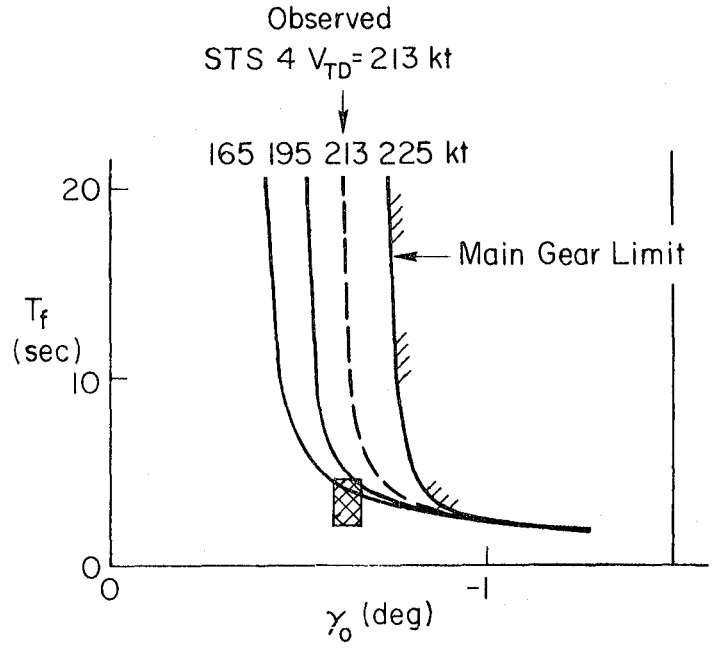

b) Touchdown Speed

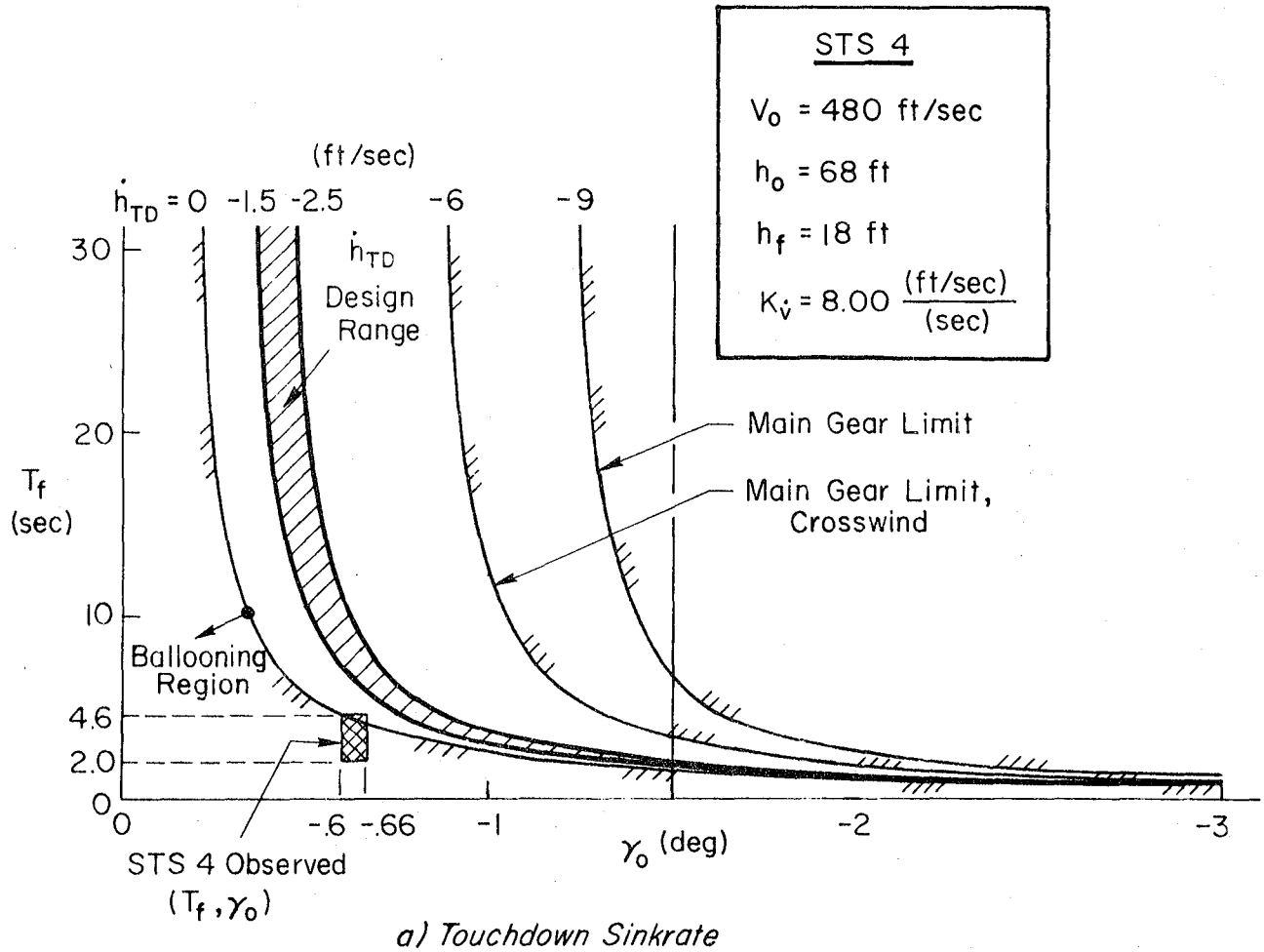

a) Touchdown Sinkrate

Figure 19. Variations of Touchdown Variables in the Pilot's T_f-γ_o Control Plane, STS-4

4. Pilot Strategy Identification with NIPIP in the Shallow Glide

Efforts to identify pilot model parameters using the NIPIP program have been made for the shallow glide region. The pilot model, Fig. 15, reduces to a $\dot{h} \rightarrow \theta_c$, $\theta \rightarrow \delta_{RHC}$ system in the flare. For application of the NIPIP program it is necessary to represent the rotational hand controller deflection in terms of the response variables $\dot{h}$ and θ and the external (precognitive) rate command $\dot{h}_c$.

$$\delta_{RHC} = Y_{p_\theta} \left\{ Y_{p_{\dot{h}}}(\dot{h}_c - \dot{h}) - \theta \right\} \tag{14a}$$

Based on the development in Phase II the expected form of the pilot elements are

$$Y_{p_\theta} = K_\theta \frac{(1/T_L)}{(1/T_I)} e^{-\tau_p s} \tag{14b}$$

$$Y_{p_{\dot{h}}} = \frac{K_{\dot{h}}^{\circ}(1/T_{L_{\dot{h}}})}{(1/T_{I_{\dot{h}}})} \doteq \frac{K_{\dot{h}}^{\circ}}{s}$$

where the approximation of $Y_{p_{\dot{h}}}$ as an integrator is made under the assumption that the outer loop crossover frequency is well below $1/T_{\theta_2}$. The result is a five parameter model with unknown parameters:

$$K_{\dot{h}}^{\circ},\ K_\theta,\ T_L,\ \text{and}\ \tau_p.$$

One of the important lessons learned from the use of NIPIP in Phase III was that relatively simple changes in the continuous (s-domain) pilot model can produce large increases in the complexity of the corresponding discrete NIPIP estimation equation. To illustrate this situation it is useful to compare the two parameter model for the series $\dot{h}$, θ model analyzed in Ref. 9, p. 61 with the above five parameter model. The two parameter model consists of a pure gain pitch attitude pilot element Y_{p_θ} and the same integral form of $Y_{p_{\dot{h}}}$ as used in the five parameter model:

$$Y_{p_\theta} = K_{p_\theta} \tag{15a}$$

$$Y_{p_{\dot{h}}} = \frac{K_{\dot{h}}}{s} \tag{15b}$$

The two parameter model may be z-transformed (using tables) directly into a two parameter estimation equation with a bias (Eq. 50 in Ref. 9)

$$\delta_n - \delta_{n-1} = \hat{a}(\theta_n - \theta_{n-1}) - \hat{b}(\dot{h}_{n-1} - \dot{h}_c) + B \tag{16a}$$

Furthermore, the estimation coefficients $\hat{a}$ and $\hat{b}$ may be directly and explicitly related to the unknown parameters in the continuous model:

$$\hat{a} = -K_\theta \tag{16b}$$

$$\hat{b} = -K_\theta K_{\dot{h}} T \tag{16c}$$

For the five parameter model the situation becomes much more complex. The first complexity arises in treating the effective pilot time delay τ_p It was found to be useful to represent the total time delay as

$$\tau_p = \tau_o + \Delta\tau \tag{17}$$

where

$$\tau_o = kT$$

and

$$k = 1, 2, 3, \ldots$$

$$T = \text{data sampling time}$$

The incremental time delay $\Delta\tau$ was then approximated as a first order lag, i.e.:

$$e^{-\Delta\tau s} \doteq \frac{\Delta\tau}{(s + \Delta\tau)} \tag{18}$$

Estimates of the pilot time delay expected can be used to select a value for the integer k to make the value of $\Delta\tau$ as small as possible, thus

improving the accuracy of the first order lag representation. The resulting pilot element is thus:

$$Y_{p_\theta} \doteq K_{p_\theta} \frac{(1/T_L)}{(1/T_I)} \frac{e^{-\tau_o s}}{(1/\Delta\tau)} \tag{19}$$

The second and greater more difficult problem occurs in transforming the continuous s-domain model to first a z-domain representation and then to a difference equation. To make the algebraic manipulation involved tractable, the desire to maintain a direct relationship between the estimation coefficients and the unknown parameters in the original continuous model must be foregone and only the structure (i.e., proper subscripts for δ, θ, and $\dot{h}$) of the model retained. The estimation coefficients become undetermined coefficients with no direct relationship back to the continuous parameters. The estimation equation for the five parameter model (derived in Appendix A)

$$\begin{aligned}\delta_n = {} & a_1\delta_{n-1} + a_2\delta_{n-2} + a_3\delta_{n-3} + b_o\theta_{n-k} + b_1\theta_{n-1-k} + b_2\theta_{n-2-k} \\ & + c_o\dot{h}_{n-k} + c_1\dot{h}_{n-1-k} + c_2\dot{h}_{n-2-k} + B\end{aligned} \tag{20}$$

has nine unknown coefficients. In spite of this relative complexity, the NIPIP algorithm applied to the STS-4 data converges and computes the estimation coefficients which appear valid at least on the basis of the correlation parameter.

The problem at that point is one of interpretation of the identified model's frequency response. It was found in the Phase III work that use of the w′ transformation (Ref. 16) provided a good solution to this problem. After running NIPIP to obtain the coefficients, estimation equations in the z-domain may be transformed to the w′ domain through

$$z^{-1} = -\frac{w'-2/T}{w'+2/T} \tag{21}$$

where T^{-1} is the data sample rate in Hz. The value of this transformation derives from the fact the w′ frequency response approximates that of the s-domain well below the sample rate, i.e.,

$$G(w') \doteq G(j\omega) \text{ for } \omega, w', \ll 2\pi/T \text{ rad/sec}$$

The overall procedure developed for representation and intepretation of complex pilot models in NIPIP may be summarized as:

- Form continuous analytic model (s-domain)
- Transform to z-domain
- Simplify, preserving model structure
- Transform to difference equation (estimation equation)
- Run NIPIP and obtain estimation coefficients
- Transform from z-domain wo w'-domain
- Interpret w'domain response as jω frequency response for $\omega << 2\pi/T$

An example of a NIPIP result as interpreted in the w'-domain is shown in Fig. 20. The difference between the s-domain and w'-domain frequency response is only a few percent at 10 rad/sec and is even closer at lower frequencies. There is considerable uncertainty about the validity of this solution for the pilot model based on large changes in the model result as the fixed portion of the pilot time delay τ_o is varied -- a result not entirely unexpected due to the approximation of $\Delta\tau$ as a lag. However, further investigation of the behavior of this solution indicated certain data problems that must be resolved before further progress can be made in using NIPIP.

D. SUMMARY OF FLIGHT DATA PROBLEMS AND RECOMMENDATIONS FOR OFQ

The flight data analyses done in Phase III have revealed a number of shortcomings in the available data, i.e., that in the (STS-4) MMLE file,

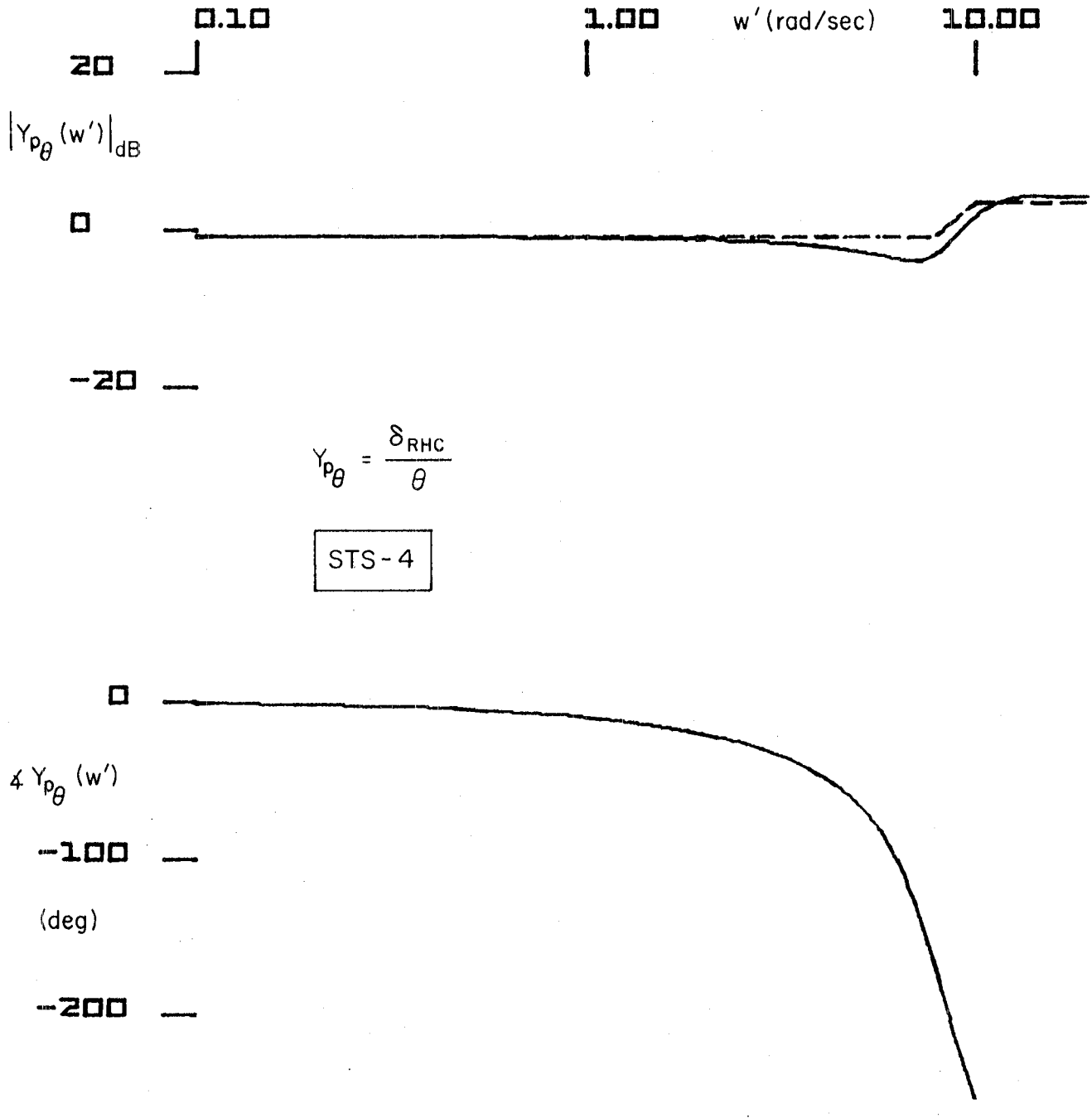

Figure 20. Y_{p_θ} From NIPIP Interpreted in w' Domain

which must be remedied for the OFQ. Fortunately, it appears that the needed data are probably available, the problem is primarily one of extracting the relevant variables from the large amount of data available from a number of sources. The primary problem identified in Phase III is the need for better altitude and sinkrate signals and it appears that this problem could be resolved through the use of available cinetheodolite data. This section will review the data problems, summarize OFQ data needs and present recommendations. A primary recommendation is that the Shuttle flight data be assembled into well-documented 'OFQ archive data files' containing all variables needed for vehicle dynamics and control and flying qualities studies. These files would be treated as an important OFQ 'product' and be available on the DFRF Cyber computer for use by local and outside groups.

1. Altitude and Sinkrate Data Problems

Altitude and sinkrate are of secondary importance for aerodynamic parameter identification, the primary use of the MMLE data files to date. However, they are essential for analysis of piloting technique in landing, either by phase plane methods or the NIPIP program. In addition, the definition of effective body reference point becomes very important at altitudes on the order of the Shuttle body length. The altitude data is available on the MMLE file from two sources, the IMU channel and radar altimeter channel, and there is some inconsistency between the two. There is no sinkrate data available from the IMU channel and the radar sinkrate channel on the MMLE file was found to be unusable, due apparently to calibration problems, thus a computer file was created from Fig. 15 in Ref. 17.

Figure 21 compares the radar and IMU altitude traces for the final 30 sec of the landing from the MMLE file. It may be seen that there are some differences particularly at low altitudes. To avoid the dynamic range problem inherent in looking at the altitude signal over the entire period from the start of preflare Fig. 22 shows radar altitude for the shallow glide and final flare. The linearly interpolated signal indicates some ballooning just before touchdown. A bias of several feet below the runway is indicated at touchdown but this could easily be

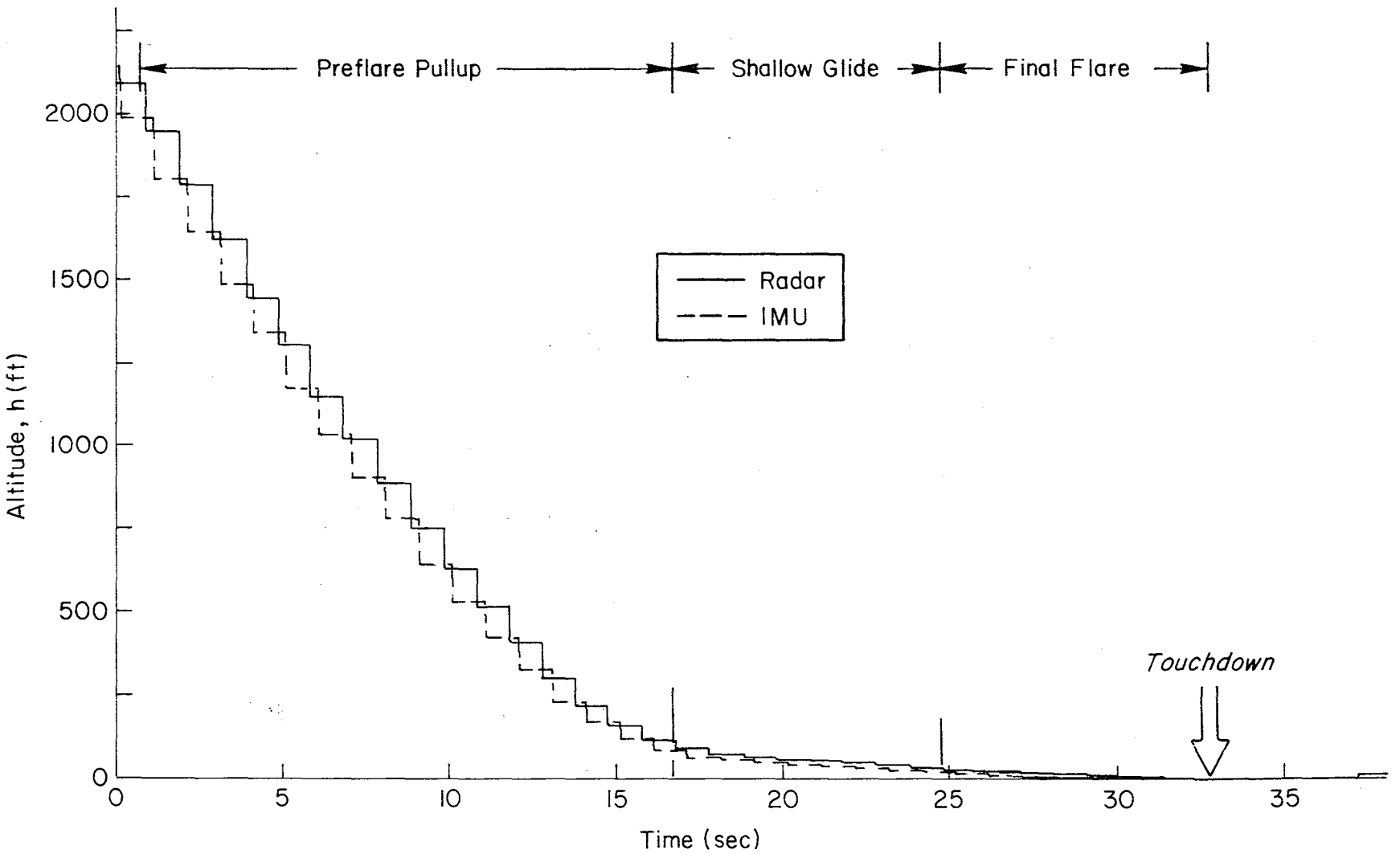

Figure 21. Comparison of Altitude Time Histories from Radar and IMU Channels in DFRF STS-4 MMLE Files

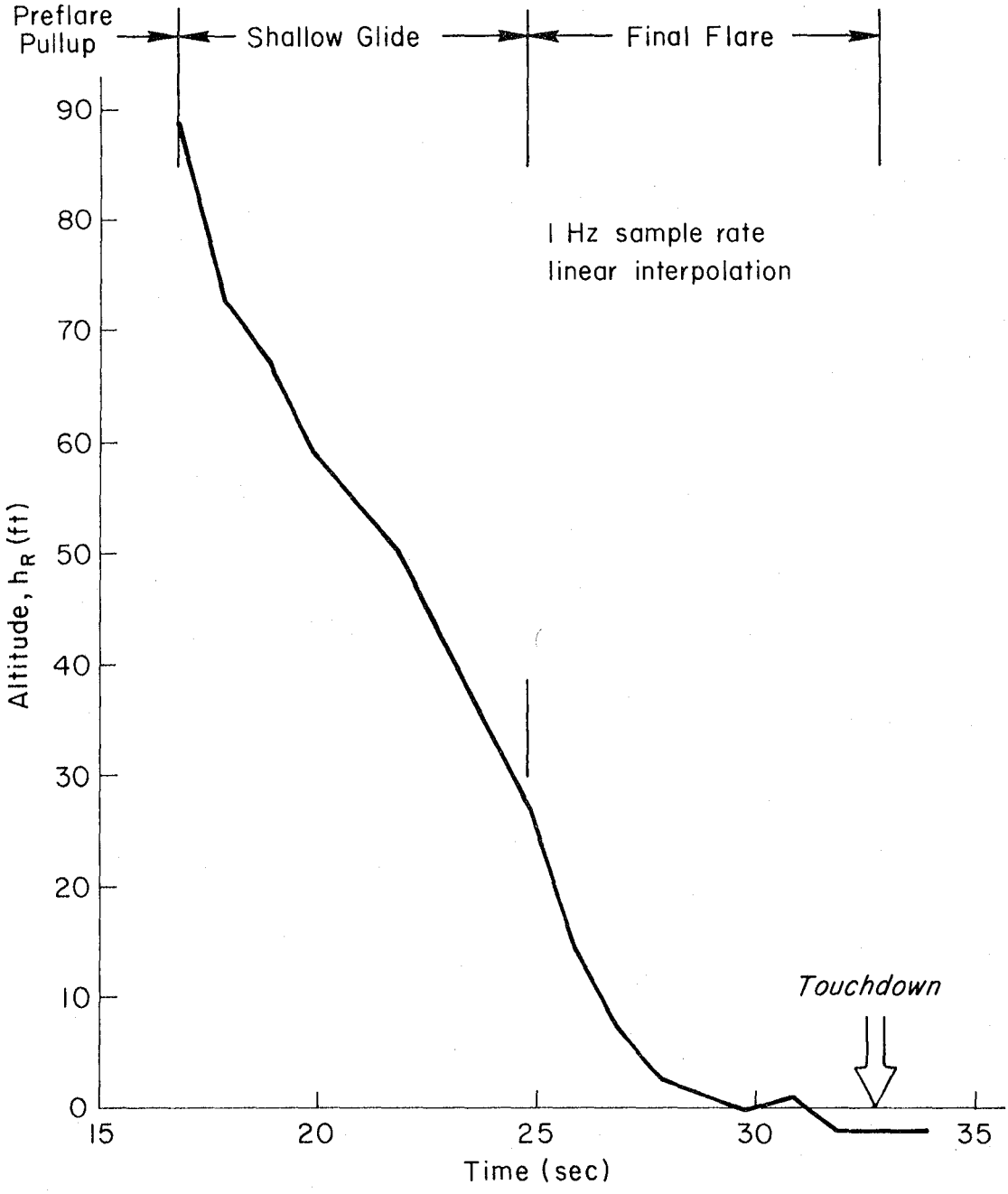

Figure 22. Interpolated Radar Altitude, Shallow Glide and Final Flare

accounted for by uncertainties in the body position reference for the signal.

The radar sinkrate plot created from the computer file generated from Ref. 17 is shown in Fig. 23 (dashed line). This signal was generated at DFRF by differentiating the radar altimeter signal, and thus retains artifacts of the 1 Hz sample rate. For comparison, a sinkrate trace was computed from

$$\dot{h} = V_T \sin \gamma$$

$$= V_T \sin (\theta - \alpha)$$

and is also shown (dotted line) in Fig. 23. When compared to the radar derived signal, there is considerable difference in basic dynamic characteristics as well as absolute levels over substantial periods.

Given the inconsistency between the available data, a sinkrate signal was generated by complementary filtering normal acceleration from the ACIP accelerometers and altitude from the IMU source. The filter form is shown in the block diagram of Fig. 24a. It may be seen that the complementary filtered sinkrate consists of washed out altitude (i.e., low frequency differentiation of altitude) combined with a pseudo-integrated accelerometer signal as indicated in the Bode amplitude sketch of Fig. 24. The expression for the filtered $\dot{h}$ is

$$\dot{h}_c = sh + \frac{n_a + asn_h}{(s + a)} \tag{23}$$

It may be seen that the high frequency accelerometer noise and low frequency altitude errors are filtered out. This s-domain expression was converted to a difference equation for use with the digital data, i.e.,

$$\dot{h}_{c_n} = e^{-aT}\dot{h}_{c_{n-1}} + a(h_n - h_{n-1}) + \frac{1-e^{-aT}}{a} a_{z_n} \tag{24}$$

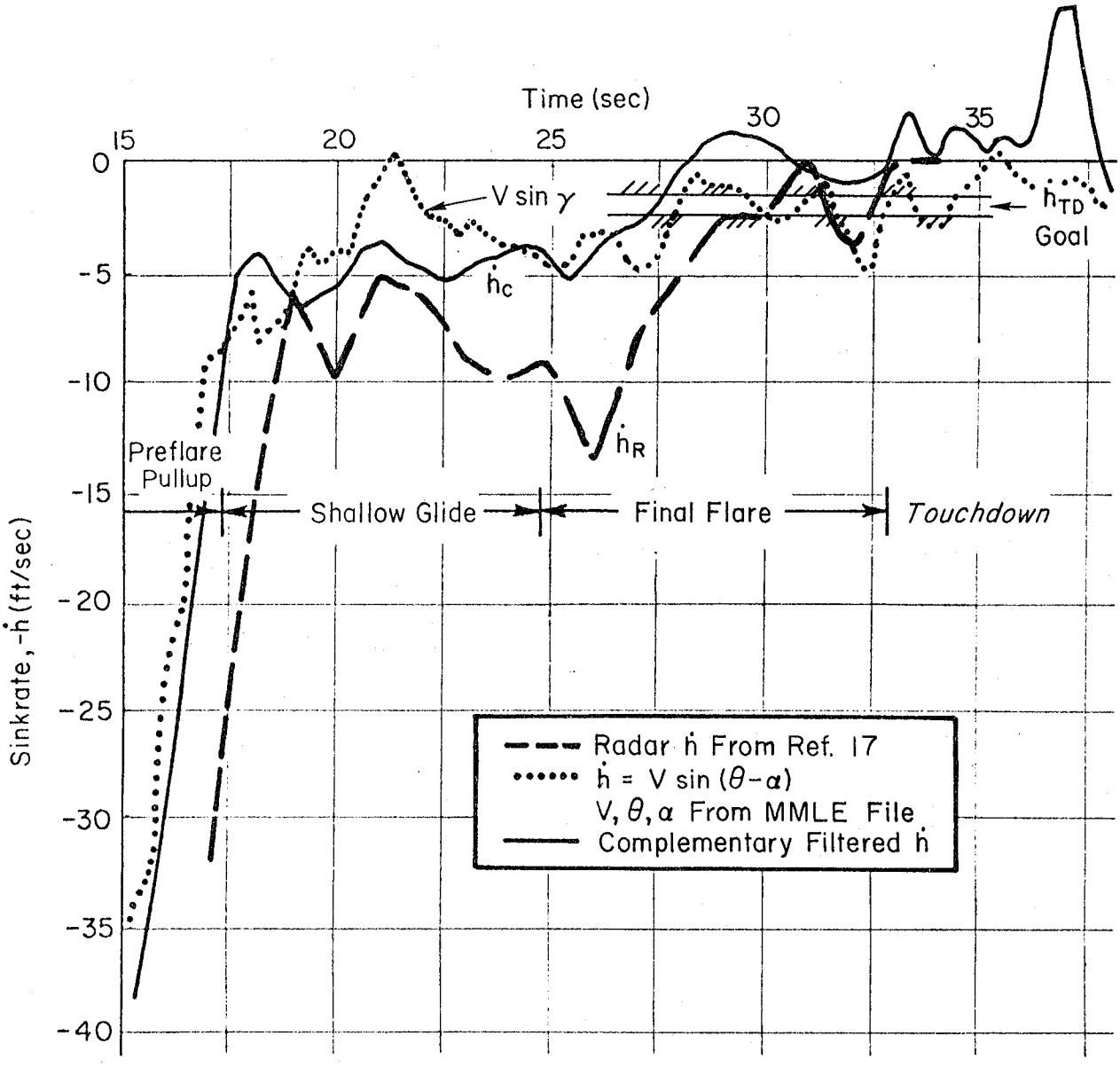

Figure 23. Comparison of Sinkrate Signals

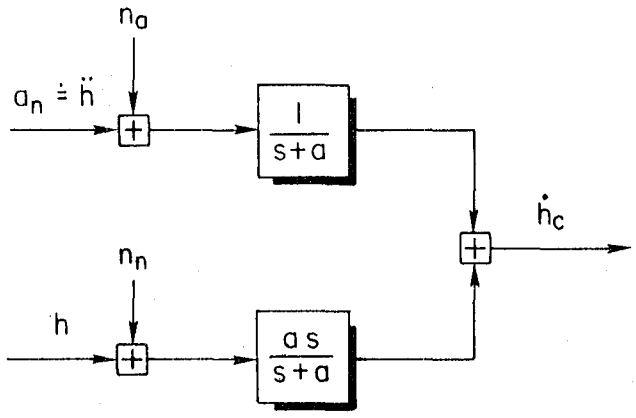

a) Filter Block Diagram

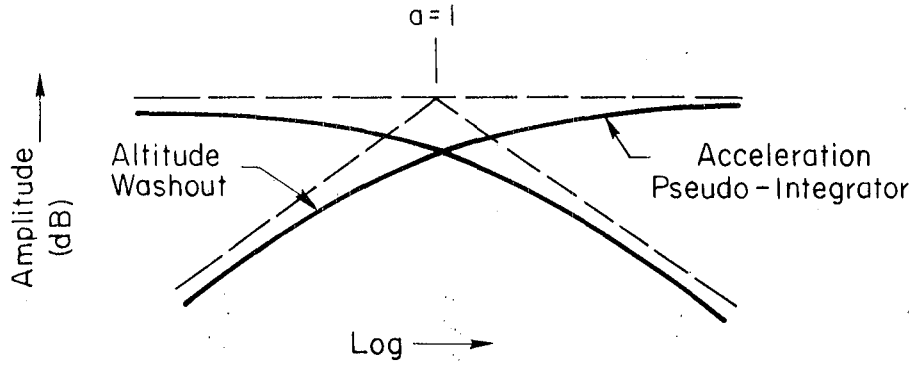

b) Frequency Domain View

Figure 24. Sinkrate from Complementary Filter

The complementary filtered sinkrate, compared to the other sources in Fig. 23, shows considerable smoothing with respect to the radar derived trace with more nearly constant sinkrate in the shallow glide region and lower sinkrate through the flare including negative sinkrate (i.e., climb) beyond t = 28 sec. This indication of ballooning is qualitatively consistent, except for time of occurrence, with the radar altitude trace shown in Fig. 21. The complementary filtered sinkrate appears to lie generally between the radar and computed sinkrates.

To emphasize the importance of high quality sinkrate data the phase plane trajectory using the radar sinkrate (dashed line Fig. 23) is shown in Fig. 25. An interpretation of this plot might allow one to consider it consistent with the basic pilot model and Fig. 18, however, it is much less obvious or convincing.

2. Other Data Questions and Needs (STS-4 MMLE File)

a. Attitude (Euler) Angle Frequency Response

The attitude signal used in the NIPIP identification of the pilot pitch control element was the pitch attitude signal from the onboard GPC attitude processor. Pitch attitude should be consistent in frequency response with the integral of q from the ACIP (except for p and r contributions). Lateral directional motions are small in the shallow glide, however, there does appear to be some difference in frequency response in the pilots crossover region (Fig. 26), particularly in phase angle, which has not yet been explained.

b. Earth Referenced X and Y Position

In addition to altitude, the location of the Shuttle with respect to the Earth's surface (X, Y) is needed but not available in the (STS-4) MMLE file. X position is of particular interest for the landing to conveniently and precisely define landing distance for each flight.

c. Manual Control

RHC deflection data appears to contain a calibration uncertainty which may be due to the use of the backup flight control system as the

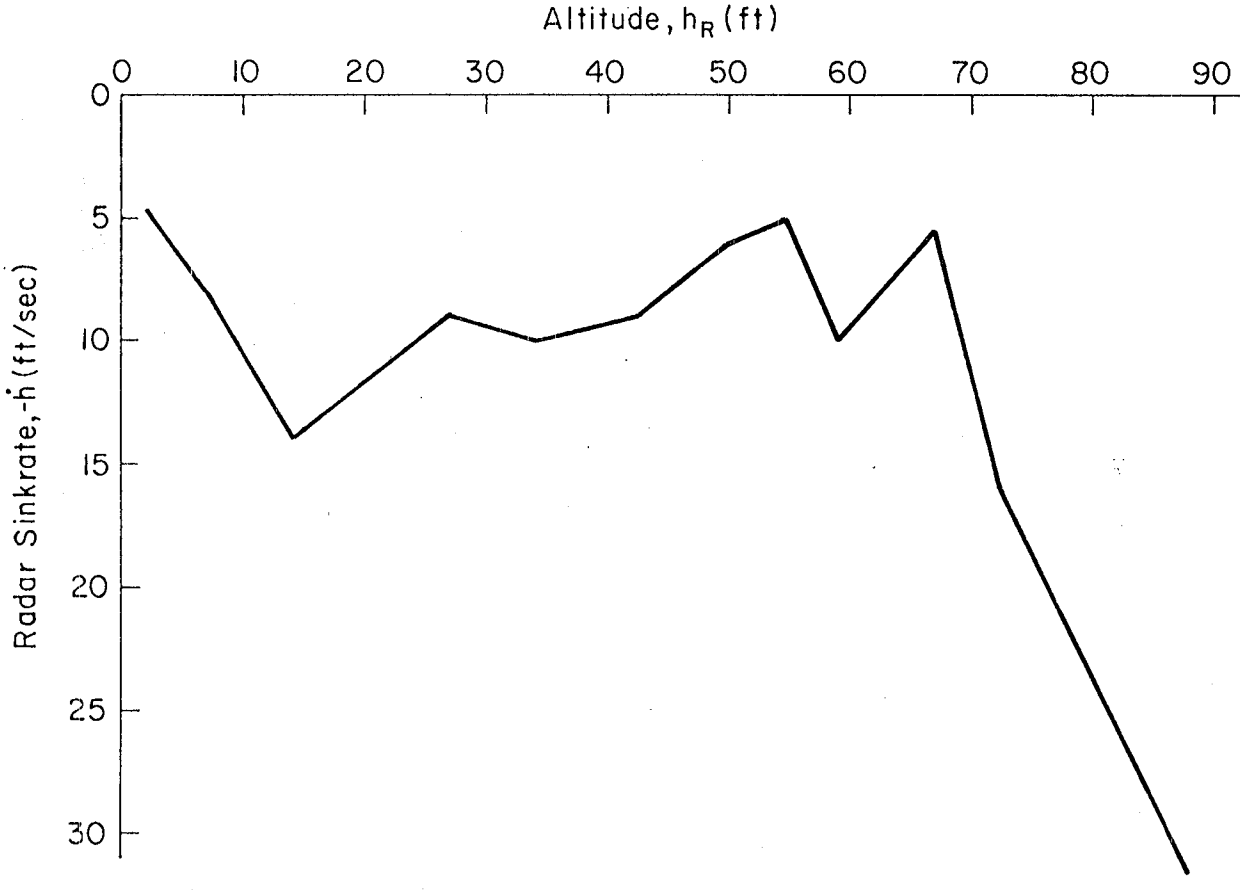

Figure 25. Altitude-Sinkrate Trajectory, STS-4 Shallow Glide and Final Flare, $\dot{h}$ from Reference 17

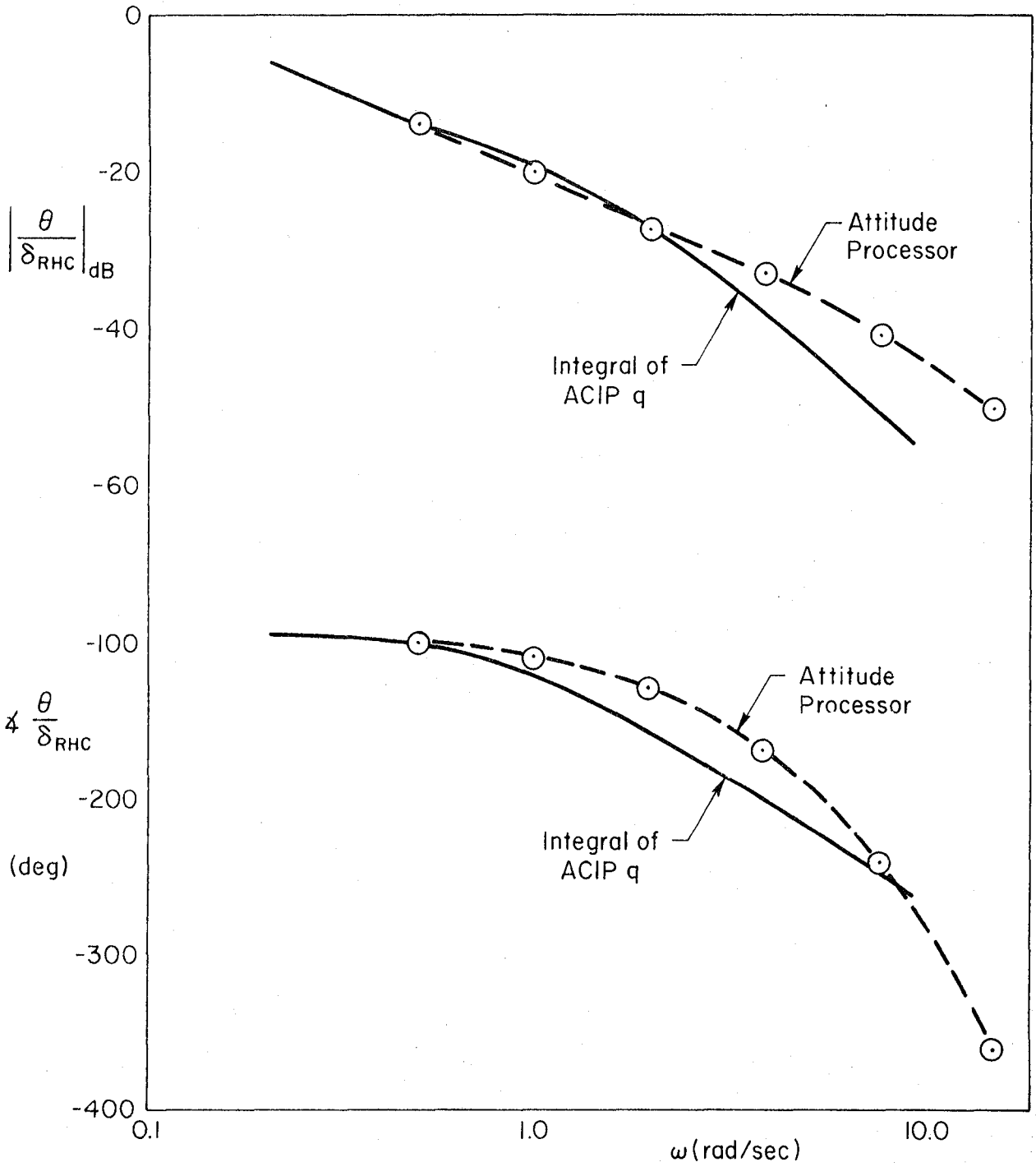

Figure 26. Frequency Response Comparison of θ/δ_{RHC} from Attitude Processor and ACIP

source for this data. Further, the highest available δ_{RHC} sample rate is 12.5 Hz (BFCS) rather than the 25 Hz actually used in the flight control system and this signal is the sum of the pilot's and commander's inputs.

There are no speedbrake or body flap control signals or manual trim data available in the STS-4 MMLE file.

d. FCS Mode Discretes

There are some limited data available in the MMLE file for switching discretes. This data has not been exercised but appears to be adequate to define AUTO/MANUAL status for the pitch, roll, yaw, body flap, and speed brakes channels. However, there are a number of discretes of interest (Table 9, Ref. 2) which are not available.

3. Summary of OFQ Data Requirements and Sources

Table 4 summarizes the present view of the data needed for the OFQ and the available sources (indicated with X's). The first four columns relate the data available on the DFRF MMLE files to onboard sources. The last four columns indicate data availability from four sources which have been investigated but not used to date. It is felt that these additional sources should be adequate to resolve most of the data problems noted above.

a. Theodolite Measurements

Problems with altitude and sinkrate data in landing are of particular concern. It is proposed that available theodolite data be used to augment onboard altitude data. Theodolite data is available from Air Force Flight Center (AFFTC) on magnetic tape in digital form and it should be possible to enter this data into the DFRF Cyber computer with reasonable effort. Data is available from the Contraves cinetheodolite system (Ref. 18) for STS-1 through 6 and provides position, rate, attitude, speed, and wind data. Data is also available for STS-4 through 6 from the 'takeoff and landing towers' parallel to EAFB runway used for

TABLE 4. SUMMARY OF SHUTTLE FLIGHT DATA DESIRED AND SOURCES FOR OFQ

VARIABLE	MMLE FILE				GROUND BASED THEDOLITE MEASUREMENTS		BEST ESTIMATED TRAJECTORY DATA (DFRF & LRC)	NASA JSC MPDB
	ACIP	GPC	OI	BFCS	TAKEOFF & LANDING TOWERS	CINETHEODOLITE		
TRANSLATIONAL ACCELERATION A_Z A_Y A_Z	X	X (NO AX)				X		ALL DATA EXCEPT ACIP
ANGULAR ACCELERATION $\dot{P},\dot{Q},\dot{R}$	X							
TRANSLATIONAL RATE (AIR DATA) $\alpha,\beta,\dot{H},V_{TRUE},V_{EAS},\bar{q},M$		X				X	X	
TRANSLATIONAL RATE (EARTH REFERENCED) $\dot{X}$, $\dot{Y}$, $\dot{Z}$					X	X	X	
ANGULAR RATE P,Q,R	X	X						
EARTH REFERENCED POSITION X, Y, H,		X (H_{IMU} H_R only)		X	X	X		
EULER ANGLES ψ, θ, ϕ		X				X		
CONTROL SURFACE DEFLECTION δ_e, δ_a, δ_r	X		X					
δ_{SB}		X						
δ_{BF}								
MANUAL CONTROLS (COMMANDER AND PILOT SEPARATE) δ_{QRHC}, δ_{PRHC}		X[1]	X	X[2]				
δ_{PED}								
δ_{SBC}, δ_{BFC}								
MANUAL TRIM CONTROLS								
SWITCHES AND FCS DISCRETES		X[3]						
DISPLAY AND HUD VARIABLES								
WIND DATA						X	X	

[1] Pilot's input, 1 Hz sample rate

[2] Pilot + commander input, 12.5 Hz sample rate

[3] AUTO/MANUAL FCS status only

the Shuttle. This data is somewhat more accurate than that from the Cine system, but is limited to X, Y, Z positions and rates. There are apparently no plans to obtain theodolite data for Shuttle landings at Cape Kennedy and it is proposed that the feasibility of obtaining such data be seriously considered.

b. Best Estimated Trajectory Data

Contacts with personnel at NASA LRC have been made concerning the Best Estimated Trajectory (BET) tapes and documentation has been requested but not yet received. In the interim, however, it has been learned that data already available at DFRF (Ref. 19) may be more suitable. This work merges data from four sources through use of a linearized Kalman filter to obtain a best estimate of vehicle and wind velocities. This effort is particularly useful because it is being done at DFRF, it should relate well to the MMLE files, and it is unusually well documented. It should be possible to extend to additional variables which could be useful in resolving data frequency response consistency problems (e.g., Fig. 26).

c. NASA JSC Master Products Data Base

A final source of data which was investigated in the Phase III effort is the official post-flight data from the NASA JSC 'Master Products Data Base' (MPDB). The data flow and maintenance of this system is indicated in Fig. 27. Certain problems have made use of this data source impractical to date. First, the MPDB is extremely large and general and includes much data irrelevant to this program. Thus, adequate documentation is critical to extracting the small subset of relevant data. A large number of specialized 'data products' (e.g., tapes, tabulations, plots, etc.) are generated from the MPDB after each flight for specific users and computer generated reports listing the specific variables available on each tape, etc., have been received from JSC, Ref. 20. These reports (a typical page is shown in Fig. 28) are, however, not appropriate for specifying a request for a unique OFQ tape. What is needed is an organized listing of the variables available on the MPDB

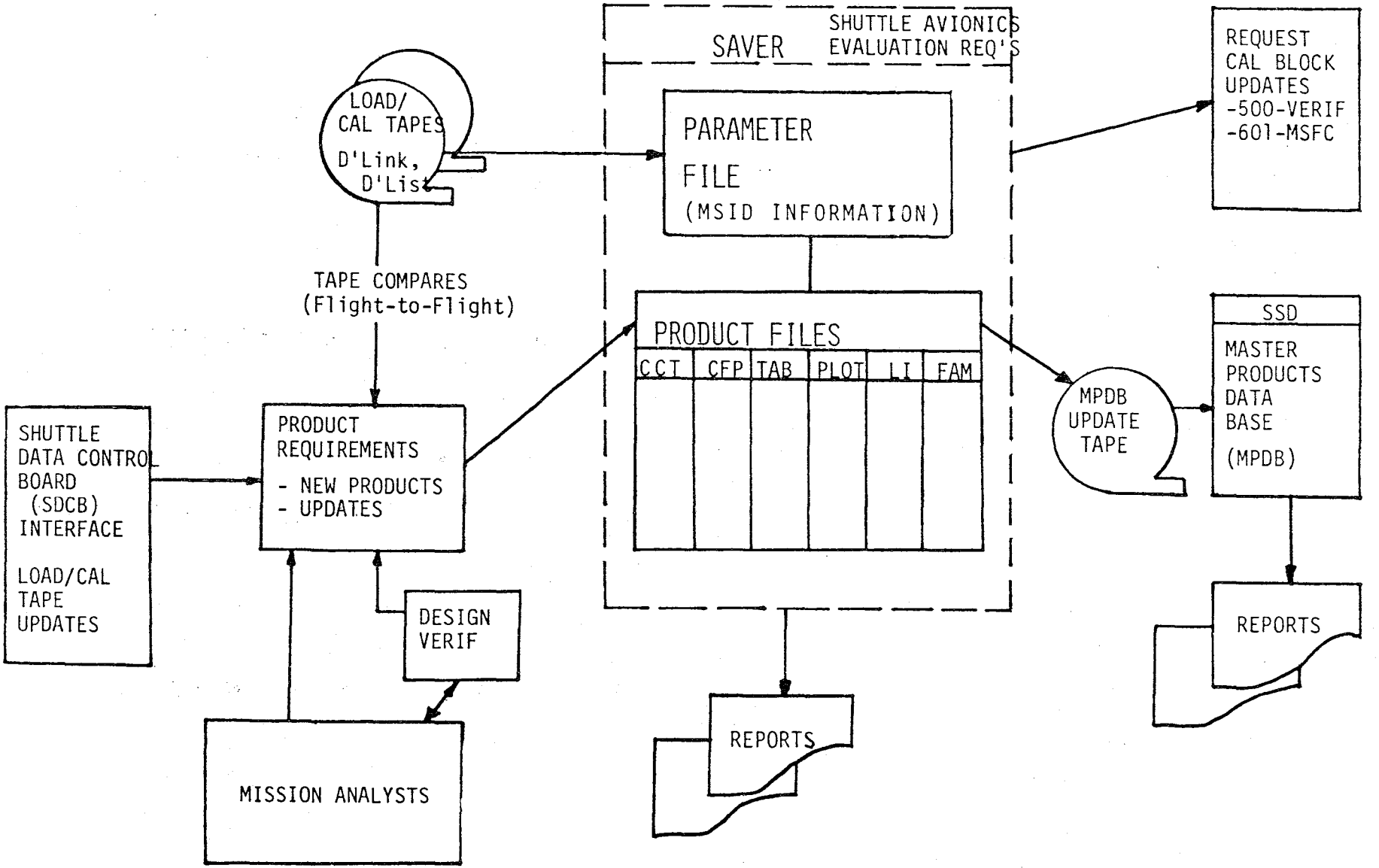

Figure 27. NASA JSC Master Product Data Base for Shuttle

MSID	NOMENCLATURE	CALF	LIFL	UNITS	TYPE
CG010F	LACY				
V98*L*0143*C	Z-VELOCITY BFS	Y		FT/S	SPL
V98*W*0150*C	GREENWICH MEAN TIME BFS	Y		US	BSU
V98*X*0431*X	TACAN 1 RANGE DATA GOOD BFS	Y		EVENT	BD
V98*X*0432*X	TACAN 2 RANGE DATA GOOD BFS	Y		EVENT	BD
V98*X*0433*X	TACAN 3 RANGE DATA GOOD BFS	Y		EVENT	BD
V98*X*0434*X	TACAN 1 BEARING DATA GOOD BFS	Y		EVENT	BD
V98*X*0435*X	TACAN 2 BEARING DATA GOOD BFS	Y		EVENT	BD
V98*X*0436*X	TACAN 3 BEARING DATA GOOD BFS	Y		EVENT	BD
V98*W*1430*C	ACC SENSED VEL TIME WORD 1 BFS	Y		S	EPL
V98*R*1550*C	ROLL RATE BFS	Y		DEG/S	HPL
V98*R*1551*C	PITCH RATE BFS	Y		DEG/S	HPL
V98*R*1552*C	YAW RATE BFS	Y		DEG/S	HPL
V98*H*1560*C	ROLL EULER ANGLE BFS	Y		DEG	HPL
V98*H*1561*C	PITCH EULER ANGLE BFS	Y		DEG	HPL
V98*U*1590*C	ALPHA BFS	Y		DEG	HPL
V98*U*1591*C	BETA BFS	Y		DEG	HPL
V98*U*1597*C	HEADING REL TO MAG NO BFS	Y		DEG	HPL
V98*L*1790*C	EARTH RELATIVE VELOCITY BFS	Y		FT/S	SPL
V98*W*1888*C	TIME TO MAIN ENGINE CUTOFF BFS	Y		S	SPL
V98*L*1917*C	MACH BFS	Y		ND	SPL
V98*H*2160*C	NAV DERIVED ALPHA BFS	Y		DEG	HPL
V98*U*2340*C	NAV DERIVED Q BAR(D) BFS	Y		LBF/FT2	HPL
V98*H*2350*C	ADI ROLL SINE POSN BFS	Y		ND	HPL
V98*H*2351*C	ADI PITCH SINE POSN BFS	Y		ND	HPL
V98*H*2352*C	ADI YAW SINE POSN BFS	Y		ND	HPL
V98*H*2355*C	ADI ROLL COS POSN BFS	Y		ND	HPL
V98*H*2356*C	ADI PITCH COS POSN BFS	Y		ND	HPL
V98*H*2357*C	ADI YAW COS POSN BFS	Y		ND	HPL
V98*U*2408*C	MAJOR MODE BFS	Y		ND	HXU
V98*H*3100*C	FIL SEL TACAN RANGE BFS	Y		FT	SPL
V98*H*3110*C	FIL SEL TACAN BEARING BFS	Y		RAD	SPL
V98*P*3117*C	DYNAMIC PRESS BFS	Y		LBF/FT2	SPL
V98*U*3155*C	ALPHA CMD BFS	Y		DEG	HPL
V98*H*3160*C	ROLL ANGLE CMD BFS	Y		DEG	HPL
V98*U*3444*C	TACAN AZIMUTH RESIDUAL BFS	Y		DEG	SPL
V98*U*3446*C	TACAN RANGE RESIDUAL BFS	Y		NM	SPL
V98*H*3762*C	TACAN 1 BEARING DATA BFS	Y		DEG	BSU
V98*H*3768*C	TACAN 1 RANGE A BFS	Y		NM	BCD
V98*H*3805*C	TACAN 2 BEARING DATA BFS	Y		DEG	BSU
V98*H*3854*C	TACAN 2 RANGE A BFS	Y		NM	BCD
V98*H*3905*C	TACAN 3 BEARING DATA BFS	Y		DEG	BSU
V98*H*3954*C	TACAN 3 RANGE A BFS	Y		NM	BCD
V98*W*3956*C	TACAN TIME TAG BFS	Y		S	DPL
V99*U*3450*C	CLUSTER TO M50/IMU-1 COMPONENT 1,1	Y		ND	SPL
V99*U*3451*C	CLUSTER TO M50/IMU-2 COMPONENT 1,1	Y		ND	SPL
V99*U*3452*C	CLUSTER TO M50/IMU-3 COMPONENT 1,1	Y		ND	SPL
V99*U*3453*C	CLUSTER TO M50/IMU-1 COMPONENT 1,2	Y		ND	SPL
V99*U*3454*C	CLUSTER TO M50/IMU-2 COMPONENT 1,2	Y		ND	SPL

Figure 28. Typical Page from the STS-6 Computer Compatible Tape (CCT) Report for the NASA JSC MPDB

with precise definitions and their MSID numbers. Further definition of data characteristics (e.g., sample-rates, sensor locations, corrections for time skews, etc.) is also necessary. It is believed that documentation of this sort exists and efforts are being made to obtain it. However, in addition to documentation difficulties, discussions with programmers at DFRF have indicated that the JSC tapes are written in UNIVAC formats difficult to read on the DFRF Cyber computer. Some data tapes presently are available at DFRF and may be read onto the Cyber; however, it appears that these tapes do not have much of the data required for the OFQ.

4. Recommendations for Obtaining OFQ Data

An initial task for the OFQ, which should be accomplished as soon as possible is the assembly of the required flight data from the above sources into a form that may be used with high efficiency. It is anticipated that 'OFQ archive' files can be created for each flight beginning with STS-1 and made available on the DFRF Cyber computer. These files would be considered an important 'product' of the OFQ which could be used at DFRF or (through transmission over phone lines) at remote facilities. This would avoid the all too common situation in which flight test data, obtained at great expense, is either destroyed or becomes effectively unusable shortly after the original study.

It is proposed that these archive files be based on the DFRF MMLE files augmented with trajectory and wind data from the Ref. 19 work and the AFFTC theodolite data. Data from the JSC MPDB may be added as practical and as needed. The OFQ archive files can probably be limited to the region from $M \doteq 3$ to touchdown and rollout, at least initially. Figure 29 shows the envisioned generation and use of the archive files. The 'data merge' program must be developed, but it is believed that this could be an expansion of existing DFRF programs. It will be essential (but difficult) to have the important aspects of the OFQ files defined and documented (perhaps including basic documentation on the Cyber). This should include

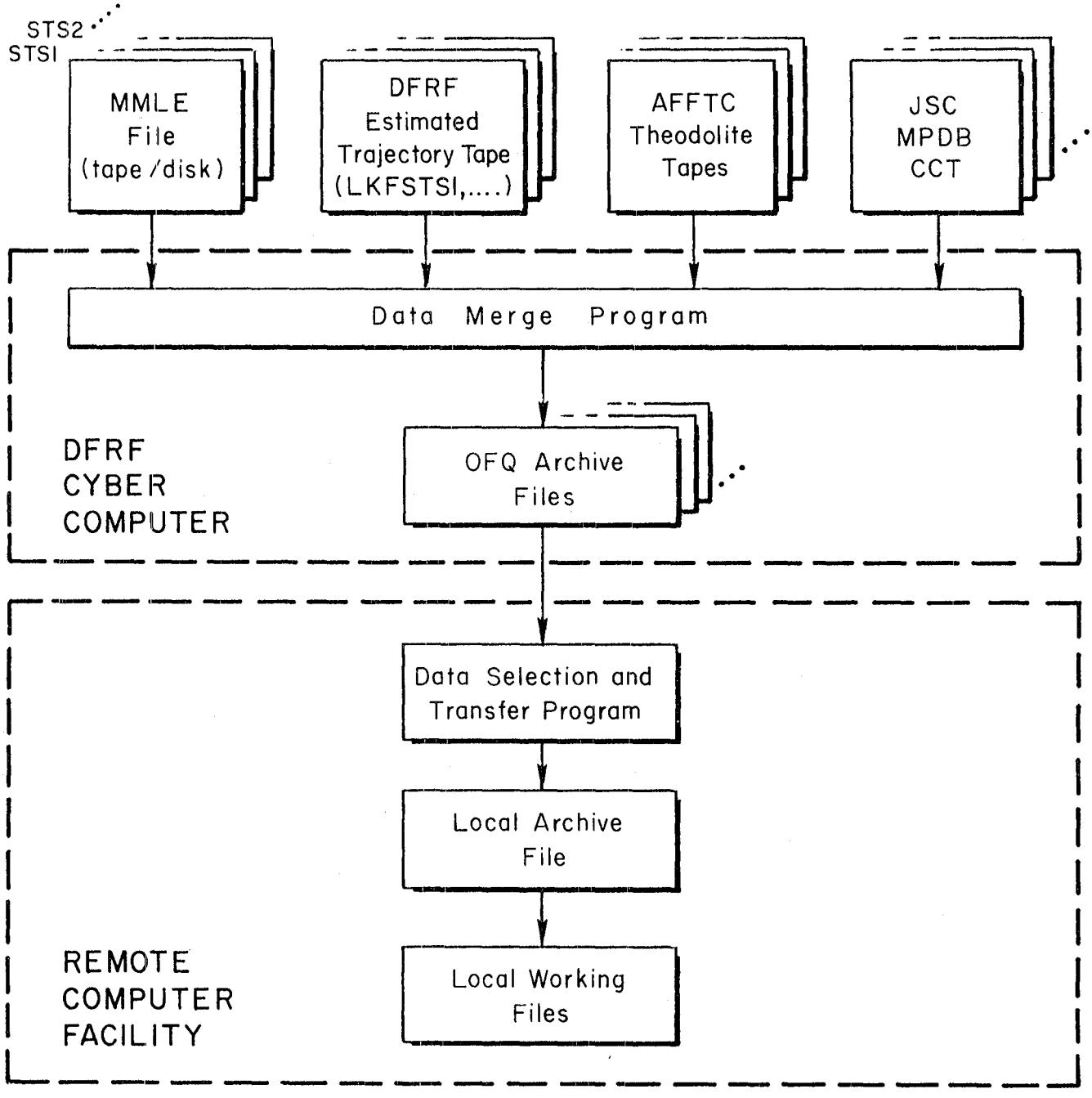

Figure 29. Generation and Use of the OFQ Archive Files

- definition of each variable with name, code, and MSID number when appropriate
- original data source (e.g., ACIP, etc.) and/or post flight processed source (e.g., MPDB, etc.)
- auxiliary information (sensor location, axis system, reference points)
- units
- data characteristics (sample rate, resolution, accuracy)
- applied processing (interpolation, filtering, time skew correction, bias corrections)

Reference 19 is perhaps the best model of the level of documentation desired. The archive files should be created for all flights beginning with STS-1 and continuing through the end of the OFQ.

SECTION III

CREW QUALITATIVE ASSESSMENTS

A key initial, and continuing, goal of this program has been to conduct in-depth, face-to-face debriefing interviews with the individual flight crews. Ideally the debriefing would take place as early as possible after each flight to discuss the events, maneuvers, etc., examined on the flight records, to solicit suggestions and recommendations concerning any additional flight segments requiring analysis, and to obtain commentary or pilot ratings pertaining to vehicle flying qualities and flight control system performance. In practice, this has not yet been successfully accomplished for several reasons. One pertains to the many responsibilities, complex schedules, and general NASA sequestering of the crews which make it difficult to gain access for in-depth interchange. Others pertain to the time lapse between the flight, the availability of flight traces suitable for flying qualities analysis, and the actual analysis of the flight records.

It has therefore been necessary, to date, to extract possible flying qualities information from crew comments volunteered in the general systems debriefing held at the Johnson Spacecraft Center (JSC) or in other press releases (e.g., Aviation Week and Space Technology). This information is then used to help interpret the flight traces (as in the previous section) and to formulate a detailed questionnaire which will be used to guide the actual flying qualities debriefing when, or if, it should come to pass.

The following subsection summarizes the key comments obtained from the STS-5 and -6 systems debriefings and associated press releases. Similar information from STS-1 through -4 is contained in Ref. 2. The second subsection outlines considerations which led to the latest version of the questionnaire for crew in-depth debriefing. The revised questionnaire is contained in Appendix B.

A. STS-5 AND -6 CREW COMMENTARY

1. STS-5

This entry and landing was initially planned to be flown essentially all automatic (autoguidance and autoland). Per Ref. 21, very brief periods of manual control were scheduled during the steep approach (outer glideslope) segment to provide the crew with a "feel" of the aircraft in case they had to take over manually during the autoland segment. The guidance system incorporated the new Optional Terminal Area Targeting program which provided a "shrinking" Heading Alignment Cone (instead of cylinder) for improved energy control during the descending turn. A computer graphics generated "shrinking HAC" was displayed on a CRT to augment the flight director needle display. This flight was also the first to use the "ball/bar" Precision Approach Path Indicator (PAPI) on the ground to insure proper execution of preflare and final glide. The external visual view is that the "ball" will approach a bar of lights at a specific rate if the approach is being flown properly. The aircraft commander (Brand) views the external reference while the pilot (Overmyer) calls out altitude and airspeed. Thus the new aids were planned to assist the crew in their primary function of monitoring performance of the autoguidance and autoland systems.

A few weeks before launch the above plan was revised, because of unresolved discrepancies in autoland performance between the mission simulator and shuttle training aircraft, to allow manual control from about Mach 1 on to touchdown. The landing was also rescheduled from the lakebed to the EAFB runway 22 due to moisture on the lakebed.

In the STS-5 Systems Debriefing at the JSC, Brand indicated that he waited until about 0.85 M (and 40,000 ft) to take over manually due to a very pronounced shaking of the aircraft from Mach 1 to 0.85. Specific comments covering the manually controlled descent and terminal phase included:

> "at 30 to 40,000 ft the orbiter handling qualities are very pleasant"

"Shuttle felt 'crisper' than the STA"

"Easy to follow the error needles" (during the HAC; 275 Kt and 1.6 g)

"The handling of the orbiter during preflare and flare felt like the STA... The STA is a good trainer for manual landings"

"It is good to fly the airplane from Mach 1 to landing as this gives continuous experience with the aircraft so that the pilot is comfortable flying it by preflare"

"...would hate to take over at 300 ft"

Brand indicated he mostly looked out the window after they broke through the cloud deck (on steep glideslope)... that the ball-bar indicator is a good aid for doing the preflare... that he had no problem knowing how much input to put in at the preflare (which he contrasted to Mattingly's uncertainty on STS-4 where the ball-bar was not available). The landing gear was lowered at 400 ft altitude instead of the originally prescribed 200 ft (presumedly to minimize workload and/or perturbation during the final flare). Brand indicated he paid no attention to the roll needle while on final -- (Overmyer) called out airspeed and altitude -- (Brand) thought they were still 3-4 ft above the runway when the main gear touched down.

In summary, the general impression obtained is that attitude control and flight director tracking is precise and relatively easy in the Shuttle. However, as the vehicle nears the surface and the crew becomes concerned with precise flight path control, the task becomes quite demanding, external visual aids are high desirable, and any path corrections, disturbances, or configuration changes during the last few seconds of final glide and flare can be troublesome.

2. STS-6

This was the first flight of Challenger, the second vehicle. It incorporated a Head-Up-Display (HUD) with improved visual information for the terminal phases of flight. This was flown manually from the

Heading Alignment Cone (HAC) through touchdown (Ref. 22). The landing was again made on the EAFB runway 22 due to the lakebed being covered with water.

The pilot (Bobko) commented in the systems debriefing that it had been their experience in the STA that if the orbiter got off the nominal trajectory in the HAC turn it was impossible to get back on nominal track using the HUD alone. Thus it was their strategy to use the HUD as another piece of information, not as a sole guidance source. The commander (Weitz) said that he flew the (head down) flight director error needles rather than the HUD.

The HUD is also useful on the steep glide slope along with the flight director needles and out-the-window visual aids. White triangular markings that correspond to steep glide slope intercepts are placed on the ground (Ref. 14). According to the report of the debriefing the crew was told to use the high-wind, close-in aim point. This caused some confusion in that the crew was not sure whether or not the HUD guidance was displaying the high wind or nominal aim point. Weitz said that the HUD aim point was not where he expected it to be, and Bobko said it is not an easy task to decide where the aim point should be if the marker on the ground is not visible. (The lakebed aim point marker was washed out or covered with water.) Weitz found that the relationship between the HUD aim point and the PAPI light location was not as he was expecting, but by preflare the aim point looked good. He also said the HUD helps a lot from 2,500 ft on down. The HUD displays among other things (Ref. 23) pitch and roll attitude, reference flight path, velocity vector, altitude, airspeed, cross track error, and speed brake position.

The commander (Weitz) said that he did not fly the HUD tightly, that is he did not tighten his gains to the point of putting the velocity vector on the guidance diamond and used the "normal" inside cockpit scan (Ref. 22).

The crew said that the orbiter flew through gusts at 4,000 ft and again at 400 ft, and that it was unresponsive to the gusts. Weitz said

that no pilot inputs were required as a result of these gusts. Overall, Weitz said that the "subsonic handling qualities were more crisp than he was expecting... there was no sloppiness or overcontrol tendencies... the orbiter was a good, solid, nice flying machine... he had no recommendations for manual flight control improvements."

B. REVISED CREW INTERVIEW/DEBRIEFING QUESTIONNAIRE

The format of the initial questionnaire (Refs. 1 and 2) were devoted solely to vehicle flying quality considerations. As our understanding of the uniqueness of superaugmented vehicle dynamics has increased and with the additional experience gained on each Shuttle flight has concluded, it has become increasingly apparent that

a) each flight (landing) has been unique in terms of

   -- manual vs. auto control of various segments of the approach and landing,

   -- ground and airborne visual aids available to the pilot, and therefore

   -- closed loop strategy and techniques available to and employed by the crew, and

   -- pilot training, background, and experience in flying qualities evaluation

b) we often do not know how to intepret crew comments and/or what we see in the flight traces

Therefore the crew interview/debriefing questionnaire needed to be rearranged and expanded into two sections (see Appendix B). The first covers crew perception of the control tasks and flying techniques in each entry flight segment. This includes identification of closed loop structure employed, strategy in transitioning from one flight segment to another or from one closed loop structure to another, tasks which were performed on a precognition basis (i.e., highly trained, open loop reaction), etc. The second section covers crew evaluation of the Shuttle dynamic response, workload, and flying qualities associated with the perceived control tasks. In both sections five flight segments are addressed:

-- Supersonic bank reversals

-- Heading alignment circle or cone (HAC) turn

-- Descent on the steep glide slope

-- Preflare

-- Shallow glide and final flare to touchdown

The information obtained from the first section will be directly applicable in modeling the pilot/vehicle control loop structure and extraction (via the identification techniques previously discussed in Section II) of model parameters, pilot adaption (or settling) time, etc. The information from the second section should provide qualitative and quantitative data, together with data extracted from flight trace analysis, from which to establish flying quality and/or flight control criteria and design guides for future Shuttle craft.

SECTION IV

HAND CONTROLLER EXPERIMENT

It was noted in Ref. 1 that the Shuttle Rotational Hand Controller (RHC) force/displacement characteristics differed drastically from those considered to be acceptable-to-good in past in-flight simulations (Refs. 24 and 25). The Shuttle RHC exhibits much greater displacement per unit applied torque than the largest ratio tested in Ref. 24 while the motion response command per unit torque was much lower. Concern was expressed in Ref. 1 that these characteristics might contribute to degraded flying quality ratings and also might lead to a larger effective time delay (latency) within the pilot's neuromuscular system. [It was shown in Ref. 26 that loose vs. stiff manipulator force/displacement characteristics have a significant influence on the human operator effective time delay in a tracking task.]

Later it became apparent that the RHC force/displacement characteristics presented in Ref. 1 represented the ALT vehicle. Information contained in Ref. 27 indicated these RHC pitch and roll force gradients were considered undesirable, a possible contributor to the PIO experienced in the ALT-5 landing, and were doubled for the OFT vehicles. However, it may be noted from Fig. 30 that there is still a very large discrepancy between the force/displacement and response/force ratios of the OFT and those considered acceptable in the Ref. 24 flight tests.

A simple experiment was proposed in Ref. 2 to quantify any difference in pilot time delay induced by the OFT RHC and a manipulator exhibiting supposedly "good" characteristics. It is based upon the STI developed Critical Instability Tracking Task (CITT) in which the operator attempts to stabilize a controlled element having a steadily increasing divergence. The experiment was further detailed as a part of this Phase III effort and preliminary runs were accomplished at the DFRF by DFRF personnel. The following subsection briefly describes the theory behind the measurements, the experimental plan, and results which

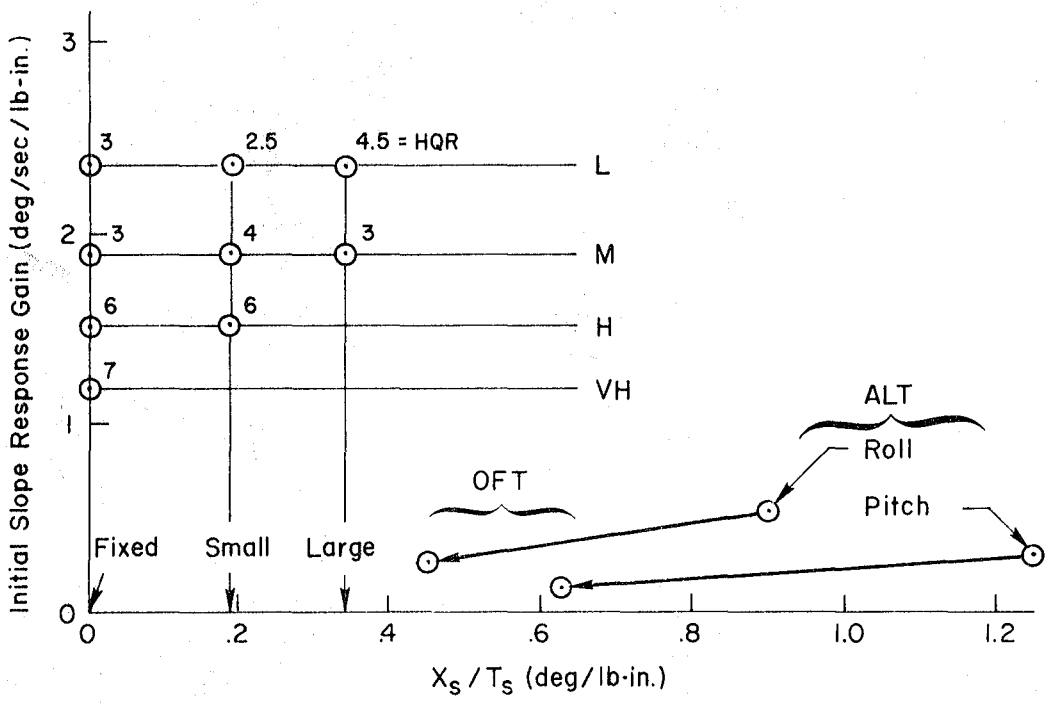

Figure 30. Shuttle Orbiter RHC Feel/Command Gradient Characteristics in Landing

lead to the conclusion that the Shuttle RHC configuration and force/displacement characteristics are such that they increase the pilot's neuromuscular time delay.

A. KEY CONCEPTS FOR ASSESSING SENSITIVITY TO TASK VARIABLES

Operational manual control systems are typically designed to require far less than the pilot's ordinary limiting capabilities. Therefore performance decrements due to task variables such as manipulator or display dynamics are seldom observed except for extreme values of the variables. However, skill-factor decrements due to task variables do become apparent when the pilot is near his limiting performance. Thus intrinsic skill limits can be measured only under high task-induced stress conditions which push the pilot to his limits.

Particular control tasks can be designed to emphasize particular skill factors. The Critical Instability Tracking Task is specifically designed to measure the lag induced into a closed loop control task by

the pilot. The task is shown in block diagram form in Fig. 31a (from Ref. 28). The output of a first order divergent controlled element is displayed to the operator as an error. The operator attempts to stabilize the divergence through application of a force (and/or displacement) to a manipulator. The divergence inverse time constant, λ, is increased as a function of time and error magnitude until the operator can no longer maintain control. The λ value at loss of control is the critical instability, λ_c, which is approximately the inverse of the dynamic delay, τ_e. Typical time traces of the rate of λ increase and the various motion quantities are shown in Fig. 31b.

The reason for the difference in pilot lag contribution with a stiff (force) vs. a free (position) manipulator may be observed from the detailed block diagram of operator dynamic elements shown in Fig. 32 (from Ref. 29). On the right side of Fig. 32 it may be observed that the neuromuscular actuation system has two feedbacks. One is via the force sensing spindle/tendon organ ensembles directly to the spinal cord where the error signal in generated to further control the muscle. The second feedback path is via the proprioceptive (joint) receptors which sense the various joint angles. This information is fed back to the central system (brain) for integration and equalization and generation of a new motorneuron command which then progresses back down the spinal cord as a command to the spindle/tendon ensemble. Thus the neuromuscular actuation system consists of an inner, force, servo system and an outer, position, servo system. The inner loop inherently has less delay than the outer loop.

Typical differences in critical instability with different types of manipulator restraint and controlled element complexity are shown in Fig. 33 (from Ref. 30). The upper plot is for a controlled element consisting of a divergent first order lag. The middle plot is for a second order controlled element consisting of an integration and first divergence. The bottom data point is for a third order controlled element consisting of a double integration and first order divergence. It can be seen from Fig. 33 that the critical instability (pilot lag) is influenced most by task order and secondarily by manipulator characteristics. However, manipulator characteristics become more significant as

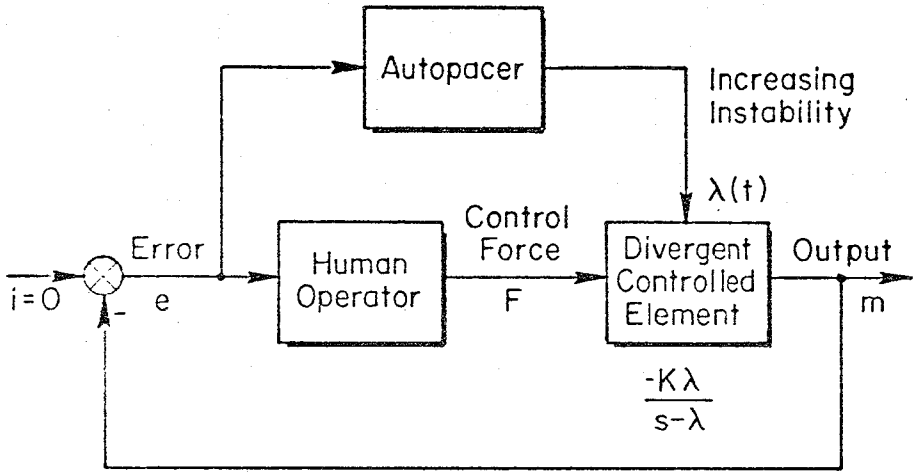

Concept:

$\lambda(t) \rightarrow \lambda_c$, the "Critical Instability"

Interpretation:

$$\text{Critical Instability} \approx \frac{1}{\text{Dynamic Delay}}$$

$$\lambda_c \approx 1/\tau_e$$

a) Block Diagram

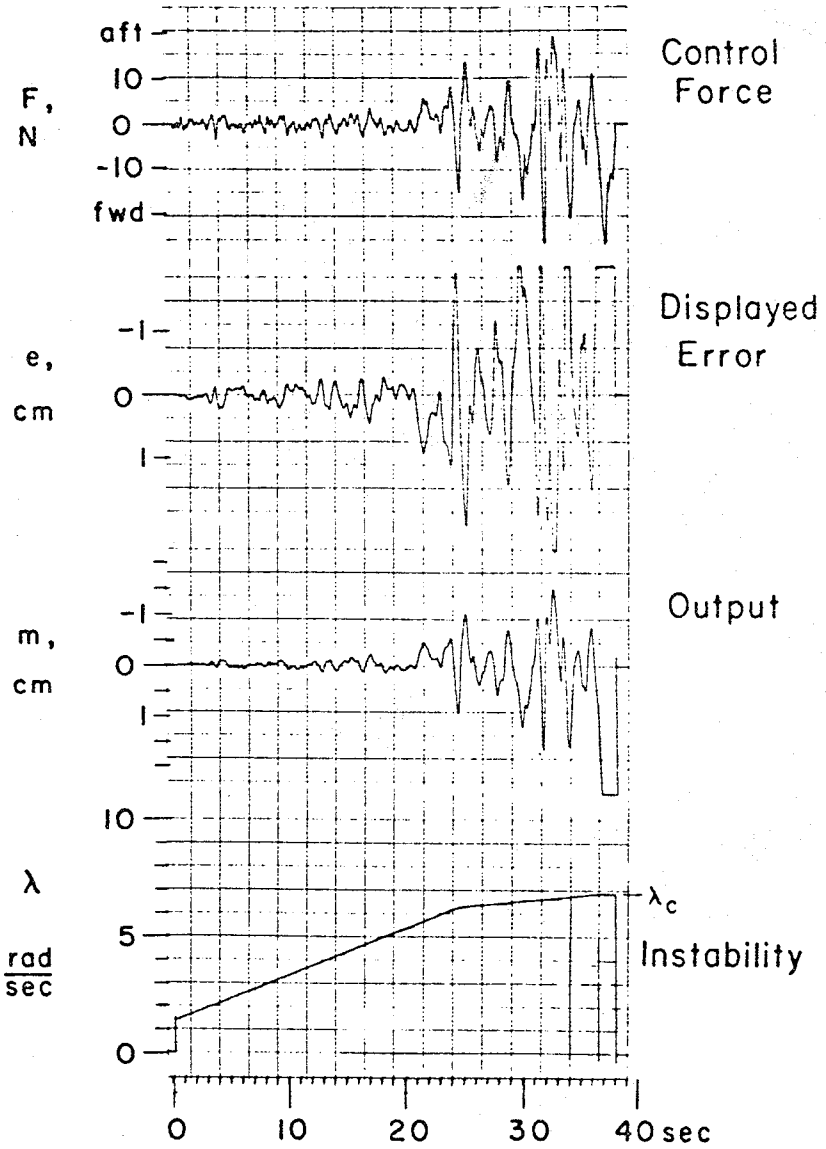

b) Typical Trial

Figure 31. The "Critical-Instability" Task (First Order)

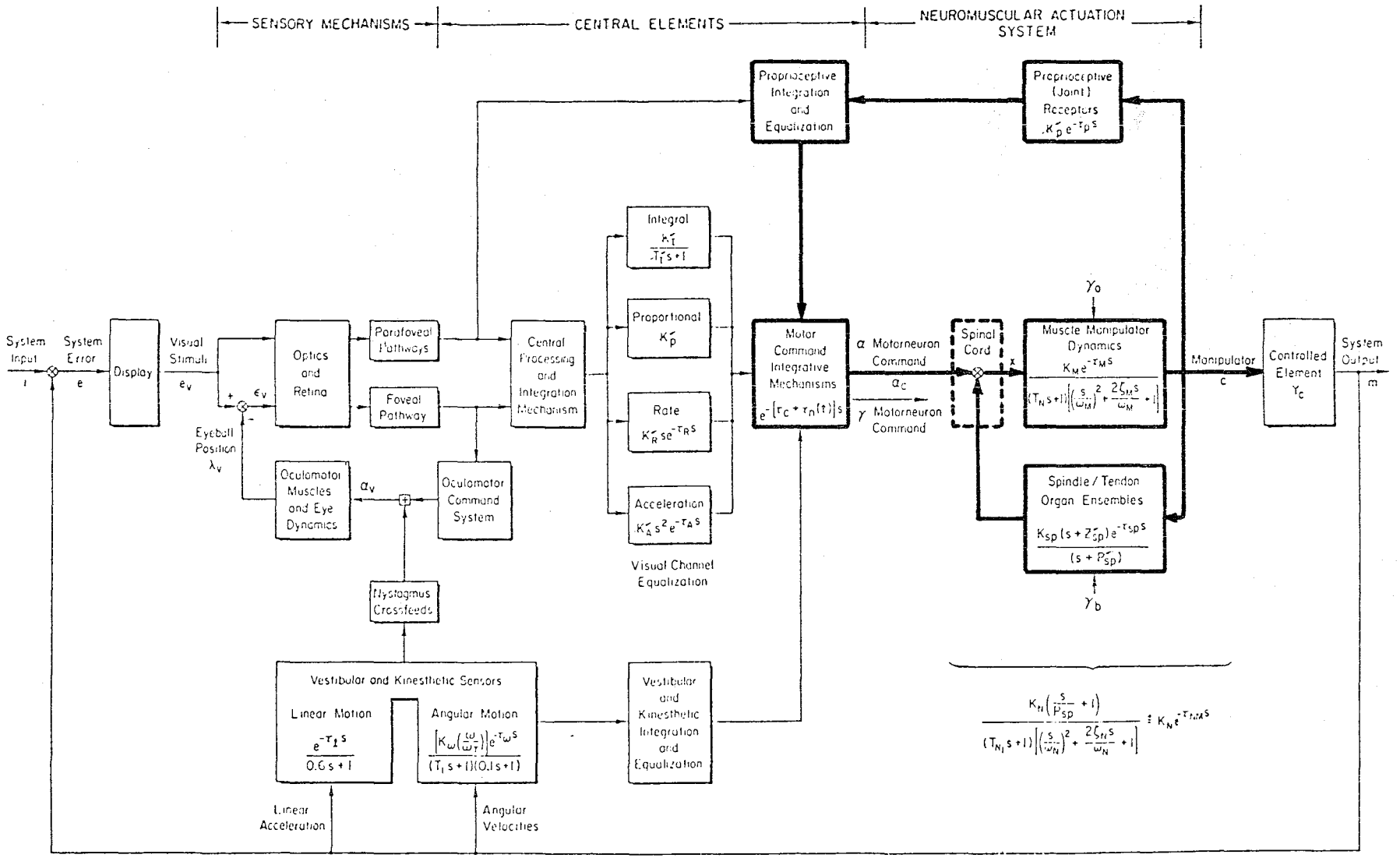

Figure 32. Structural-Isomorphic Model of Pilot-Aircraft System

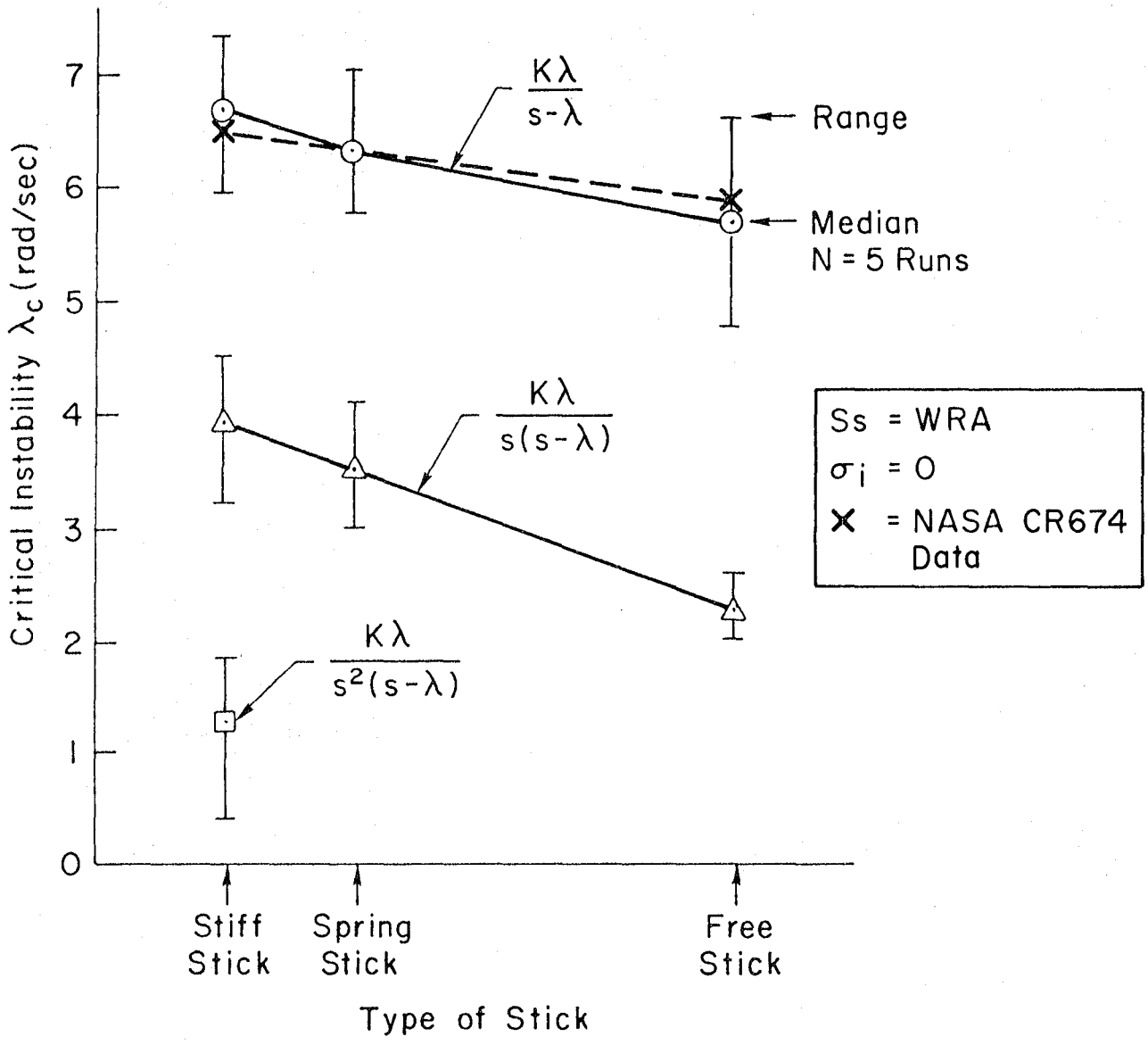

Figure 33. Critical Instability vs. Type of Control Stick

the task order increases. The λ_c decreases approximately 1 rad/sec ($\Delta\tau_e \doteq 0.025$ sec) between the stiff and free stick configurations for a first order critical task. With the second order critical task the λ_c decreases about 1.8 rad/sec ($\Delta\tau_e \doteq 0.205$ sec).

B. EXPERIMENTAL PLAN

The initial intent of the experiment was to compare the Shuttle RHC with a sidestick configuration given good (HQR = 3) ratings in the Ref. 24 flight test. The only stick available for comparison was from the DFRF fixed base simulation cockpit and, unfortunately, the gradient adjustment range was insufficient to achieve the desired values. The maximum gradient achievable remained quite close to that of the Shuttle RHC. Therefore, the tactic adopted was to adjust the DFRF stick breakout and gradient to "best" values for this experimental task as judged by DFRF research pilots. These values were somewhat different from the Shuttle RHC and did provide for some comparison.

Possibly of greater significance, the geometric characteristics of the two manipulators were quite different. The Shuttle RHC configuration is approximately that shown in Fig. 34. The pitch axis pivot point is at the middle of the hand palm. The roll axis pivot is about five inches below the pitch pivot. Thus deflection of the RHC is accomplished by wrist movement. Stop to stop deflection (exclusive of an override) is ±19.5 deg in each axis. The DFRF simulation stick is fairly conventional with the pitch and roll pivot points roughly a foot below the grip. The stop to stop deflection was ±2 in. in both axes, therefore the hand grip displacement was considered to be mostly longitudinal or lateral translation and involved arm, rather than wrist, motion.

In both cases the manipulator grip was centered in front of the pilot.

A block diagram of the experimental setup is shown in Fig. 35. The Shuttle RHC electrical output was processed through its basic digital flight control system computation and shaping elements and extracted

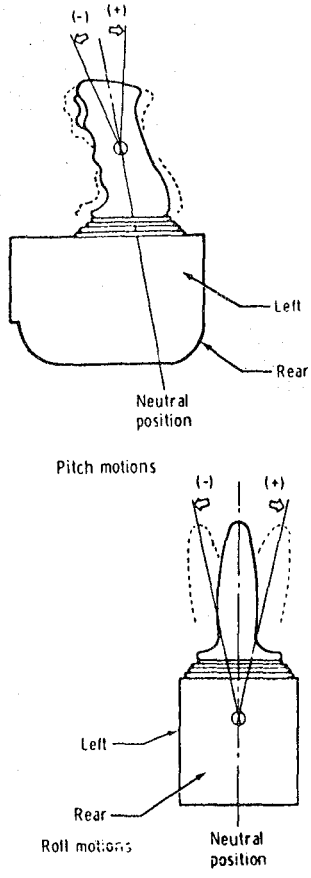

Figure 34. RHC Configuration

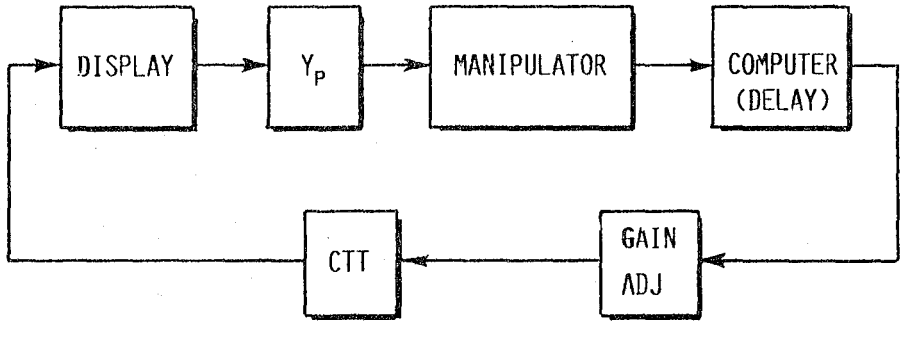

Figure 35. Manipulator Experiment Set-Up

from the computer as a pitch or roll rate command. This digital computation introduced an effective time delay of 0.046 sec. To keep the experiment focussed on manipulator characteristics, a similar time delay was inserted between the DFRF simulation stick output and the input to the critical task test unit. A gain adjustment was placed between the computer output and the CTT for proper electrical scaling.

The tracking task was single axis, e.g., pitch or roll independently, using the first order instability:

$$Y_C = \frac{K\lambda}{s - \lambda}$$

Five test subjects were employed. After initial task familiarization and training, each was given five groups of three trials with each manipulator. The critical instability, λ_c, scores were recorded at the conclusion of each trial and the subjects were challenged to make the highest possible scores.

C. RESULTS

The experiment was accomplished on a non-interference basis with the subjects normal workload and the simulator schedule. Therefore the training sessions for some configurations were somewhat shorter than desired and learning effects were noted in 5 of 20 sessions as a general increase in λ_c scores through the 15 trials. However, the impact on overall results is considered to be minor.

Mean and 1σ λ_c scores for the pitch axis task are shown in Fig. 36. The L above a score identifies sessions where learning was evidenced throughout the 15 tasks. Figure 36 shows 4 of the 5 subjects had better scores with the conventional stick but this could have ended as 3 of 5 if subject 2 had more training with the Shuttle RHC.

Mean and 1σ λ_c scores for the roll axis are presented in Fig. 37. Again 4 of 5 show better scores for the DFRF stick but this could have been 3 of 5 if learning had levelled off.

It might be observed that the scores obtained in this experiment are lower than those of Fig. 33. This is because of the 0.046 sec

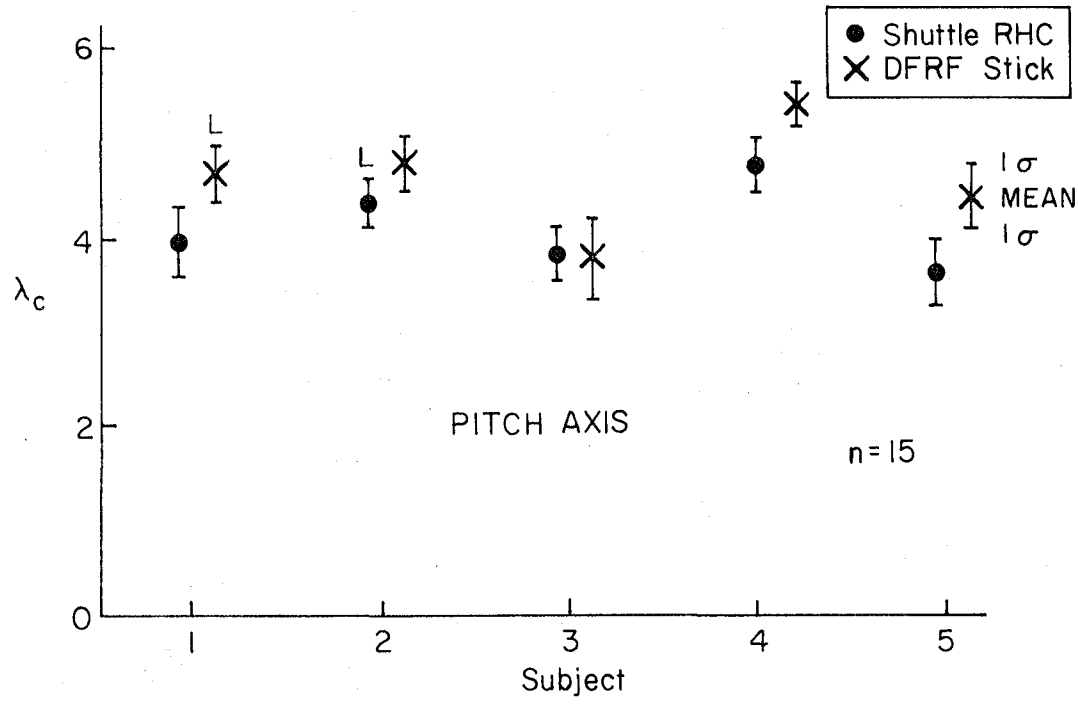

Figure 36. Pitch Axis CCT Raw Scores

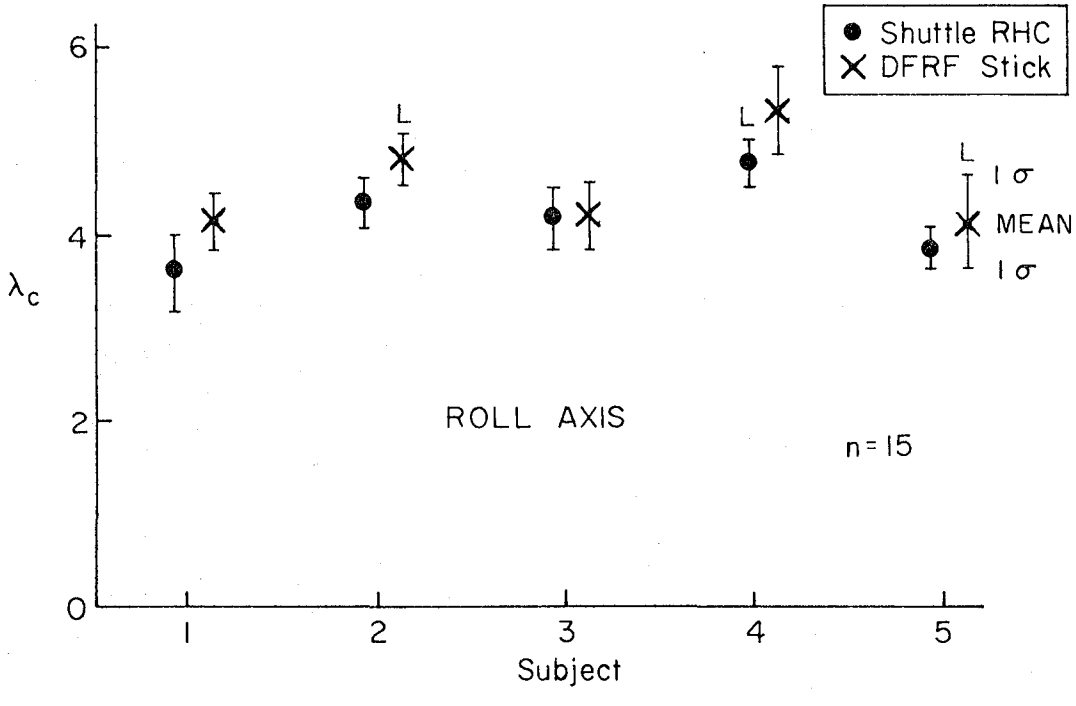

Figure 37. Roll Axis CCT Raw Scores

computational time delay which became a part of the controlled element dynamics. The effective controlled element dynamics seen by each test subject was

$$Y_e = \frac{K_\lambda e^{-0.046s}}{(s - \lambda)}$$

This could be expected to place the scores somewhere between the first and second order critical tasks of Fig. 33.

The effective pilot latency with the computational delay, τ_d, removed is

$$\tau_p = \frac{1}{\lambda_c} - \tau_d$$

The average values calculated across the five subjects (Figs. 36 and 37) are presented in Fig. 38. These show the Shuttle RHC resulted in increased pilot latency (delay) of about 25 millisec in pitch and 20 millisec in roll. This may be due to the RHC force/displacement characteristics, the wrist type motion, or both.

With the computational time delay removed as above, the resulting τ_p values can be compared with the inverse of first order critical instability task scores from Fig. 34. This is done in Fig. 39 and shows the DFRF simulation stick to result in pilot neuromuscular lags comparable to the unrestrained (free) stick configuration of Ref. 26. Again the Shuttle RHC fares somewhat worse.

D. CONCLUSIONS

It is concluded on the basis of this preliminary experiment that the Shuttle RHC may be inducing extra lag in the pilot because of its force/displacement characteristics, wrist action pivot point location, or both. The difference in this experiment is about 0.020-0.025 sec more delay in each axis with the Shuttle RHC.

The experiment has demonstrated that the simple CTT approach can measure the influence and could be employed as one task in optimizing manipulator characteristics for future shuttlecraft.

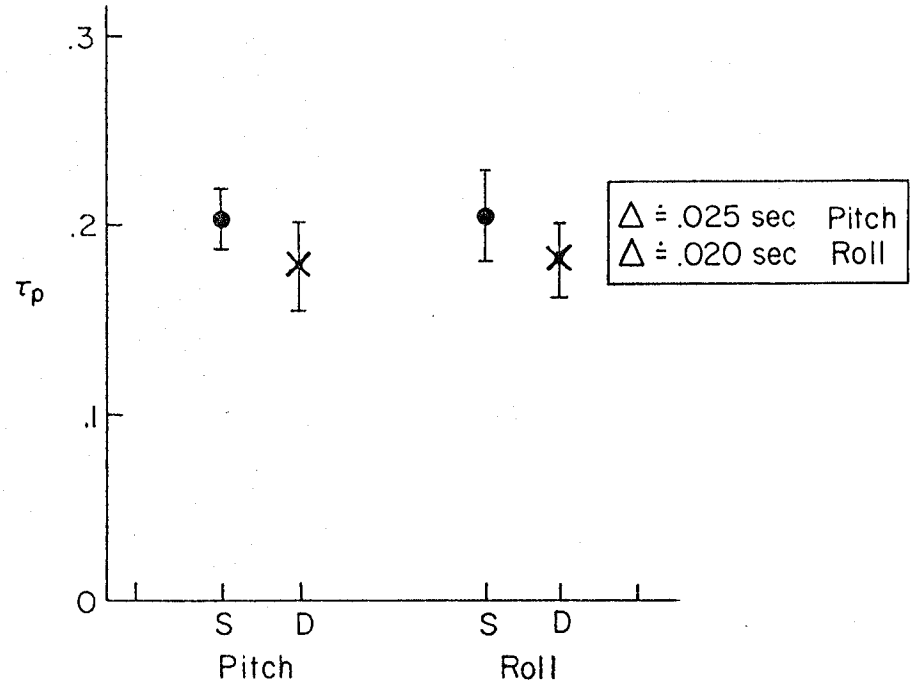

$$\tau_p = \frac{1}{\lambda} - \tau_d$$

Figure 38. Effective Pilot Latency; Shuttle vs. DFRF Simulation Controller

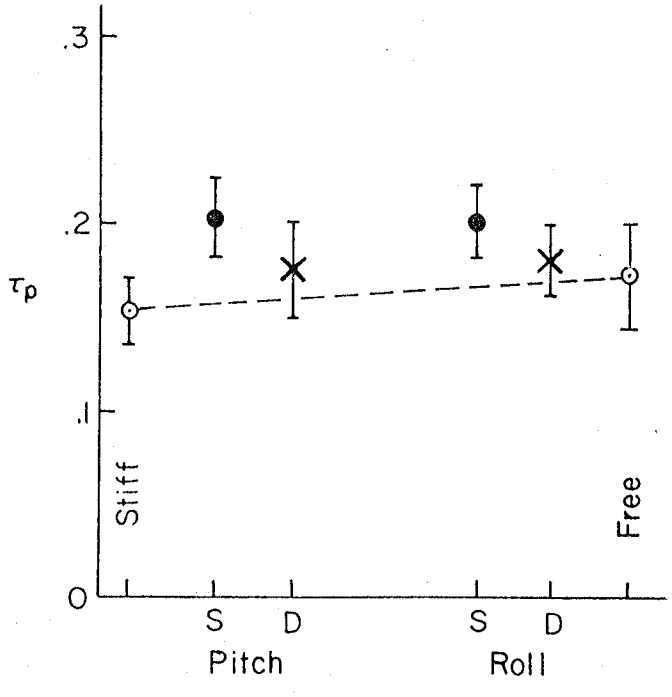

Figure 39. Comparison of Experimental Results with Free and Stiff Manipulator Data of Reference 30

SECTION V

RESULTS, CONCLUSIONS, AND RECOMMENDATIONS

A. MAJOR RESULTS

- Shuttle flight data (STS-4) has been transferred over telephone lines from the DFRF Cyber computer to the STI PDP-11 computer for analysis. This procedure has proven practical and efficient.

- The superaugmentation model has been used to study the identification of the effective augmented pitch response of the Shuttle and explain results obtained from (STS-4) flight data.

- Identification of the effective Shuttle pitch response in landing from STS-4 flight data has been performed using a spectral method (the FREDA program) and also by use of the NIPIP program.

- The pilot-vehicle-task model for shallow glide and final flare developed in Phase II has been refined based in part on flight data analysis.

- The altitude-sinkrate phase plane method has been further developed and applied to the STS-4 flight data. It has been possible to extract pilot-vehicle-task parameters, in particular, γ_0 and T_f for STS-4.

- An attempt has been made to use the NIPIP program for pilot model identification but satisfactory results have not been obtained. This is due in part to procedural complications and data uncertainties for this application, but progress has been made in developing modified procedures (e.g., use of the w′ transformation).

- A number of data problems and needs have been uncovered in the flight data analysis effort which need to be resolved for the OFQ. The most critical of these is the need for better altitude and sinkrate data in landing.

- Several additional sources of data (beyond the MMLE files) have been investigated and appear to be applicable to resolve the data problems. These include the AFFTC cinetheodolite tapes, the Kalman filtered BET data from DFRF, and the JSC Master Products Data

Base. Additional work is needed to access these sources.

B. CONCLUSIONS

- The effective augmented vehicle identification effort provides support for the superaugmentation model and, in particular, indicates that the effective attitude lead is $(1/T_q)$ rather than $(1/T\theta_2)$. The approximate time-invariance of the q/qc response in the preflare through touchdown region has been verified.

- Normal pilot RHC activity in landing apears to be adequate for identification purposes. This indicates the feasbility of the indirect non-intrusive OFQ approach proposed in Phase II.

- The NIPIP program appears to be capable of vehicle identification from flight data.

- Examination of the STS-4 time histories (in particularly the RHC trace) indicates (expected) variations in pilot technique among landing flight segments, discrete RHC inputs to transition between segments and pulsive RHC inputs in shallow glide and final flare.

- The form of the STS-4 altitude sinkrate phase plane trajectory is consistent with the Phase II shallow glide and flare pilot-vehicle-task model. The initial conditions, h_o and h_f, are lower than the 'nominal' values estimated in Phase II, but when STS-4 initial conditions are inserted in the model the results are consistent with the γ_o and T_f values extracted from the phase plane analysis. The oscillatory nature of the h-$\dot{h}$ trajectory indicates pilot difficulty in accomplishing the landing.

- Procedures for pilot model identification with NIPIP needs further refinement and h-$\dot{h}$ phase plane analysis should be used for guidance in NIPIP model formulation.

- The CTT experiment has demonstrated that this simple simulation approach can measure the influence of different manipulators and could be employed as one task in optimizing manipulator characteristics for future Shuttlecraft.

- The Shuttle RHC may be inducing extra lag in the pilot because of its force/displacement characteristics, wrist action pivot point location, or both.

The difference in this experiment is about 0.020-0.025 sec more delay in each axis with the Shuttle RHC.

C. RECOMMENDATIONS FOR OFQ

- First priority should be given to bringing the required flight data sources together into documented OFQ archive files on the DFRF Cyber. Before any data is formally analyzed, data checks for consistency (e.g., altitude from radar, IMU, barometric and theodolite sources), biases, calibration, etc., should be made with adjustments, filtering, etc., made as required.

- Vehicle identification should be performed for all flights to develop an ensemble average for q/δ_{RHC}. Both FREDA and NIPIP should be used to gain further experience with NIPIP in flight data applications.

- Altitude/sinkrate trajectories should be generated and analyzed for each flight with emphasis on pilot technique variations among flights. The pilot model should be refined as required.

- The pilot-vehicle-task model for landing should be implemented as a simple digital simulation (STI PDP-11 or Apple). A primary use of this simulation would be to analyze NIPIP pilot identification problems and procedures using a known pilot model.

- When preliminary work has been done, pilot identification efforts with NIPIP should be continued for each flight.

This Page Intentionally Left Blank

REFERENCES

1. Myers, Thomas T., Donald E. Johnston, and Duane McRuer, Space Shuttle Flying Qualities and Flight Control System Assessment Study, NASA CR-170391, Dec. 1981.

2. Myers, T. T., D. E. Johnston, and D. T. McRuer, Space Shuttle Flying Qualities and Flight Control System Assessment Study, Phase II, Systems Technology, Inc., TR-1187-1, Dec. 1982.

3. McRuer, D. T. and E. S. Krendel, Mathematical Models of Human Pilot Behavior, AGARDograph No. 188, Jan. 1974.

4. Hess, Ronald A., "A Rationale for Human Operator Pulsive Control Behavior," J. Guidance and Control, Vol. 2, No. 3, May-June 1979, pp. 221-227.

5. Systems Technology, Inc., "Flying Qualities and Control System Alternatives for Superaugmented Aircraft," NAS2-11388.

6. Aerodynamic Design Data Book, Orbiter Vehicle, Rockwell International, Report SD72-SH-0060, Vol. 1, Nov. 1980.

7. Hoey, Robert G., et al., AFFTC Evaluation of the Space Shuttle Orbiter and Carrier Aircraft -- NASA Approach and Landing Test, AFFTC-TR-78-14, May 1978.

8. Magdaleno, R. E., The STI Frequency Domain Analysis Routine (FREDA), Systems Technology, Inc., WP-407-2, June 1978.

9. Hanson, Gregory D. and Wayne F. Jewell, Non-Intrusive Parameter Identification Procedure User's Guide, NASA CR-170398, Apr. 1983.

10. Bendot, Julius S. and Allen G. Piersol, Engineering Applications of Correlation and Spectral Analysis, John Wiley & Sons, NY, 1980.

11. Mooij, H. A., W. P. de Boer, and M. F. C. Van Gool, Determination of Low-Speed Longitudinal Maneuvering Criteria for Transport Aircraft with Advanced Flight Control Systems, National Aerospace Lab., NLR TR 79127 U, Dec. 1979.

12. Requirements/Definition Document, Flight Control, Part 1 Configuration Performance and Functional Requirements, Report SD72-SH-0105, Vol. 1, Book 2, Part 1A, July 1977.

13. Heffley, Robert K., Gregory D. Hanson, Wayne F. Jewell, and Warren F. Clement, Analysis of Pilot Control Strategy, NASA CR-170399, Apr. 1983.

14. Tsikalas, G. M., "Space Shuttle Autoland Design," AIAA Paper 82-1604-CP, Aug. 1982.

15. Stapleford, Robert L., Irving L. Ashkenas, Graham Dunstan, John J. Best, and J. Alfred Tennant, Analysis of Several Handling Quality Topics Pertinent to Advanced Manned Aircraft, AFFDL TR-67-2, June 1967.

16. Whitbeck, R. F. and L. G. Hofmann, "Digital Control Law Synthesis in the w' Domain," J. Guidance & Control, Vol. 1, No. 5, Sept-Oct. 1978, pp. 319-326.

17. Preliminary Analysis of STS-4 Entry Flight Data NASA TM-81375, Sept. 1982.

18. "Final Analysis Output Progam (FALOUT)," Kentron International, Inc., Memo. No. K4E-007B-81, 10 Dec. 1980.

19. Whitmore, Stephen A., "Reconstruction of the Shuttle Reentry Air-data Parameters Using a Linearized Kalman Filter," NASA DFRF proposed Technical Paper, 1983.

20. "Master Products Data Base," NASA Johnson Space Center DDC Accession No. Z06-5-000515, 21 Mar. 1983.

21. Covault, Craig, "Liftoff Time Pivotal to Shuttle Events," Aviation Week and Space Technology, Vol. 117, No. 8, Nov. 1, 1982, pp. 57, 59, 61-63.

22. Covault, Craig, "Shuttle 6 Reentry Aids Program Data Base," Aviation Week and Space Technology, Vol. 118, No. 16, 18 Apr. 1983, pp. 18-20.

23. Looney, B. J., "Post-DETAC HUD Monitor Description," Sperry Autoland Memo 57, 4 Nov. 1980.

24. Hall, G. Warren and Rogers E. Smith, Flight Investigation of Fighter Side-Stick Force-Deflection Characteristics, AFFDL-TR-75-39, May 1975.

25. Black, G. Thomas and David J. Moorhouse, Flying Qualities Design Requirements for Sidestick Controllers, AFFDL-TR-79-3126, Oct. 1979.

26. McDonnell, J. D. and H. R. Jex, A "Critical" Tracking Task for Man-Machine Research Related to the Operator's Effective Delay Time. Part II: Experimental Effects of System Input Spectra, Control Stick Stiffness, and Controlled Element Order, NASA CR-674, Jan. 1967.

27. Hartsfield, Henry W., "Space Shuttle Orbital Flight Testing," Society of Experimental Test Pilots 22nd Symposium Proc., SETP Technical Review, Vol. 14, No. 2, 1979, pp. 11-20.

28. Sadoff, M. E., D. T. McRuer, and H. R. Jex, "Human Transfer Function and Dynamic Response Properties During Extended Orbital Flight," Systems Technology, Inc., WP-175-19A, presented at NASA-Ames/National Academy of Sciences Experiment Jury, 14 Oct. 1970.

29. McRuer, D., "Human Dynamics in Man-Machine Systems," Automatica, Vol. 16, May 1980, pp. 237-253.

30. Jex, H. R. and R. W. Allen, "Research on a New Human Dynamic Response Test Battery," 6th Annual Conference on Manual Control, 7-9 Apr. 1970.

This Page Intentionally Left Blank

APPENDIX A

DERIVATION OF NIPIP ESTIMATION EQUATION FOR THE SHALLOW GLIDE AND FLARE MODEL

Simplifying notation

$$Y_{p_\theta}(s) = \frac{K_{p_\theta}(1/T_L)e^{-\tau_o s}}{(1/T_I)(1/\Delta\tau)}$$

$$\equiv \frac{K_\theta(\nu)e^{-kTs}}{(\alpha)(\beta)}$$

$$\delta(s) = Y_{p_\theta}\left\{Y_{p_{\dot{h}}}[\dot{h}_c - \dot{h}] - \theta\right\}$$

$$= \frac{K_{\dot{h}}K_\theta(\nu)[\dot{h}_c - \dot{h}]e^{-kTs}}{(0)(\alpha)(\beta)} \quad \frac{K_\theta(\nu)\theta e^{-kTs}}{(\alpha)(\beta)}$$

From the Z transform table, Smith, J. A., Mathematical Modeling and Digital Simulation for Engineers and Scientists, John Wiley & Sons, NY, 1977, p. 100.

$$\delta(Z) = \frac{K_{\dot{h}}K_\theta}{\alpha\beta}\left\{\frac{\nu Z}{Z-1} + \frac{\beta(\nu-\alpha)Z}{(\alpha-\beta)\left(Z-e^{-\alpha T}\right)} + \frac{\alpha(\beta-\nu)Z}{(\alpha-\beta)\left(Z-e^{-\beta T}\right)}\right\}(\dot{h}_c - \dot{h})Z^{-k}$$

$$- \frac{K_\theta}{(\beta-\alpha)}\left\{\frac{(\nu-\alpha)Z}{\left(Z-e^{-\alpha T}\right)} + \frac{(\beta-\alpha)Z}{\left(Z-e^{-\beta T}\right)}\right\}\theta Z^{-k}$$

Multiplying through by $\frac{Z^{-1}}{Z^{-1}}$ and establishing a common denominator

$$\delta(Z) = \frac{K_n^{\cdot} K_\theta}{\alpha\beta(\alpha-\beta)} \left\{ \frac{\begin{array}{l}(\alpha-\beta)\nu\left(1-e^{-\alpha T}Z^{-1}\right)\left(1-e^{-\beta T}Z^{-1}\right) \\ + \beta(\nu-\alpha)\left(1-Z^{-1}\right)\left(1-e^{\beta T}Z^{-1}\right) \\ + \alpha(\beta-\nu)\left(1-Z^{-1}\right)\left(1-e^{\alpha T}Z^{-1}\right)\end{array}}{\left(1-Z^{-1}\right)\left(1-e^{-\alpha T}Z^{-1}\right)\left(1-e^{-\beta T}Z^{-1}\right)} \right\} (\dot{h}_c - \dot{h})Z^{-k}$$

$$- \frac{K_\theta}{(\beta-\alpha)} \left\{ \frac{(\nu-\alpha)\left(1-Z^{-1}\right)\left(1-e^{-bT}Z^{-1}\right) + (\beta-\nu)\left(1-Z^{-1}\right)\left(1-e^{-\alpha T}Z^{-1}\right)}{\left(1-Z^{-1}\right)\left(1-e^{-\alpha T}Z^{-1}\right)\left(1-e^{-\beta T}Z^{-1}\right)} \right\} \theta Z^{-k}$$

$$\equiv \frac{-c_o - c_1 Z^{-1} - c_2 Z^{-2}}{1-a_1 Z^{-1} - a_2 Z^{-2} - a_3 Z^{-3}} (\dot{h}_c - \dot{h})Z^{-k} + \frac{b_o + b_1 Z^{-1} + b_2 Z^{-2}}{1-a_1 Z^{-1} - a_2 Z^{-2} - a_3 Z^{-3}} \theta Z^{-k}$$

Multiplying through by the denominator leads directly to the estimation (difference) equation for $\dot{h}_c \equiv 0$

$$\delta_n = a_1\delta_{n-1} + a_2\delta_{n-2} + a_3\delta_{n-3} + b_o\theta_{n-k} + b_1\theta_{n-1-k} + b_2\theta_{n-2-k}$$

$$+ c_o\dot{h}_{n-k} + c_1\dot{h}_{n-1-k} + c_2\dot{h}_{n-2-k} + B$$

APPENDIX B

SPACE SHUTTLE FLYING QUALITIES QUESTIONNAIRE

Respondent's Name _____

Flight _____ on (date) _____

The Shuttle Orbiter, as a large highly augmented, fly-by-wire, delta glider has some entry flying characteristics which are considerably different from more conventional aircraft. The current flying qualities criteria data base is drawn from experience with the latter and may not be appropriate for Shuttle-like vehicles. This questionnaire has been prepared to obtain information on manual control of Shuttle entry for development of improved criteria for advanced aircraft.

This questionnaire has two sections, the first concerns the crews' perception of the task and flying techniques in each entry flight segment. The second section concerns the crews' evaluation of Orbiter dynamics, flying qualities and workload.

In both sections, five flight segments are of interest:

1. Supersonic bank reversals (M = 18, 9, 5, 2.5)
2. Heading Alignment Circle (HAC) turn
3. Descent on the steep glide slope
   - auto speed brake
   - manual speed brake
4. Preflare
5. Shallow glide and final flare to touchdown

SECTION I

QUESTIONS ON TASKS AND FLYING TECHNIQUE

As noted on the previous page, the Shuttle Orbiter has some flying characteristics which are considerably different from conventional aircraft, not the least of which is the lack of thrust or power to maintain constant energy flight segments and/or extract the vehicle from hazardous flight conditions. The questions contained in this section are intended to help us establish

a) the control loop structure in use by the pilot (e.g., what parameter is being controlled, what is being tracked)

b) the pilot control strategy (e.g., constant θ, g, $\dot{h}$, γ,...; pitch attitude; maintain __?__ within ± __?__; switch to another strategy when __?__)

c) pre-programmed (highly learned, open-loop) maneuvers

We will also use this information in analyzing data recorded during your flight (or simulation). For example, it will assist us in

a) identifying the different flight segments on the flight traces

b) modeling the pilot's control loop structure and strategy so as to extract (via parameter identification techniques) information concerning pilot workload, pilot adaptive time to each control task or flight segment, etc.

c) identifying influence of the Orbiter nonconventional flying and control characteristics

d) preparing criteria and design guides for improving the flying qualities of future Shuttle-type aircraft.

Please feel free to add any comments, suggestions, criticism, or whatever which you feel may be of assistance in achieving the above goals. Your cooperation is greatly appreciated.

A. General questions for each flight segment:

1. Please check the control channels flown manually in each flight segment

	PITCH	ROLL/YAW	SPEED BRAKES	BODY FLAP
Supersonic Bank Reversals (Please identify specific maneuvers)				
HAC Turn				
Steep Glide				
Preflare				
Shallow Glide and Final Flare				

2. What were the primary objectives of each flight segment flown manually, the primary variables controlled (tracked) and the allowable range of these variables?	
Supersonic Bank Reversals (Please identify specific maneuvers)	
HAC Turn	
Steep Glide	
Preflare	
Shallow Glide and Final Flare	

3. What cues and conditions are used to transition from each flight segment to the next, what information sources are used, what controller inputs are employed?	
Supersonic Bank Reversals (Please identify specific maneuvers)	
HAC Turn	
Steep Glide	
Preflare	
Shallow Glide and Final Flare	

4. To what extent is each flight segment an "open loop" (learned) maneuver? To what extent is "closed loop" tracking significant and what response variables from what sources are involved?	
Supersonic Bank Reversals (Please identify specific maneuvers)	
HAC Turn	
Steep Glide	
Preflare	
Shallow Glide and Final Flare	

5. To what extent are manual trim (pitch, roll, yaw, body flap) controls used?	
Supersonic Bank Reversals (Please identify specific maneuvers)	
HAC Turn	
Steep Glide	
Preflare	
Shallow Glide and Final Flare	

6. To what extent did the commander operate in a "head-up" visual mode, what factors determined "head-up" operation?	
Supersonic Bank Reversals (Please identify specific maneuvers)	
HAC Turn	
Steep Glide	
Preflare	
Shallow Glide and Final Flare	

7. What is the extent of occupation with secondary axes of control? (e.g., heading control in Preflare, etc.).	
Supersonic Bank Reversals (Please identify specific maneuvers)	
HAC Turn	
Steep Glide	
Preflare	
Shallow Glide and Final Flare	

8. What (if any) disturbances (crosswinds, turbulence) were significant, what techniques were used to regulate against these disturbances?	
Supersonic Bank Reversals (Please identify specific maneuvers)	
HAC Turn	
Steep Glide	
Preflare	
Shallow Glide and Final Flare	

B. Specific Questions for Individual Manually Controlled Flight Segments

1. Steep glide slope acquisition and glide

   a. To what extent is manual control of speed with speedbrakes similar to conventional use of throttles?

   b. Is speedbrake operation basically "open loop" or "closed loop," continuous or discrete?

   c. Are there any significant interactions between manual (or automatic) speedbrake control and attitude/path control with the RHC? If so, how does this effect piloting technique?

2. Preflare Pullups

   a. What cues are used to initiate preflare?

   b. Do you prefer to fly this

      as a constant load factor maneuver? Why?

      as a constant pitch rate maneuver? Why?

      other? Why?

c. Any comments as to the RHC force/displacement/sensitivity/ lat-long harmony during this maneuver?

d. What determines speedbrake retraction?

e. What determines gear extension, is the gear light used?

3. Acquisition of and glide on the shallow glideslope and final flare

a. Is the shallow glide basically constant sinkrate, constant flight path angle or neither, how is the controlled variable maintained?

b. Is there a distinct final flare maneuver? Is it basically open or closed loop? What determines the initiation of flare? Is flare due to ground effect noticeable or explicitly accounted for?

c. Is there any conscious effort to "schedule" sinkrate with altitude in this flight segment?

d. What are the relative priorities and criteria in the control of: energy, touchdown sinkrate, touchdown speed, touchdown point?

e. What are the principal attitude and path references? What is the relative use of "out the window," HUD and panel displayed information? How are verbal callouts from other crew members used?

f. Is the selection of the shallow glideslope and flare characteristics essentially preplanned or are they modified as the landing unfolds? Would the strategy be modified in crosswinds?

g. What situations might lead to ballooning? To a pilot induced oscillation (PIO)?

h. What procedures are used to control (touchdown) speed?

i. Is attitude control basically open or closed loop? Are attitude commands basically discrete or continuous?

j. Are you conscious of any pulse type RHC control activity? Does this seem "natural"? necessary?

SECTION II

A. General Evaluation of Orbiter Dynamics, Flying Qualities and Workload

The following is a list of flying quality related characteristics which may or may not have adversely impacted manual control workload, task difficulty, attitude or path control precision, etc. These have not been integrated into a question format in order to avoid restricting the nature of your response. Comments are therefore solicited on any aspect in which a particular factor may stand out in your memory as adversely impacting the above during the flight segments of interest. Please identify the flight segment being commented on.

1. Longitudinal control

   a. Rotational hand controller (RHC) characteristics

      RHC displacements

      RHC force gradient

      Breakout sensitivity

      Gain (rate command/force input) and shaping

      Longitudinal-lateral displacement, gradient, or sensitivity harmony

   b. Pitch attitude response (to inputs required to perform task)

      Effective time delay

Initial response onset (rise time)

Overshoot

Settling time

Predictability

Sensitivity

PIO tendency

c. Path response/control

Effective motion delay time

Predictability

PIO tendency

Any special control techniques employed? required?

d. Airspeed control

Precision

Predictability

e. Disturbances

Turbulence

Wind shear

Ground effect

f. Workload

Is control workload significant? dominant?

Does other task workload detract from control task performance?

Cooper-Harper rating (if possible)

2. Lateral-Directional Control

a. Rotational hand controller characteristics

RHC displacements

RHC force gradient and shaping

Breakout sensitivity

Lateral-longitudinal harmony

Gain (rate command/force input) and shaping

b. Roll attitude response

Effective time delay

Initial response onset (rise time)

Overshoot

Settling time

Predictability

Sensitivity

PIO tendency

Lateral acceleration at pilot

Roll ratcheting

c. Heading response/precision

Roll into turns

Roll out of turns

d. Workload

Is control workload significant?

Does other task workload detract from control task?

e. Cooper-Harper rating (if possible)

3. Summary (Brief)

a. Major problems

b. Good features

B. Specific Questions on Flying Qualities and Workload

1. In landing, are there any unusual characteristics of the Shuttle pitch attitude response to the rotational hand controller? Does the response appear to be "rate command," "attitude command" or neither?

2. Are there any unusual characteristics of the Shuttle path (altitude, flight path angle) response to pitch attitude changes?

3. What differences in pitch trim and airspeed control, as compared to conventional aircraft, are required because of the zero stick force/speed gradient of the Shuttle's pitch rate command system?

4. What is the relative difficulty of speed control with the speed-brakes (steep glideslope)?

5. In the shallow glide and final flare are there any conflicts in simultaneous control of touchdown point, speed and sinkrate?

6. Are there inadequacies in the availability of information (pitch attitude, sinkrate, etc.)? What display changes would help? How adequate is the view "out the window" for attitude, altitude, heading, and flight path control?	
Supersonic Bank Reversals (Please identify specific maneuvers)	
HAC Turn	
Steep Glide	
Preflare	
Shallow Glide and Final Flare	

7. Do you foresee any operational conditions (turbulence, cross-winds, night landing, etc.) which might approach flying qualities limits? What response characteristics of the Shuttle might be limiting in these situations?

8. To what extent did the actual Shuttle Orbiter flying characteristcs in approach and landing differ from ground simulations and STA flights? What, if any, changes would be valuable for pre-flight ground and STA simulations?

9. What portion (rough percentage) of the total crew workload capacity was used in each flight segment?

	NO WORKLOAD 0	50%	LIMIT OF CAPACITY 100%
Supersonic Bank Reversals (Please identify specific maneuvers)			
HAC Turn			
Steep Glide			
Preflare			
Shallow Glide and Final Flare			

1. Report No.	2. Government Accession No.	3. Recipient's Catalog No.
NASA CR-170407		

4. Title and Subtitle	5. Report Date
Space Shuttle Flying Qualities Criteria Assessment – Phase III	February 1984
	6. Performing Organization Code

7. Author(s)	8. Performing Organization Report No.
T. T. Myers, D. E. Johnston, and D. T. McRuer	TR-1197-1
	10. Work Unit No.
9. Performing Organization Name and Address	
Systems Technology, Inc. 13766 South Hawthorne Boulevard Hawthorne, California 90250	11. Contract or Grant No. NAS4-3005
	13. Type of Report and Period Covered
12. Sponsoring Agency Name and Address	Contractor Report - Final
National Aeronautics and Space Administration Washington, D.C. 20546	14. Sponsoring Agency Code RTOP 506-63-40

15. Supplementary Notes

NASA Technical Monitor: Donald T. Berry, Ames Research Center, Dryden Flight Research Facility, Edwards, CA 93523. Phase I of this study is published as NASA CR-170391; phase II, as NASA CR-170406.

16. Abstract

This study continues the development of flying qualities experiments as part of the Orbiter Experiments Program (OEX). Phase I, published as CR-170391, reviewed flying qualities criteria and initial Shuttle data. Phase II, published as CR-170406, proposed a program implementation consisting of inflight experiments correlated with extensive simulator programs, a preliminary review of instrumentation and data analysis requirements and a review of STS 1 through 4 flying qualities. This report explores the crucial flight data measurement and reduction techniques required for the experimental approach. An overview of available flight data is presented, identification of the effective augmented vehicle and pilot models determined, a summary of flight data problems compiled, and further recommendations for the Orbiter Flying Qualities (OFQ) experiment provided.

17. Key Words (Suggested by Author(s))	18. Distribution Statement
Space shuttle orbiter Flying qualities Flight control Pilot models	Unclassified-Unlimited STAR category 08

19. Security Classif. (of this report)	20. Security Classif. (of this page)	21. No. of Pages	22. Price*
Unclassified	Unclassified	128	A07

*For sale by the National Technical Information Service, Springfield, Virginia 22161.

End of Document